UNIVERSITA' DEGLI STUDI DI PARMA

Dottorato di ricerca in Fisica

Ciclo XXVII

Archaeological Biophysics:

Structural study of ancient collagen in archaeological skin and bone samples.

Coordinatore:
Chiar.mo Prof. Cristiano Viappiani
Tutor:
Chiar.ma Dr.ssa Maria Grazia Bridelli

Dottoranda:
Chiaramaria Stani

March 18th 2015

In qualsiasi circostanza vi troviate
non cedete alla sconfitta.
Non abbandonate ciò che avete raggiunto
se vi trovate ad un punto morto.
Un grande futuro vi attende.
Per questo motivo dovete perseverare e studiare.

(Daisaku Ikeda)

A Clara e alla mia dolcissima famiglia!!!

Acknowledgements

I would like to thank all the people that took part to this project.

Many thanks to the Prof. Emma Rabino Massa and to the Dr. Rosa Boano, curator of the museum of Anthropology and Enthography "G. Marro" of the University of Turin for the possibility to work on the Egyptian mummified remains.

Thank to the Dr. Mirko Traversari of the University of Bologna for his great availability and for providing the Roccapelago mummified remains.

Thank to the Prof. Paola Iacumin for providing the ancient bone samples.

I would like to thank the whole BioArCh research group and in particular the Prof. Matthew Collins, Dr Stephen Buckley, Prof. Joann Fletcher, Dr. Sarah Fiddyment and Rianca Vogels of the University of York, for their great hospitality and for the opportunity to participate to the "Mummifying Alan project" and to the study regarding the use on Natron in ancient Egypt.

Thank to the Dr. Giovanni Magno of the University of Padua for the possibility to collaborate to the experimental archaeology project about the funerary practices of cremation of the ancient Veneti population.

I would like to thank all the people who supervised me in these years with great patience and availability. Many thanks to the Dr. Roberta Bedotti, Dr. Lucia Dramis and Dr. Daniele Menozzi for teaching me laboratory procedures and sample preparations. Thank to the Dr. Victor Erokhin and the Prof. Rosangela Cinquetti for the opportunity to perform SEM measurements and Histological analyses, respectively. Thank to the Dr. Roberta Bedotti and the Dr. Mara Bertolotti for the CD measurements.

And, in closing, hoping I have not forgotten anyone, I would like to thanks my supervisor, Dr. Maria Grazia Bridelli, for supported, helped and teached me every day in these three years of Ph.D.

Table of Contents

Preface

This thesis work is focused, oriented on the study of a series of ancient remains, such as mummified skin and fossilized bones, coming from different archaeological contexts, to investigate their state of preservation. The mummified skin samples belong to the Egyptian collection of the Museum of Anthropology and Ethnography of the University of Turin and to the Roccapelago anthropological findings while the bone samples come from Central Anatolia and Friuli (Italy). Previous works showed that the state of preservation of these ancient materials is correlated to the mechanism of transformation or degrade of the constituting biological macromolecules. The main macromolecule constituting skin and bone is represented by type I collagen. Collagen is a structural fibrous protein that shows an incredible survival capability during time and in extreme environmental conditions. Dehydration mechanism and glycation reactions are the main factors that influence the structural modification of the collagen secondary structure.

This work is organised in two main part. In Part I the main structural modifications of collagen secondary structure are investigated. The biochemical mechanisms that lead to modification of fibrous proteins can cause, primarily, a loss of protein functionality. However, biological remains coming from the archaeological contexts probably survived across historical ages due to the collagen structural modifications. With the aim to understand the mechanisms allowing the preservation of the ancient remains, two parallel approaches were developed. The first one, consisting in a series of *in vitro* experiments performed in order to gain information on the hydration structure of collagen and the biochemical mechanism of interaction with sugars. Experiments of controlled dehydration-rehydration and glycation with different types of sugars were carried out, on a rat tail type I collagen, assumed as reference, in the native conformation. FTIR Spectroscopy and Circular Dichroism Spectroscopy were employed to characterize the sample changes consequent to the treatments. This biochemical modification can be considered the main processes producing the mummification or the fossilisation of the ancient remains exposed to various environmental conditions. For this reason the second approach was essentially archaeometric one, consisting in analyses on several archaeological samples by means of FTIR spectroscopy, Scanning Electron Microscopy and histological analyses. However each kind of sample required a different measurement protocols, in dependence of its nature, age and the archaeological significance. A great amount of results was collected and interpreted in the lights of the results obtained from the *in vitro* experiments. It was then possible to assess a preservation degree to the archaeological remains in dependence on aging,

different mummification processes, natural or anthropogenic, and on different burial environmental conditions. Moreover, in some cases it was possible to accomplish the characterization of some embalming materials used during the Egyptian embalming procedures and to detect on some remains traces of infestant organisms responsible of particular forms of biodegrade.

In Part II two cases of experimental archaeology were faced, representing two of the most debated and controversial questions of the modern archaeology. The first one is concerning the use of Natron, the salt employed by ancient Egyptian embalmers to dehydrate corpses before mummification procedures, and its evolution during the Egyptian historical ages. The second one is a study of the funerary practices of cremation exploited by Ancient Veneti peoples of bronze age. The colour and microstructure of charred bones were investigated and related to funerary practice proposed in the study.

PART I

Chapter 1

Collagen structure and aging mechanisms

1.1 - Collagen family: types, localisations and functions.

Collagens belong to the family of fibrous proteins. They are the most important proteins in mammals, as they constitute 25% of the whole protein mass in these animals. They are secreted by connective tissue cells and in these tissues they are multipurpose: they bind body structures together and they provide support and protection. As a matter of fact, they are the main element in skin, bones, tendons, ligament, and teeth. (Whitford 2005)

All collagens are structured in a triple helix and they are put together by three polypeptide chains. About 25 distinct collagen α-chains have been identified, each one encoded by a separate gene. 30 distinct genes have been approximately identified. Different combinations of these genes are expressed in each tissue. Since polypeptide chains may be combined in more than one combination, many different collagens may exist and several of them have been identified. They may form about 30 distinct collagen types in animals and at least 19 different collagens in humans.

Collagens may be distinguished among them depending on their structure, localisation and function. In most connective tissues, matrix macromolecules are secreted by cells called fibroblasts. In some specialised connective tissue, such as cartilage and bone, however, they are secreted by cells belonging to the fibroblast family, whose cells have more specific names: chondroblasts, for example, create cartilages, and osteoblasts create bones.

Four major classes have been identified:

- fibrillar collagens;
- fibril-associated collagens;
- network-forming collagens;
- filamentous collagens. (Bailey et al. 1998; Alberts 2001)

Fibrillar collagens are the most common collagens, which constitute the most of the collagen in the human body. Types I, II, III, V and XI belong to this class. They have the rope-like structure of a typical collagen molecule. After being secreted into the extracellular space, these collagen molecules are assembled into ordered polymers, called collagen fibrils: they are thin structures (10-300 nm in diameter) which are hundreds of micrometers long. The collagen fibrils often aggregate into larger, cable-like bundles called collagen fibers which have a diameter of several micrometers. (Alberts 2001)

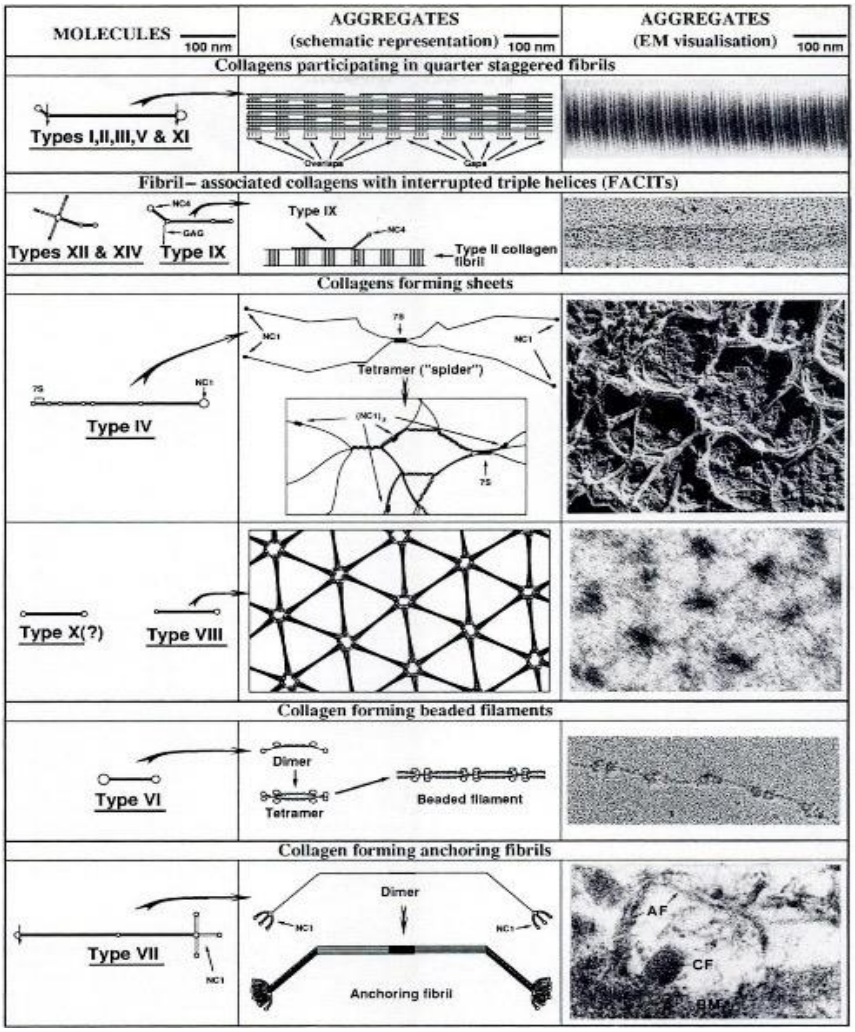

Figure 1.1: Main classes of collagens

- **Type I** collagen: it is the most common type and it constitutes 90% of the whole collagen in the human body and it may be found in bones, skin, tendons, ligaments, cornea, internal organs and dentine.
- **Type III** collagen has been found in skin, blood vessels and internal organs.
- **Type V** collagen is usually associated to Type I molecules.
- **Type II** collagen: it is the major collagenous constituent of cartilaginous tissues, intervertebral discs and vitreous humours.
- **Type XI** is often associated to type II.

Network collagens are involved in the formation of sheets or protein membranes which surround tissues and organisms. (Rest and Garrone 1991)

- **Type IV** molecules assemble into felt-like sheet or meshwork that constitute the major part of the mature basal laminae.
- **Type VII** molecules form dimers which assemble into specialised structures called anchoring fibrils, which, by their extremities, help to attach the basal lamina to the underlying connective tissue. They are abundant especially in the skin.
- **Type VIII** collagen molecules are the main element of the hexagonal lattice of Descemet's membrane, one of the layers of the cornea. Its structure bears no clear similarity to basement membrane type IV collagen, but it looks to be closely related to type X collagen.
- **Type X** collagen molecules were synthesized by hypertrophic chondrocytes. Its function and mode of aggregation is still a matter of controversy. There is not a clear evidence that type X collagen would form a sheet structure, yet.

The **fibril associated collagens** do not form proper fibers or networks, but they are associated with others fibers, forming collagens which link them to other fibrils, or to other components in the extracellular matrix. They do not form typical quarter-staggered fibrils. The structure of these molecules may be divided into three main functional regions. The first region, consisting of one or two triple helical domains, serves for the interaction and adhesion of these molecules to the fibrillar collagens. A second region, consisting of another triple helical domain, serves as a rigid arm that projects out of the fibril; a third region, which does not include triple helices, may serve to interact with other matrix elements or with cells. (Rest and Garrone 1991)

- **Type IX** is the best-characterised molecule of this group. It consists of three collagenous domains, separated by non-triple helical regions. It is aligned on the surface of type II collagen fibers in an antiparallel manner.
- **Type XII** and **Type XIV** are usually associated with the surface of Type I and III collagens. They are localised in embryonic tendons and skin, periodontal ligaments, foetal skin and cartilages.

Finally, **Type VI** collagen, defined as **filamentous collagen**, shows a loosely packed filamentous structure, with an axial repeat of 100 nm and it is formed by end-to-end alignment of tetramers. These kind of fibers occur in many tissues and it has been suggested that Type VI collagen may separate and align larger Type I collagen fibers. It has been proven that its amino acid sequences play a central role in the interaction of matrix constituents, in particular fibronectin, with cell receptors of the integrin type.

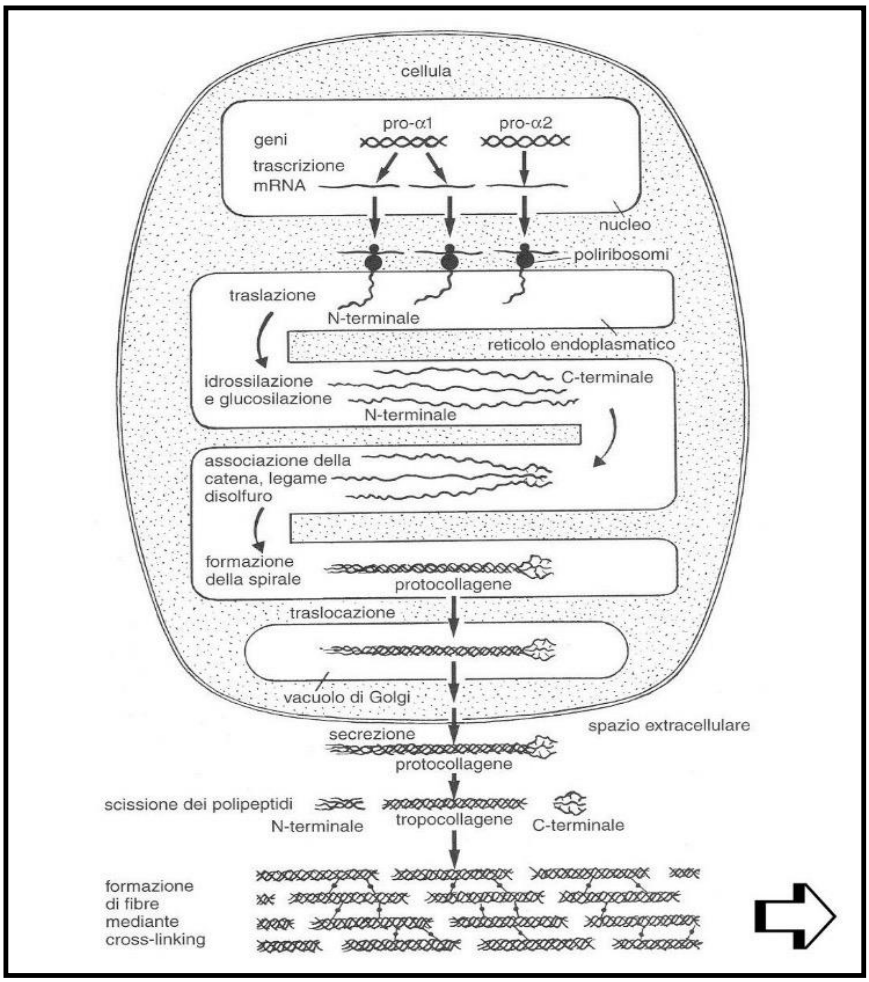

Figure 1.2: Collagen synthesis

1.2 - Collagen synthesis

The biosynthesis of collagen is divided into reactions which differ not only in the nature of modification but also in their cellular location.

In the cell nucleus, the polymerase RNA begins the transcription of the two genes COL1A1 and COL1A2 to obtain mRNA. This messenger RNA, the pre pro-α chains, contains a signal sequence at its N-terminal, that directs the precursors and facilitates its recognising and binding on the membrane-bound ribosomes, associated to the rough endoplasmic reticulum (RER). Inside the ribosomes, the transfer RNA encodes the mRNA, giving rise to the primary amino acid sequences. They are injected in the lumen of the endoplasmic reticulum, where the signal peptide are cleaved by the action of specific proteases and large collagen precursors are synthesized. Now they are called pro-α chains. As they enter into the RER proline and lysine residues were hydroxylated, respectively from the action of prolyl hydroxylase and lysyl hydroxylase and by the presence of oxygen and vitamin C.

Furthermore, glycosylation take place, through the hydroxyl group of hydroxylysines by the attachment of sugars, chiefly glucose and galactose. Frequently, the sugars are added as disaccharide units. The procollagen molecule contains polypeptide extensions (extension peptides) of 20–35 kDa at both its amino and carboxyl terminal ends, neither of which is present in mature collagen. Both extension peptides contain cysteine residues. While the amino terminal propeptide forms only intrachain disulfide bonds, the carboxyl terminal propeptides form both intrachain and interchain disulfide bonds. Formation of these disulfide bonds assists in the registration of the three collagen molecules to form the triple helix, winding from the carboxyl terminal end. Thus, the propeptides have at least two functions:

1. They guide the intracellular formation of the triple-stranded collagen molecules;
2. As they are removed only after secretion, they prevent the intracellular formation of large collagen fibrils, which could destroy the cell.

After having formed the triple helix, no further hydroxylation of proline or lysine or glycosylation of hydroxylysines take place. Following **secretion** from the cell, through the Golgi Apparatus, extracellular enzymes, called **procollagen aminoproteinase** and **procollagen carboxyproteinase**, remove the extension peptides at the amino and carboxyl terminal ends. Once the propeptides are removed, each pro-α chain, containing approximately 1000 amino acids per chain, combines with two others, in order to form a hydrogen-bonded, triple-stranded helical molecule known as tropocollagen, that spontaneously assemble into collagen fibers. The fibrils begin to form close to the cell surface, often in deep infolding of the plasma membrane formed by the tandem fusion of secretoty vesicles with the cell surface. The cortical cytoskeleton can influence the sites, rates and orientation of the fibrils assembly. These fibrils are further stabilized by the formation of inter- and intrachain cross-links through the action of lysyl oxidase. (Harvey; Alberts 2001; Whitford 2005; Murray et al. 2009)

1.3 - Collagen Structure

The main feature of a typical collagen molecule is its long, stiff, and triple-stranded helical structure, in which three collagen polypeptide chains, called α-chains, wound around one another in a rope-like superhelix. At the end of collagens, proline and glycine are added, as both are important in the formation of the triple-stranded helix. Proline, because of its ring structure, stabilises the helical conformation in each α-chain, while glycine is regularly spaced at every third residue throughout the central region of the α-chain. Being the smallest amino acid,

glycine allow the three helical α-chain to pack tightly together, in order to form the final collagen superhelix.

Type I collagen consists of two identical chains called α_1 (I) chains and a third chain called α_2 (II). The α-chains differ from one another just for their amino acid sequences. In contrast, type II collagen contain three identical α_1 chains. (Whitford 2005)

Tropocollagen is a triple helix of three similarly sized polypeptide chains, each one has on average about 1000 amino acid residues, and they weight around 95000 Da each. This leads to an approximate MW of 285000, an average length of ~300 nm and a diameter of ~1.4 nm. Collagen has an extremely elongated and filamentous nature.

1.3.1 - Polyproline helix

Proline does not form helical structure for the obvious reason that the absence of an amide proton (NH) preclude hydrogen bonding, whilst the side chain covalently bonded to the N atom restricts backbone rotation. (Whitford 2005)

But it may form two very particular kinds of helical structure, and they do not contain hydrogen bonds. They are called polyproline I and polyproline II.

The polyproline I is a left-handed helix with 10 residues for three turns. All peptide bonds take a cis conformation, which is quite rare. On the other hand, the polyproline II is a similar left-handed helix, but all peptide bonds take a trans conformation. A solvent variation may stimulate a switch between two conformations. In a water solution, polyproline II is more stable, it shows 3 residues per turn and the rise per residue is 3.12 Å. The polyproline II helix is more open than a classical α-helix which show a rise per residue of 1.5 Å.

The repetition of many proline residues, or sequence with a high amount of proline, is quite rare in most of the proteins. For this reason, a protein with a structure similar to polyproline II is occasionally observed. Collagen is an exception.

1.3.2 - Amino acids sequence

Collagen amino acid composition is very peculiar. It is characterized by an excess of glycine and proline content showing a repetitive primary sequence, in which every third residue is glycine. The sequence of the polypeptide chain can be written as

-Gly-Xaa-Yaa-Gly-Xaa-Yaa-Gly-Xaa-Yaa-

Where Xaa and Yaa are any other amino acid residue, but they are often found to be the amino acid proline and lysine. Many of the proline and lysine residues are hydroxylated via post-traslational enzymatic modification to yields either hydroxyproline (Hyp) or hydroxylysine (Hyl). The sequence Gly-Pro-Hyp occurs frequently in collagen. (Whitford 2005)

1.3.3 - Collagen Helix

Amino acid	Percentage
Gly	**32.7**
Ala	**12.0**
Ser	**3.4**
Glx	**7.7**
Cys	**0**
Pro	**22.1**
Arg	**5.0**
Leu	**2.1**
Thr	**1.6**
Asx	**4.5**
Val	**1.8**
Tyr	**0.4**
Ile	**0.9**
Phe	**1.2**
Lys	**3.7**
Trp	**0**
His	**0.3**
Met	**0.7**

Table 1.1: Collagen amino acid percentages

Each polypeptide chain intertwines with the remaining two chains to form a triple helix. The helix arrangement is very different compared to the α-helix and it is more similar to the poly-proline II helices.

Each chain has a sequence Gly-Xaa-Yaa and forms a left-handed super helix with the other two chains. This leads to the triple helix of left-handed polypeptide chain, supercoiled in a right-handed manner on a common axis. The rise, or translation distance per residue, for each chain in the triple helix is 0.286 nm, whilst the number of residues per turn is 3.3. Combining these two figures yields a value of ~0.95 nm per helix pitch and it reveals a more extended conformation, especially if compared with α helices or 3_{10} helices (pitch ~0.50 – 0.54 nm).

Glycine, as it lacks the chiral centre and it possesses a conformational flexibility, significantly contrasts with proline. In proline, a conformational constrain exists as a result of the limited variation in the torsion angle (ϕ), allowed by the cyclic pyrrolidone ring.

The presence of a large amount of proline in tropocollagen is significant as well, because the absence of the amide hydrogen (NH) eliminates any potential hydrogen bonding with suitable acceptor groups. As a result, the presence of both glycine and proline in high frequency in the collagen, the triple helix is forced to adopt a different strategy in packing polypeptide chains. Since the glycine residues are located at every third position and make contact with the two remaining polypeptide chains, it is clear that only a very small side chain can be accommodated in this position. Any side chain bigger than hydrogen would disrupt the conformation of the

triple helix. As a result, there is very little space along the helix axis of collagen, and glycine is always the residue closest to the helix axis. The side chains of proline residues, along with lysine and other residues are on the outside of the helix.

1.3.4 - Hydrogen bonds and water bridges

Van der Waals' interactions, stabilize the collagen triple helix, but in addition, extensive hydrogen bonding takes place between polypeptide chains. The hydrogen bonds established between the amide (N-H) group of one glycine residue and a backbone carbonyl (C=O) group of the residue Xaa on adjacent chains. The direction of hydrogen bonds is transversal or it crosses the long axis of the helix. Each chain is staggered, so that Gly and Xaa and Yaa occur at approximately the same level, along the axis of the triple helix. As suggested by Whitford, interactions within the triple helix are further enhanced by hydrogen bonding, between amide groups and hydroxyl group of Hyp residue. The triple helix stabilisation is possible through hydroxylation of proline (Hyp) and the formation of hydrogen bonds with neighbouring chains (Whitford, 2005). Hyp residues stabilise collagen by participating in direct interchain hydrogen bonding, but steric constraints would not permit direct hydrogen bonding between the Hyp hydroxyl group and peptide carbonyls in the same chain, between different chains in the same molecule, or between different molecules (Whitford 2005).

Water plays a key role in maintaining the conformation of the native collagen molecule. However, the structure of water in collagen fibrils is very different from bulk water, in terms of restricted mobility and asymmetric orientation. In fact, it looks like water molecules are tightly bound to specific sites on collagen chains, filling in the spaces between collagen molecules. The stabilisation of collagen triple helix by Hyp residues take place through intramolecular water bridges, involving those carbonyl and amide groups, which are not participating in the interchain hydrogen bonding pattern (Bella et al. 1995).

Triple helix is surrounded by an extensive cylinder of hydration and Hyp residues seem to play an important role, connecting the water network to the peptide molecules (Bella et al. 1995; Kawahara et al. 2005). The solvent around a given triple helix goes beyond the immediate neighbourhood and reaches adjacent triple helices in the crystal. This suggest a role of hydration in the process of molecular association leading to the formation of collagen assemblies.

Proline carbonyl groups only participate in the interchain N-H…O=C hydrogen bonding, and do not exhibit hydration. Carbonyl groups are proportionally less hydrated than Hyp hydroxyl groups. Moreover, there is the tendency for Hyp carbonyl groups to receive hydrogen bonds from more than one solvent molecule.

Water bridges were extensively studied in crystalised collagen molecules and may be categorised as intrachain, connecting anchoring groups in the same peptide chain; interchain, connecting anchoring groups in different peptide chain from the same triple helix; intermolecular: connecting triple-helical molecules related by the symmetry elements of the crystal lattice (Bella et al. 1995). Bella et al. and Kawahara et al. identified 7 types of water bridges:

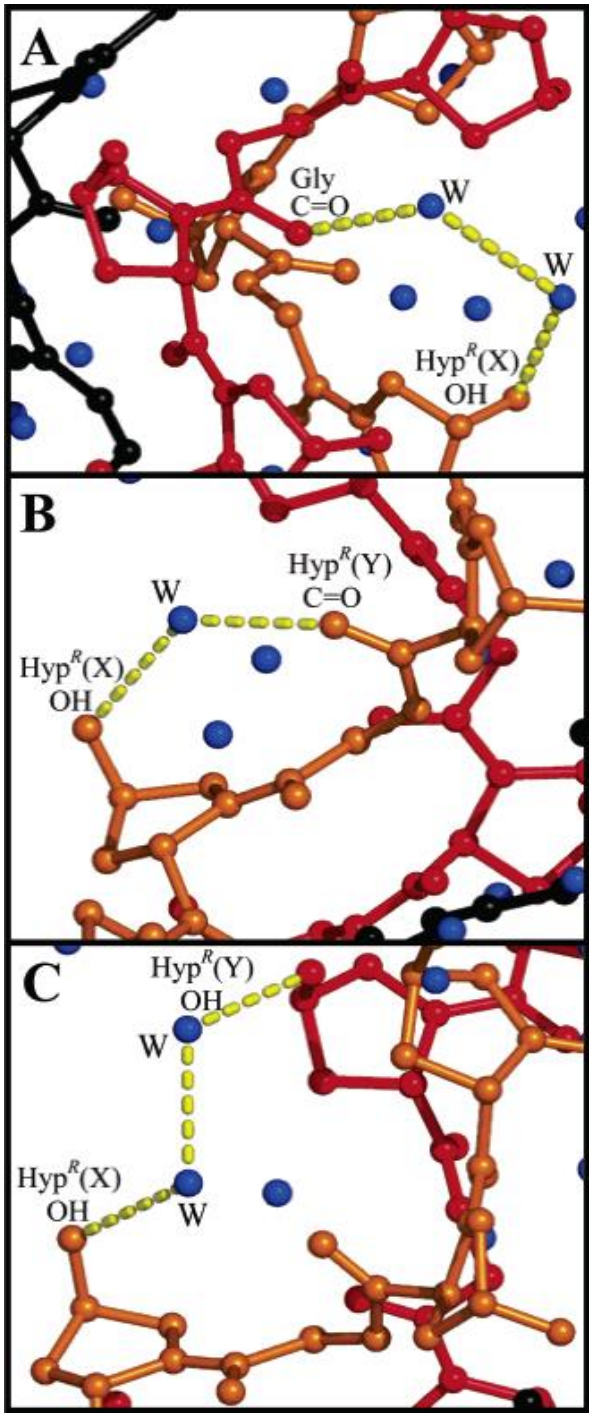

- **α**: intrachain bridges between Hyp(Y) C=O group and Gly C=O group any two residues in a triple helix;
- **β**: interchain bridges between Hyp(Y) C=O group and Gly C=O group;

α and β bridge are totally independent from the amino acid sequence, because they only interconnect carbonyl groups and could appear as connector of any two residues in a triple helix. **β** bridges seem to form interrupted filaments of water molecules which are wrapped around the triple helix.

- **γ**: intrachain bridges between Hyp(Y) O-H group and preceding Gly C=O group;
- **δ:** Interchains bridges between Hyp (Y) O-H group and Hyp (Y) C=O group on the next chain (Bella et al. 1995).

Figure 1.3: example of various types of water bridges.
Panel A: Interchain k bridge between the Hyp(X) OH group and the Gly C=O group.
Panel B: Intrachain λ bridge between the Hyp(X) OH group and the Hyp(Y) C=O group.
Panel C: Interchain μ bridge between the Hyp(X) OH group and the Hyp(Y) OH group.
Dotted lines (yellow) designate the hydrogen bonds. Water molecules (blue) which are involved in the water bridge are labeled by W.

Formation of γ and δ bridges depends on the presence of the hydroxyl group in the right place. They can involve from 1 to 3 water molecules. They are one of the dominant features in the repetitive patterns of hydration in this crystal structure. The occurrence of these bridges seems to be independent from local distortions of the triple-helical geometry. By prolyl hydroxylation, collagen triple helices acquire extra hydrogen-bonding capabilities that may reinforce their conformational structure.

- **k**: Interchain bridges connecting Hyp (X) O-H group and Gly C=O group.

They can involve 2 or 3 water molecules

- **λ**: Intrachain bridges connecting Hyp (X) O-H group and Hyp (Y) O-H group

They can involve from 1 to 3 water molecules

- **μ**: Interchain bridges connecting Hyp (X) O-H group and Hyp (Y) O-H group

They can involve 2 or 3 water molecules (Kawahara et al. 2005)

- **ω**: water bridges connecting neighbouring triple helices in the crystal (Bella et al. 1995).

ω bridges may involve any number of waters, but typically they involve two or three water molecules.

The absence of direct contacts between triple helices suggests that triple helices are already coated by a cylinder of hydration, before assembling into the crystal lattice. This cylinder is organised in successive shells. The first shell of water molecules is directly hydrogen bonded to carbonyl, hydroxyl or amide groups on the peptide surface. The second shell of water molecules is hydrogen bonded to the ones in the first shell. At this step, the filling of the superhelical groove by solvent molecules becomes more evident. Lastly, a third shell of water molecules completes the hydration of collagen triple helices.

Most of the water bridges described show a pentagonal-like appearance. Water pentagons are found in the solvent zone between two triple helices, and their water molecules participate in extensive hydrogen bonding to the anchoring groups in the peptide molecules engaged in α, γ, or δ bridges. Some of the most frequently observed water bridges may be considered as fragments of pentagons. Water around hydrophobic surface tends to form a more organised structure than the bulk water, and in a typical collagen triple helix, proline and hydroxyproline rings are facing the solvent. In addition, collagen triple helices seem to provide good anchoring points to attack this hydrophobically enforced water structure to peptide molecule.

Prolyl hydroxylation introduces extra anchoring points and extra bridges, which participate to the water structure. The result is that the water that immediately surrounds the peptide becomes highly ordered by extensive hydrogen bonding. Therefore, as Hyp hydroxyl groups are the key

to structure the water network around the triple helices, this suggests that Hyp residues not only play a crucial role in the stabilisation of isolated triple helices, but also participate to the formation of macromolecular assemblies by inducing and supporting the waterbridged network present between triple helices (Bella et al. 1995).

1.3.5 - Collagen self-assembly: Enzymatic cross-links

Collagen forms long rod-like fibers assembled by a lateral association of these triple helical units into a "quarter staggered" alignment, so that each one is displayed longitudinally from its neighbour by slightly less than one-quarter of its length. The banded appearance of these fibers, characterised by a D period of 67 nm is recognisable by means of Scanning Electron Microscope Imaging. Collagen fibers are stabilised by the formation of covalent enzymatic cross-links, both within and between the triple helical units. The divalent products of this mature spontaneously form stable multivalent cross-links (Bailey et al. 1998; Murray et al. 2009).

Enzymatic cross-linking mechanism may be divided in two steps that give rise to immature and mature cross-links, respectively. The first mechanism is based upon aldehyde formation from the single telopeptide lysine or hydroxylysine residues. The enzyme is lysil oxidase, a copper-dependent enzyme, that acts only upon telopeptide residues. After this initial enzymatic step, the subsequent reactions of the aldehydes (allysine and hydroxyallysine) are spontaneous and ruled by post-translational modifications and structural organisation of the collagen molecules, in particular by the hydroxylation of lysine residues.

The lysine aldehydes (Allysine) condense with lysine or hydroxylisine residues to form reducible Schiff bases:

- dehydro – lysinonorleucine (DeH-LNL)
- dehydro-hydroxylisino-norleucine (DeH-HLNL)

These bases undergo an Amadori rearrangement to form Lysino-Norleucine (LNL) and HydroxyLysino-norleucine respectively that are classified as Aldimines. (Bailey – collagen review)

The hydroxylysine aldehydes (hydroxyallysine), instead, condense with lysine or hydroxylisine residues to form reducible Schiff bases that undergo an Amadori rearrangement to form:

- lisyne – 5 – ketonorleucine (**LKNL**)
- hydroxylisine – 5 – ketonorleucine (**HLKNL**)

These products are called Ketoimines.

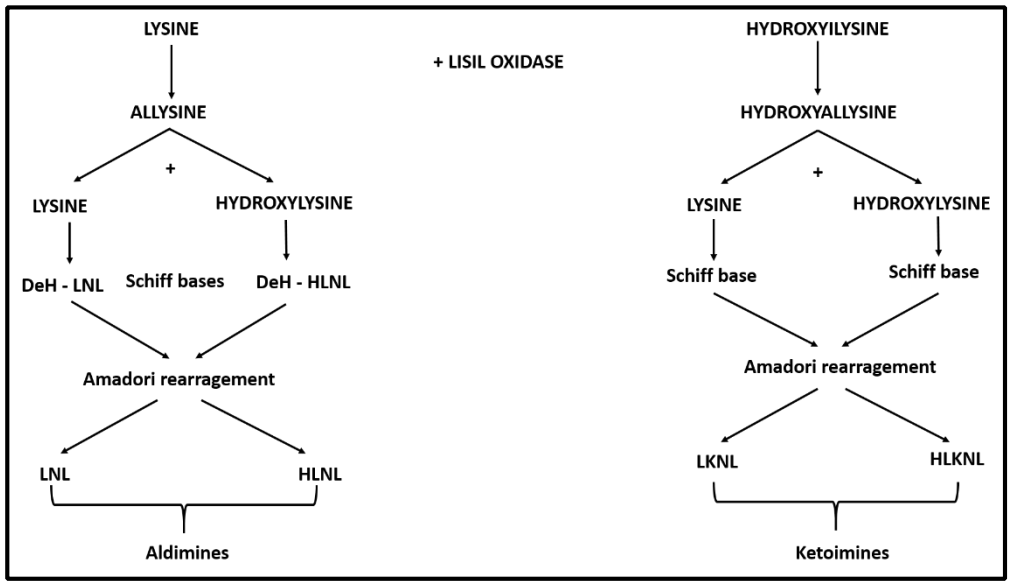

Figure 1.4 mechanism of immature cross-links formation

The second cross-linking step may form trifunctional cross-links which derive from the immature reducible ones. These mature cross-links are more stable, explaining the increase in both insolubility and strength of older collagenous tissues.

The Schiff base DeH-HLNL reacts spontaneously with histidine to form histidine-hydroxylysinonorleucine (HHL).

Ketoimines (LKNL and HLKNL) react with allysine and hydroxyallysine to form respectively:

- Lysil-Pyrrole (**L-Pyrrole**)
- Hydroxylysil-pyrrole (**HL-Pyrrole**)
- Lysil-pyrolidine (**L-Pyr**)
- Hydroxylisil-pyrolidine (**HL-Pyr**)

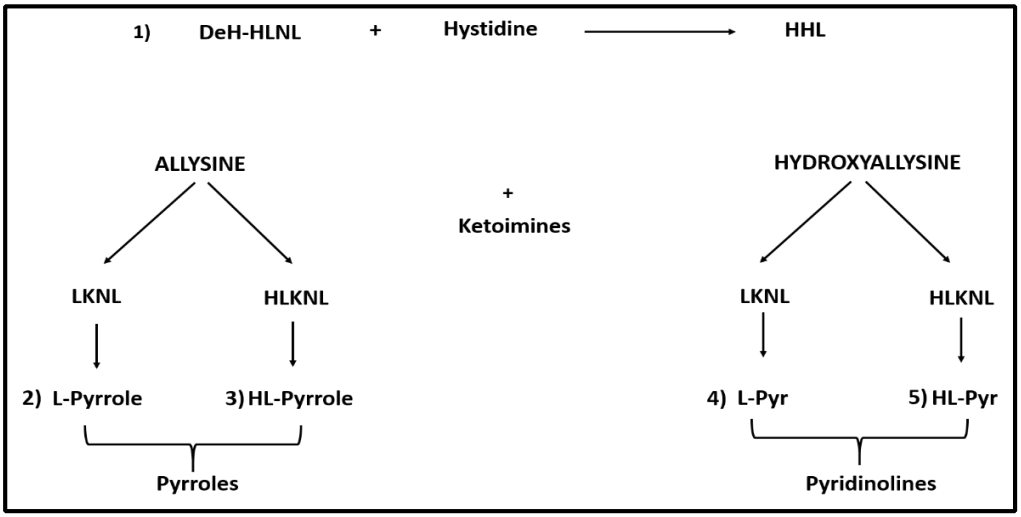

Figure 1.5: mechanism of mature cross-links formation

(a)

(b)

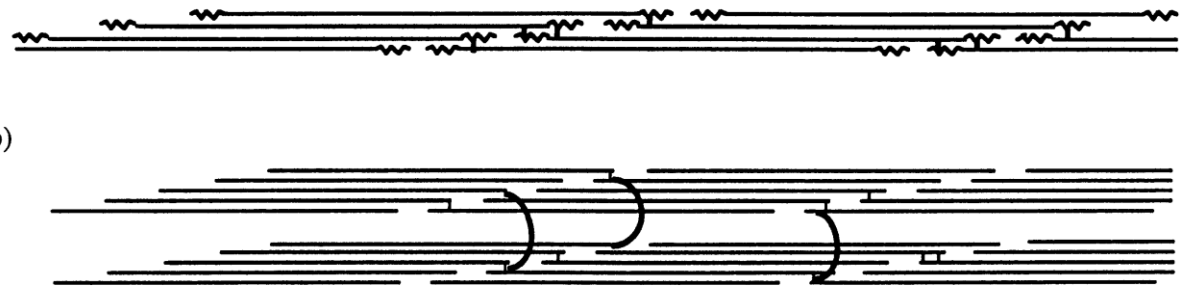

Figure 1.6: (a) Location of the divalent immature cross-links in collagen fibers aligned in the quarter-staggered arrangement. (b) Location of the trivalent mature cross-links, linking of the microfibrils.

The formation of immature and mature cross-links lead to the self-assembly and stabilisation of collagen molecules which aggregate among them to form very complex structures, through the formation of microfibrils, fibrils, fibers and bundles of fibers.

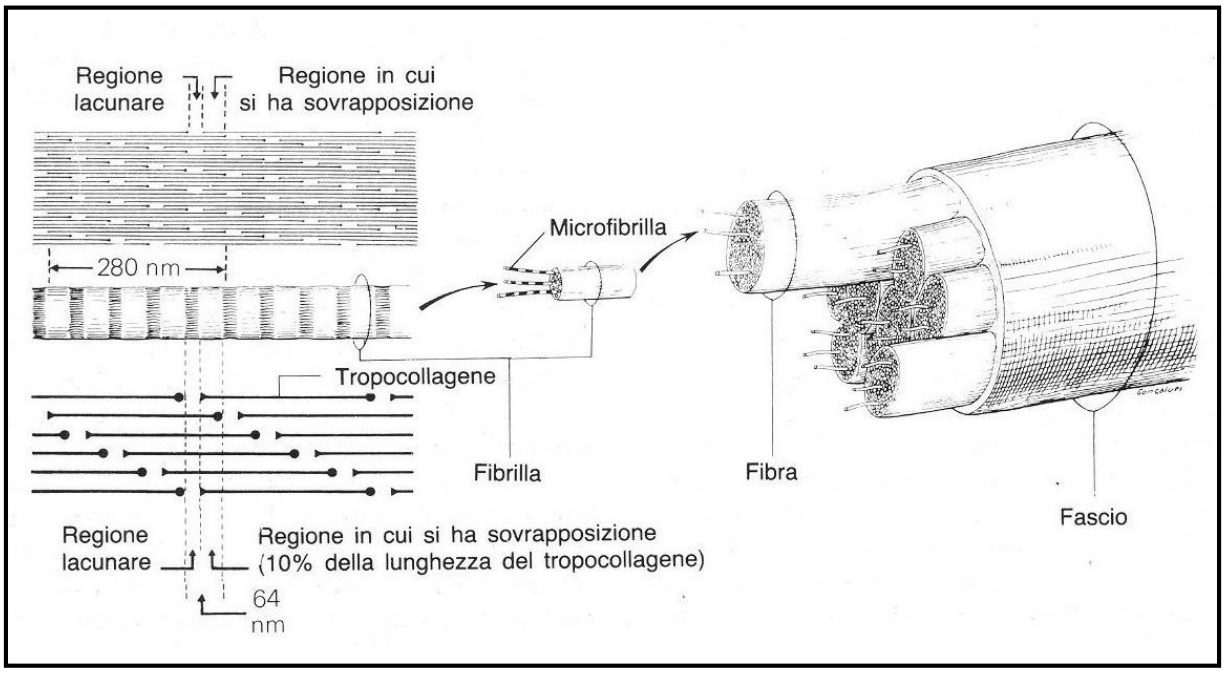

Figure 1.7: self-assembly of collagen molecules.

1.4 - Aging mechanisms

Even though the enzymatic cross-links stabilise the growing fibers and provide the optimal functional capacity of collagen, this mechanism represents the first stage of aging. The turnover of collagen is very rapid during growth and the fibers are stabilised by the divalent immature cross-links. Following maturity, these enzymatic cross-links do not increase, but as turnover slows down and the half-life of collagen increases there is an increase in the proportion of mature cross-links. In this stage, the predominant cross-links are the mature trivalent bonds that are maintained into old age (Bailey 2001).

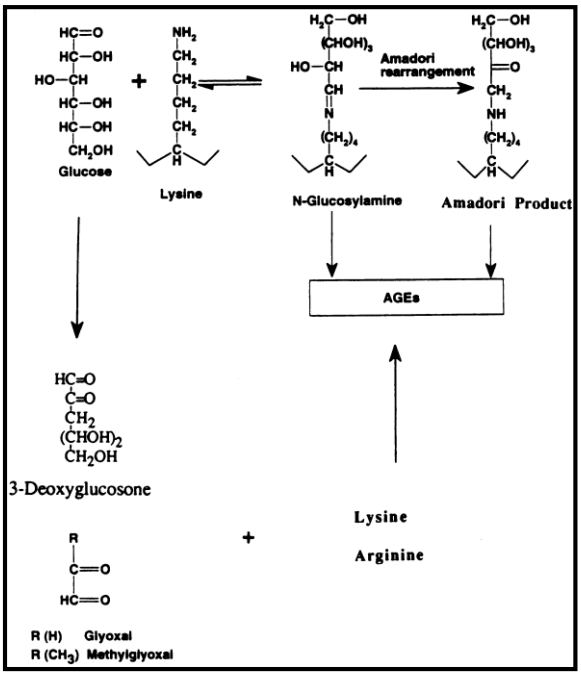

Figure 1.8 Formation of the Advanced Glycation End-products

Biological function of collagen depends primarily on its three-dimensional structure. The major modifications of the collagen structure, relating to the aging process, are mainly due to two factors: dehydration and a further increase of the intermolecular cross-links.

The loss of the shells composing the cylinder of water molecules of collagen cause a destabilisation of the protein structure (Allison et al. 1999). In the attempt to reach a structural stabilisation, collagen borrows hydroxyl groups reacting with the glucose composing the glycosaminoglycans of the extracellular matrix. This reaction lead to the accumulation of the products of Maillard reaction that give rise to non-enzymatic cross-link called Glycation(Bailey et al. 1998; Bailey 2001).

The initial reaction of glucose with collagen is with the ε-amino group of lysine to form a Schiff base, glucosyl–lysine which undergoes an Amadori rearrangement to fructose–lysine. Both these intermediate are susceptible to oxidation to deoxyglucosone and to fragmentation to smaller sugar aldehydes, such as methylglyoxal, which are many times more reactive than glucose although only present in small quantities.

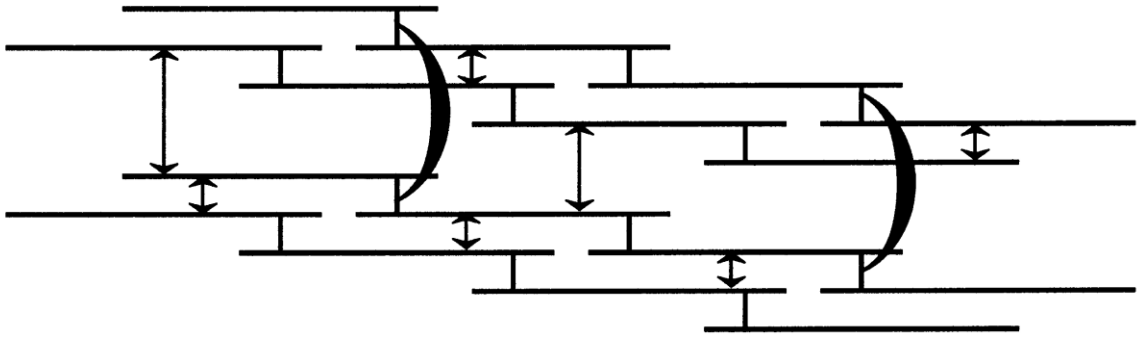

Figure 1.9: Glycation cross-links during aging of collagen fibers (indicated by arrows)

The subsequent oxidation of these initial glucose products, referred to as advanced glycation end-products (AGEs), results in the dysfunction of the collagenous tissues. AGEs in fact, form intermolecular crosslinks between the collagen molecules within the fibers.

The effect of dehydration(Shoulders and Raines 2009) and these cross-links on the fibers is to modify the physical properties of collagen, leading to an increase in stiffness and breaking load, denaturation temperature and a decrease of the solubility and in the susceptibility to degradative enzymes. Resistance to enzymatic degradation is due to two effects, blocking the enzyme sites, such as lysine and arginine, and to the closer packing of the molecules in fibers, due to cross-linking. Glycation of collagen is therefore a true ageing effect (Avery and Bailey 2006)

Chapter 2

Elements of Anatomy

2.1 - Skin Structure

The skin is a biological tissue that carries out several functions. It covers the underlying soft tissues, acting as a barrier against an inhospitable environment, by preventing pathogens from entering, and by avoiding infections. It also regulates the body temperature and the amount of water absorbed and released from the body through sweat glands and the wide capillary network. It acts as a sensory system, because it has cutaneous mechanoreceptors, nociceptors (pain) and thermoreceptors (temperature). In closing, it synthesises vitamin D3 through the action of the ultraviolet solar radiation. Skin is composed by several layers, which can be divided mainly into epidermidis, dermis and hypoderm (Leslie et al. 2009).

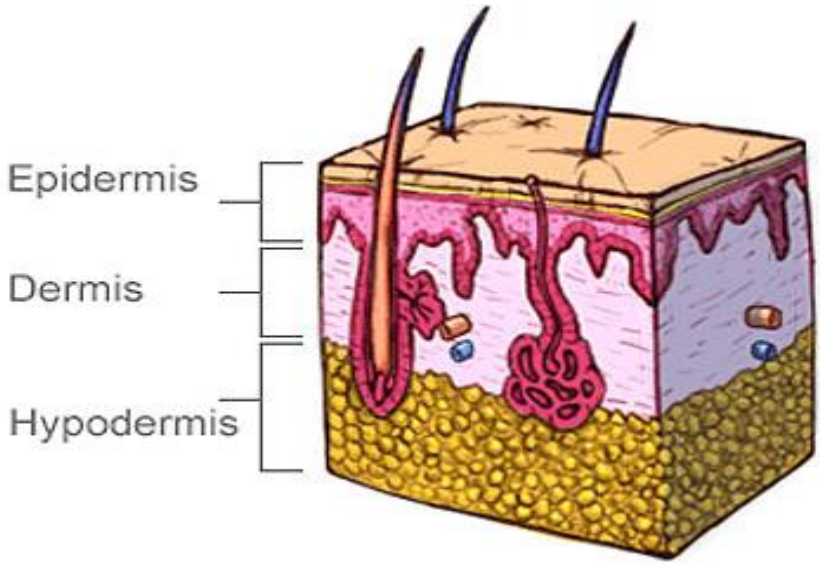

Figure 2.1: Skin structure

2.1.1 - Epidermis

Epidermis is a keratinized stratified squamous epithelium that arises from the ectoderm. It does not show blood vessels and is nourished exclusively by diffused oxygen from the surrounding air. It is composed for the 95% by keratinocytes but also contains melanocytes, Langerhans cells, Merkel cells and inflammatory cells.

The epidermis is composed by five layers, (figure 6.2) which differ among them for their level of keratinization. It increases from the inner to the outer layer. From the outer face of the skin to the inner one, those layers are:

1. **Cornified layer** - stratum corneum: it is composed of 10 to 30 layers of polyhedral, anucleated corneocytes (final step of keratinocyte differentiation). Corneocytes are surrounded, in the extracellular space, by stacked layers of lipids.

2. **Clear / translucent layer** (Stratum lucidum): it is found only in the palms and soles.
3. **Granular layer** (Stratum granulosum): in this layer, keratinocytes lose their nuclei. Lipids contained within them are released into the extracellular space, to form a lipid barrier. Those polar lipids are then converted into non-polar lipids and arranged parallel to the cells surface. Some examples are glycosphingolipid that convert into ceramides and phospholipids that become free fatty acids.
4. **Spinous layer** (Stratum spinosum): in this layer keratinocytes are connected through desmosomes and they start to produce lamellar bodies rich in different kinds of lipids. Langerhans cell are located in the middle of this layer.
5. **Basal/germinal layer** (stratum basale or germinativum): it is composed mainly of proliferating keratinocytes attached to the basement membrane by hemidesmosomes. Merkel cells are observed.

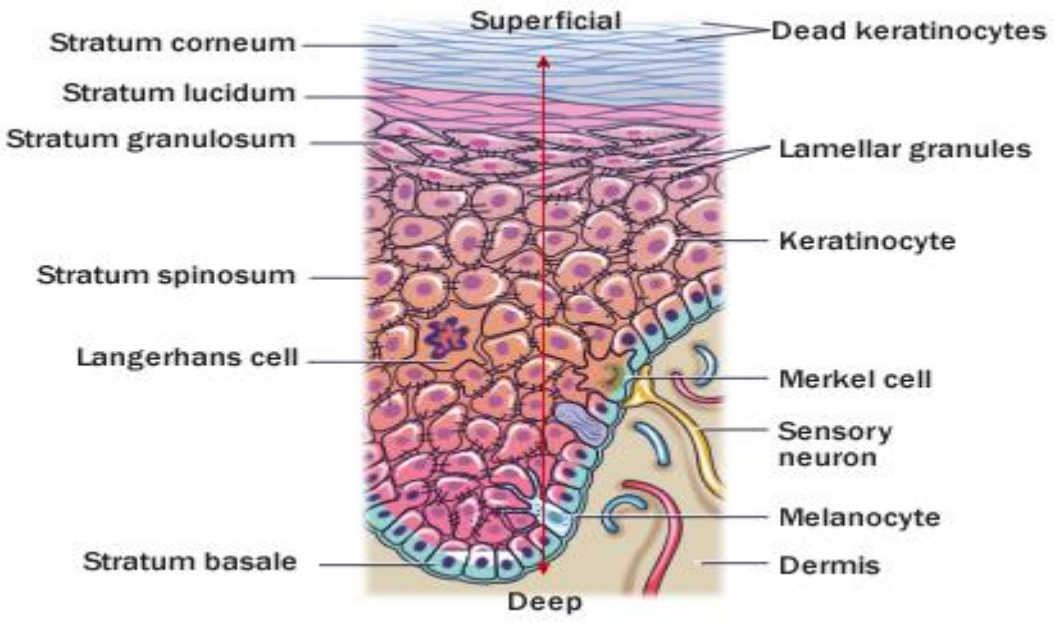

Figure 2.2: Structure of Epidermis

2.1.2 - Dermis

The dermis arises from the mesoderm and its thickness can vary from 0,6 mm in the eyelids to 3 mm in the palms and feet soles. It consists of connective tissue that can resist to strong tensile strength. It is divided into two layers, a superficial area called the papillary region and a deep thicker area known as reticular dermis.

The papillary region shows an irregular aspect and intertwines with the epidermis, forming the dermal papillae which greatly increase the surface area between the dermis and epidermis.

This layer is composed by aereolar connective tissue, containing type I collagen fibres and elastic fibres, forming a wide mesh fishnet. Anchoring collagen fibres run from the basal laminae to papillary layers, connecting epidermis and dermis. It contains several kind of cells typically present in the connective tissues as fibroblasts, macrophages and mastocytes. Moreover, it is rich in terminal networks of blood capillaries and some mechanoreceptors as Meissner's corpuscles and end-bulbs of Krause, respectively detecting tactile and cold stimulations.

The reticular layer is composed by dense irregular connective tissue characterised by big bundles of fibers of type I collagen. A large amount of sweat and sebaceous glands and hair follicles are visible.

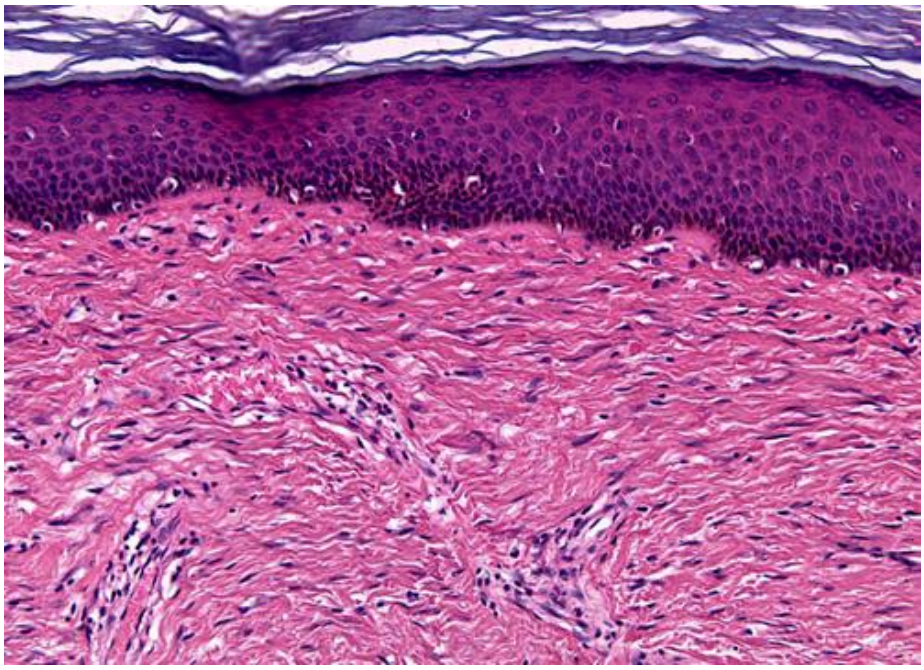

Figure 2.3: Hystological section of the skin. Dermis (lower layer) shows big bundles of collagen fibers (pink stained).

Others types of mechanoreceptors, Pacinian and Ruffinian corpuscles are sensible for vibration, pressure and tensile strength (Leslie et al. 2009).

Thus, the dermis layer is characterised by the presence of the extracellular matrix. It determines the physical properties of the connective tissue it belongs to. The matrix is composed of a variety of proteins and polysaccharides that are locally secreted and assembled into an organised meshwork in close association with the surface of the cell that produced them. The two main classes composing the matrix are (1) polysaccharides chain of the class, called glycosaminoglycans (GAGs) which are covalently linked to protein, as proteoglycans and (2) fibrous proteins of two functional types: mainly structural, collagen and elastin, and mainly adhesive, fibronectin and laminin.

Glycosaminoglycan and proteoglycan molecules in connective tissue form a highly hydrated, gel –like "ground substance", in which the fibrous proteins are embedded. The polysaccharide gel resists compressive forces on the matrix, while collagen fibers provide tensile strength. The aqueous phase of the polysaccharides gel facilitates the rapid diffusion of the nutrients, metabolites, and hormones from blood into tissue cells, while collagen fibers both strengthen and help to organise the matrix, and rubberlike elastin fibers provide resilience. Fibronectin promotes the interaction of the fibroblasts and other cells to the matrix in connective tissue, while laminin promotes the adhesion f epithelial cells to the basal lamina.

Glycosaminoglycans are unbranched polysaccharide chains composed of repeating disaccharide units. They are called GAGs, because one of the two sugar residues in the repeating disaccharides is always an amino sugar (N-acetylglucosamine or N-acetylgalactosamine), which in most cases is sulphated. The second sugar is usually an uronic acid (glucuronic or iduronic). GAGs are highly negatively charged. Four main groups of GAGs may be distinguished by their sugar residues, the bond type between these residues, and by the number and position of sulphate groups:

1. hyaluronan
2. chondroitin sulfate and dermatan sulfate
3. heparin sulphate and heparine
4. keratan sulphate.

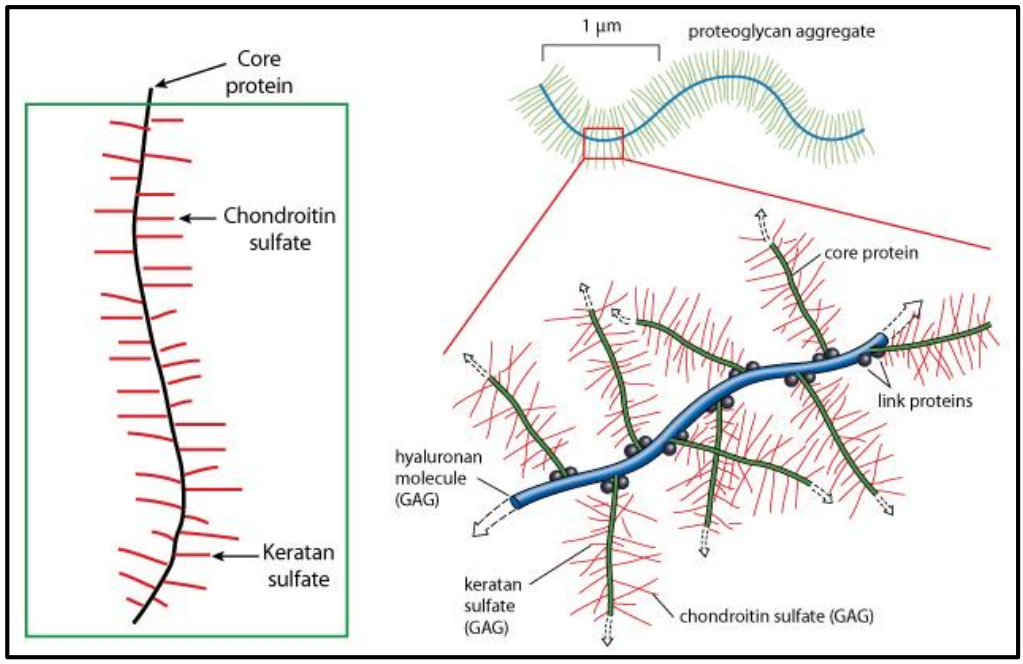

Figure 2.4: Structure of a proteoglycan aggregate

GAGs tend to adopt highly extended conformations which occupy a huge volume relative to their mass and they form a gel even at very low concentrations. The high density of negative charge attracts a cloud of cations, such as Na^+, that are osmotically active, causing large amounts of water to be sucked into the matrix. This creates a matrix swelling, that enables the matrix to withstand compressive forces (in contrast to collagen fibrils, which resist stretching forces).

The amount of GAGs in connective tissue is usually less than 10% by weight of the amount of the fibrous proteins. Since they form porous hydrated gels, the GAGs chains fill most of the extracellular space, providing mechanical support to the tissue, allowing the fast diffusion of water-soluble molecules and the migration of the cells.

2.1.3 - Hypodermis

Hypodermis is composed of adipocytes, which are assembled in lobules separated by connective tissue. The number of adipocytes varies among different areas of the body, while their size varies according to the body's nutritional state (Alberts 2001).

2.2 - Bones

Bones are composed of an organic component, represented by collagen with small amounts of proteinpolysaccharides, glycoaminoglycans (formerly known as mucopolysaccharides), such as hyaluronic acid and chondroitin sulfate, chemically bound to protein and dispersed within and around the collagen fibres, and an inorganic mineral component, in the form of rod-shaped crystals. These crystals are parallel with the long axes of collagen bundles and many actually lie in the empty space within the bundles.

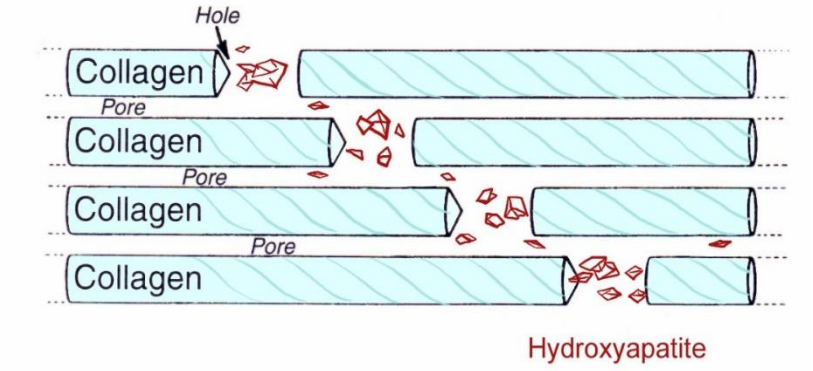

Figure 2.5: Hydroxyapatite crystals fill the empty spaces between collagen fibers

Organic material comprises 50% of the volume and 30% of the dry weight of the intercellular composite, with minerals making up the remainder. The inorganic composition of bone (bone mineral) is primarily formed from salts of calcium and phosphate, the major salt being hydroxyapatite ($Ca_{10}(PO_4)_6(OH)_2$). The exact composition of the matrix may change over time and with nutrition, with the ratio of calcium to phosphate varying between 1.3-2 (per weight), and traces of other minerals, such as magnesium, sodium, potassium. Carbonate is also present - in amounts around 8% in most mammals - and occurs in two distinct phases, calcium carbonate and carbonate apatite.

The mineral crystals are responsible for hardness, rigidity, and for the great compressive strength of bone. On the other hand, the collagen fibrils of bone possess high elasticity, little compressive strength, and considerable tensile strength. Thus, the tensile strength of bone depends not on collagen alone, but on the intimate association of mineral with collagen. A variation in the mineral-collagen ratio leads to changes in physical properties: less mineral amount tends to greater flexibility while more mineral quantity to increased brittleness. Optimal ratios, as reflected in maximal tensile strength, are observed at a mineral content of approximately 66%, characteristic of the weight-bearing bones of mammals.

Bone tissue is a type of dense connective tissue. It is organised into a variety of shapes and configurations adapted to the function of each bone. Bones have an exterior layer called cortex that is smooth, compact, continuous, and of varying thickness. In its interior, bony tissue is arranged in a network of intersecting plates and spicules called trabeculae, which vary of amount in different bones and enclose spaces filled with blood vessels and marrow. This honeycombed bone is termed cancellous or trabecular.

Microscopically, bones consist of hard, apparently homogeneous intercellular material, within or upon which may be found four main characteristic cell types: osteoblasts, osteocytes, osteoclasts.

Osteoblasts are responsible for the synthesis and deposition on bones surface of the protein matrix of new intercellular material.

Osteocytes are osteoblasts which have been trapped within intercellular material, residing in a cavity (lacuna) and communicating with other osteocytes as well as with free bone surfaces, by means of filamentous protoplasmic extensions which occupy long, meandering channels (canaliculi) through the bone substance.

Osteoclasts are usually large multinucleated cells that, located on the bone surface, which are responsible for bone resorption by direct chemical and enzymatic attack.

Depending on how the protein fibrils and osteocytes of bone are arranged, two types of bone can be identified:

1. woven, in which collagen bundles and the long axes of the osteocytes are randomly oriented,
2. lamellar, in which both the fibrils and osteocytes has a regular alignment in clear layers.

Woven bone is produced when osteoblasts produce osteoid rapidly, which occurs initially in all fetal bones. Woven bone is weaker, with a smaller number of randomly oriented collagen fibers, but forms quickly. It is soon replaced by lamellar bone, which is highly organised into units known as osteons, which consist of concentric cylindrical lamellar elements several millimetres long and 0.2–0.3 mm in diameter.

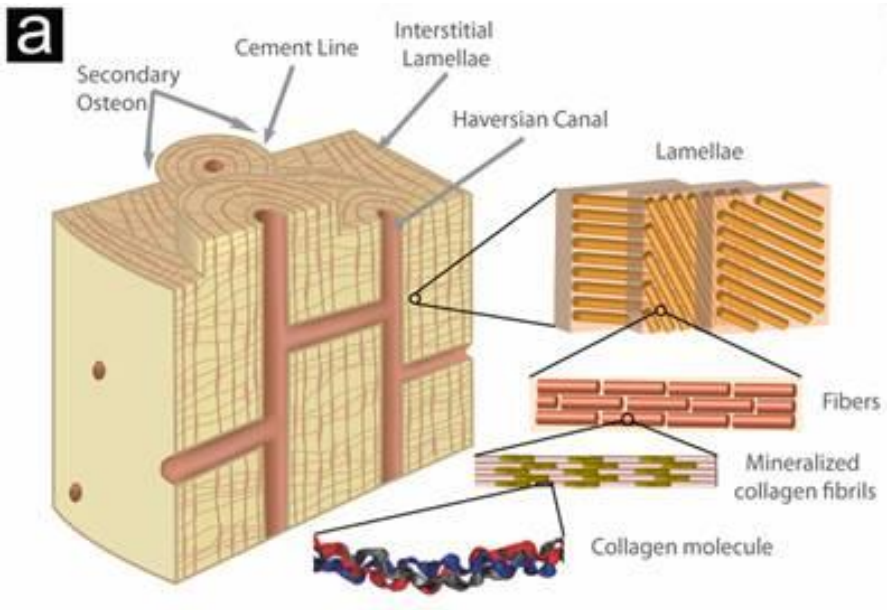

Figure 2.6: Cancellous bone structure

These cylinders comprise the haversian systems. Osteons exhibit a gently spiral course oriented along the axis of the bone. In their centre there is a canal (haversian canal) containing one or more small blood vessels, and at their outer margins there is a boundary layer known as a "cement line," which serves both, as a mean of fixation for new bone deposited on an old surface and as a diffusion barrier. Osteocyte processes do not penetrate the cement line, and therefore these barriers constitute the outer envelope of a nutritional unit; osteocytes on the opposite sides of a cement line derive their nutrition from different vascular channels. Cement lines are found in all types of bone, as well as in osteons, and in general they indicate lines where new bone was deposited on an old surface.

The biochemical and physical sequence of events that prepare matrix for mineralization includes many phases.

First of all, intracellular biosynthesis of collagen by osteoblasts, extrusion of collagen in the extracellular matrix in soluble form, maturation or polymerization of collagen into an array of fibrils (in random orientation in rapidly deposited bone, in a highly ordered regular pattern in slowly formed lamellar bone), binding of calcium to collagen fibrils, and formation of protein-glycoaminoglycan complexes.

Mineralization itself depends upon establishment of crystal nuclei within the matrix. A suitable nucleating configuration is somehow established, and, once nuclei reach a critical size, further mineralization proceeds spontaneously in the presence of usual body fluid calcium and phosphorus concentrations (Steele and Bramblett 1988; Hall and Guyton 2005; Curry 2006).

Chapter 3

Materials

3.1 - Reference samples

In order to perform in vitro experiments, two samples of type I collagen from rat tail were used. The first one was of pure and native type I collagen purchased from SIGMA-ALDRICH Co. It was used as a standard reference without any further purification.
The second one was extracted from rat tails provided by the laboratories of Cardiac Physiology, Area of Animal and Plant Biology, Department of Life Sciences of the University of Parma.
Modern samples of untreated human skin (finger of the author) and animal bone (*bos taurus* tibia) were used as standard references for the archaeological samples.

3.2 - Archaeological samples

As clearly summarized by Samadelli and coworkers, anthropologically, mummies can be distinguished in three types: spontaneous (or natural) mummies, anthropogenic (or artificial) ones and mummies caused by favourable spontaneous processes (or spontaneously enhanced processes).
Spontaneous mummies are produced as a consequence of natural events and they can be classified as "eco-facts", that means that they have not been subjected to any intervention by man. Famous examples of this category are the glacier mummies, such as the Iceman, stored in the South Tyrol Museum of Archaeology in Bolzano, Italy. It naturally mummified, after the death on the top of a mountain, at an altitude of 3200 m, in some very cold and windy conditions.
Anthropogenic mummies were produced by man action. Almost 95% of the best known mummies belong to this category, such as all Egyptian dynastic mummies.
Mummies obtained by favourable spontaneous processes, are represented by corpses which gained mummification as a result of favourable environmental conditions. Egyptian pre-dynastic mummies, South American pre-Columbian mummies, and many bog mummies belong to this category (Samadelli et al. 2013).
The mummified skin samples analysed in the present thesis work belong to two collections. Fragments of skin were taken from some mummies stored in the Museum of Anthropology and Ethnography "Giovanni Marro" of the University of Turin. From several mummified remains recovered from the crypt of the Church of the Conversion of St Paul of Roccapelago, Italy samples of skin and bones were collected.

3.2.1 - The Marro Museum Collection

The Museum of Anthropology and Etnography of the University of Turin was created in 1926, when Prof. Giovanni Marro (1875-1952), doctor, psychiatrist and anthropologist, was appointed as professor of Anthropology at the University of Turin.

In 1911, he was called by the Egyptologist Ernesto Schiaparelli to take part to M.A.I., the Archaeological Italian Mission in Egypt established in 1903, by King Vittorio Emanuele III. Marro worked with Schiaparelli until his death in 1928, then he continued to work with M.A.I., supporting the new director of the Egyptian Museum of Turin, Giulio Farina until 1937.

All the findings he collected during the six digging campaigns constitute the Collection of the Museum. It is divided into four sections: Primatology, Anthropology, Paleoethnology and Ethnography. The Anthropological collection includes more than 650 complete skeletons and 1300 isolated skulls. 59 skeletons belong to the Neolithic period. Besides the osteological remains, the collection includes 80 mummies skulls, 5 complete pre-dynastic mummies and 15 dynastic ones. All the mummies come from the dynastic necropolis of Assiut and pre-dynastic and dynastic necropolis of Gebelein. Assiut, the ancient city of Lycopolis, is located 380 km south from Cairo, was excavated from 1907 to 1913. Gebelein is located 28 km from Luxor and was excavated from 1930 to 1937.

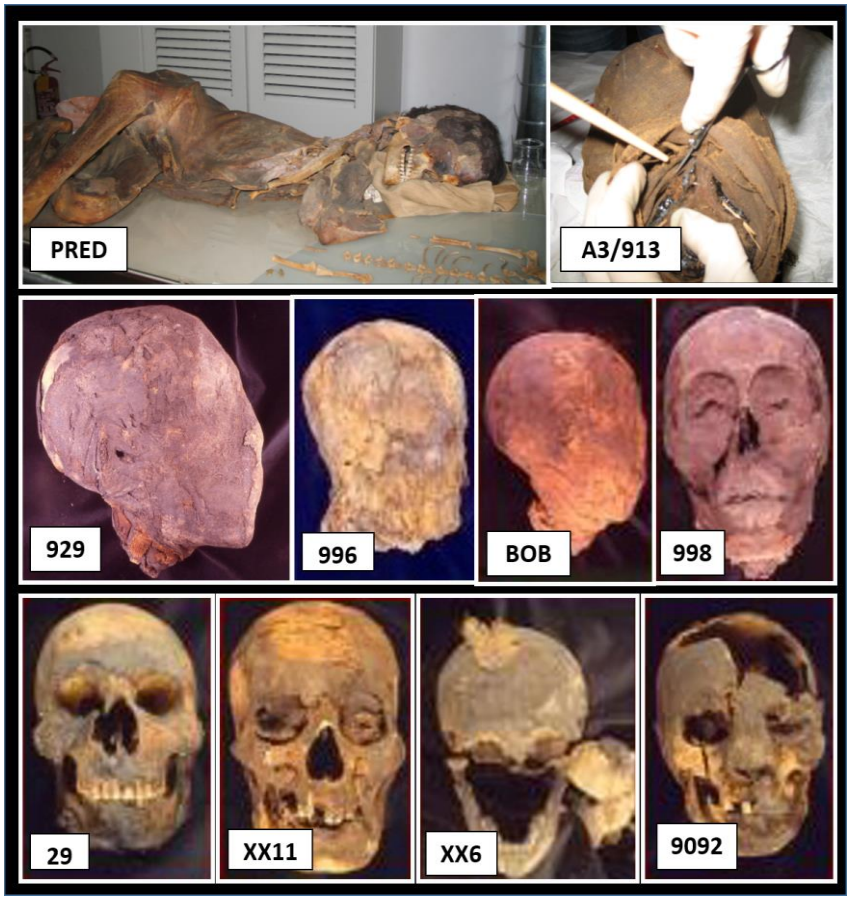

Figure 3.110: Mummified remains from the Museum Marro Collection

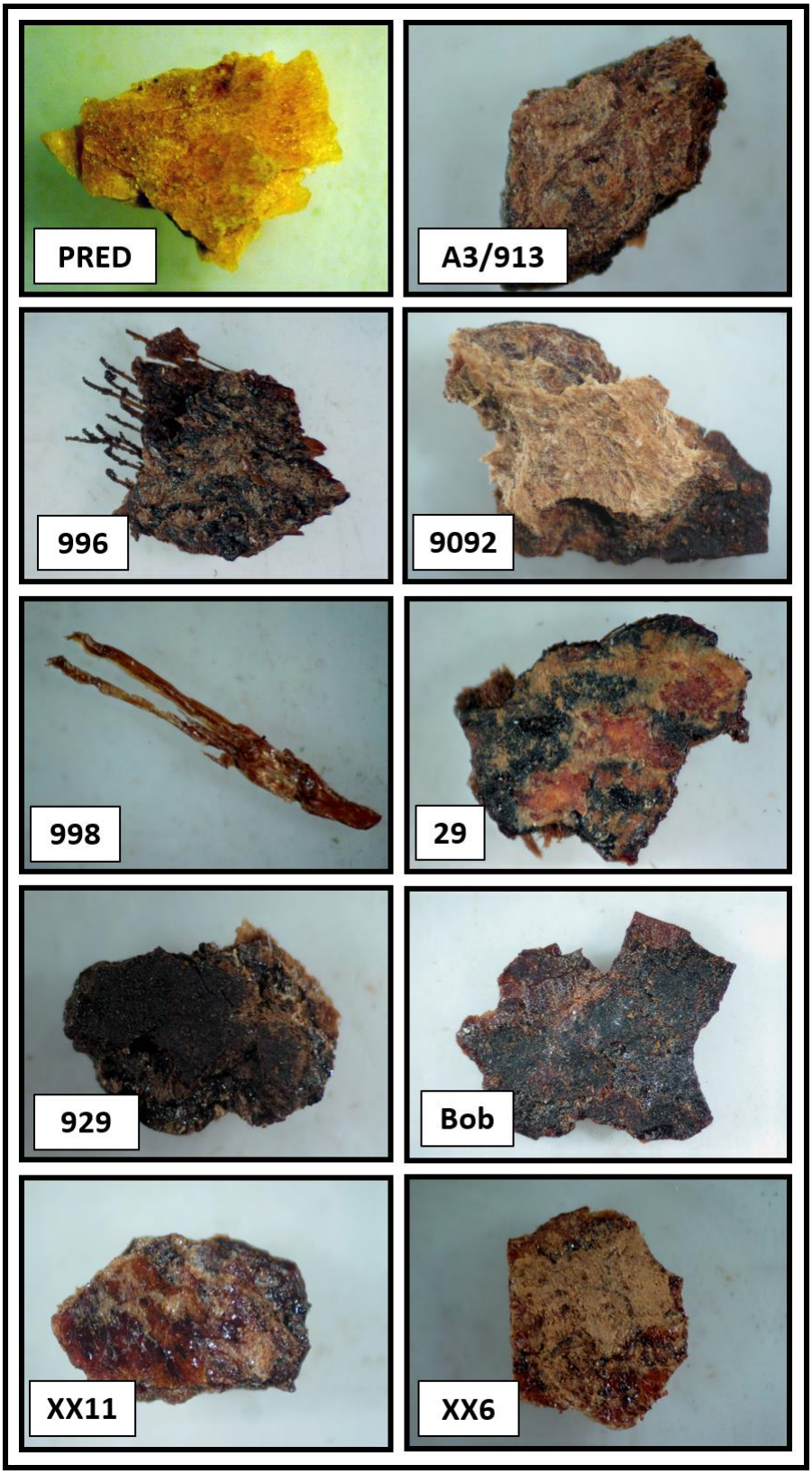

Figure 3.211: Mummified skin samples phographed by means of a optic microscope equipped with cam

The Egyptian mummies studied in this work are a pre-dynastic mummy and 10 dynastic mummy skulls. The archaeological data about the collection are missing, fragmented and not sufficiently precise. The poor information about the collection is available just from Marro's excavation diaries. When the remains were collected, in fact, a systematic method to catalogue the findings was not still set in the archaeological practice.

The pre-dynastic mummy (PRED, figure 3.1) was probably found in the pre-dynastic necropolis of Gebelein. A dating by Radiocarbon was estimated by Zink and Samadelli at 3630-3383 BC.

The ten skulls are classified by letters and numbers as A3/913, 929, 996, BOB, 998, 29, XX11, XX6 and 9092.

They were not dated by radiocarbon, but anthropologically and by relating the skulls to the period of use of the necropolis where they were found, and they have been dated between VI and XI dynasty (2500-2000 BC).

Very small pieces of skin were sampled from every mummy, trying to take them from hidden points, in order to avoid an excessive damage of the remains. The samples were photographed by an optic microscope equipped with a cam. Every sample area is around 2-3 mm^2.

3.2.2 - The mummified remains from Roccapelago

Roccapelago of Pievepelago is a small village at 1095 mt a.s.l, surrounded by the Apennines Mountains in the province of Modena. The church of the Conversion of St Paul (figure 3.3) was built in the 15th century on the top of an hill, where there was an abandoned castle. A chamber that had been used as a cannon enclosure became the church crypt, and between 16th and 18th century it was the common tomb for some of the 281 inhabitants of the small town. People of all ages and all stations in life were deposited in the crypt that, as reached its capacity after several centuries, was sealed and forgotten.

Figure 3.3: Church of the Conversion of St Paul

During the restoration of the church, in 2010, the forgotten room under the floor of the church was rediscovered. Archaeological excavations of the crypt were performed between 2010 and 2011. After the removal of the detrital layers (Stratigraphic Units 22 and 24), a striking pile of human remains was discovered (Stratigraphic Unit 23). During the digging, the big amount of remains was disassembled, one body after the other, collecting each body in a enumerated sack. Studying the arrangement of the bodies and the room structure, an hypothesis on the use of the crypt was made. Initially, the bodies were brought into the crypt by a stair running from the floor of the church nave, later they were lowered in the crypt from a trapdoor in the floor of the church. Unexpectedly, some of the bodies were completely, or partially mummified.

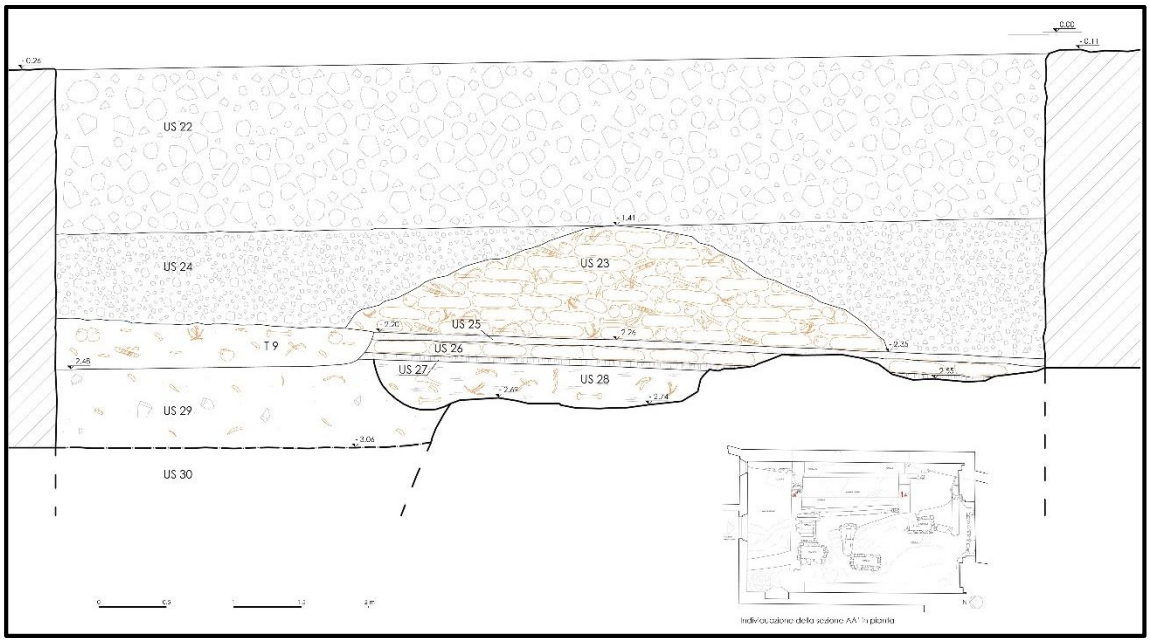

Figure 3.4: Archaeological section of the crypt reconstructed. Stratigraphic units are visible. Scale 1:20

The unusual microclimate of crypt of Roccapelago, probably due to the dry and cold temperatures, and the good ventilation of the room allowed by the small windows in the wall in east side of the crypt, resulted in a process of natural mummification, so that around 60 bodies were perfectly preserved. Much of their clothing was intact and the corpses were still clutching religious artefacts, or the tools of their trade in life.

Figure 3.5: Stratigraphic Unit 23

Figure 3.6: The small window in the east side of the crypt. Cimone Mountain on the background.

After *rigor mortis*, a very fast dehydration of the bodies fixed them in particular depositional positions. Some corpses still show the joined hands in the act of praying, or the hands laying down on the abdomen. Cases of wrists and ankles tied by laces or bandaging around the chin are very frequent, in order to avoid the disassembling of the body or the spreading out of the mouth.

Figure 3.7: Some of the Roccapelago mummified remains

Actually, after the cleaning, the consolidation and the restoration of the corpses, the most well preserved bodies were reallocated in the crypt that is visible from the glass floor of the church.

Figure 3.8: Museum exhibition. The mummies are visible from the glass floor of the church.

The skin samples analysed were collected in particular from the mummified bodies contained in the sacks n° 17, 57 and 86. The samples are covered by dust and the soil of the upper detrital layers. The skin specimens show a very hard consistence, stiffness and rigidity. The epidermal layers and big bundles of fibres are still visible at the naked eye.

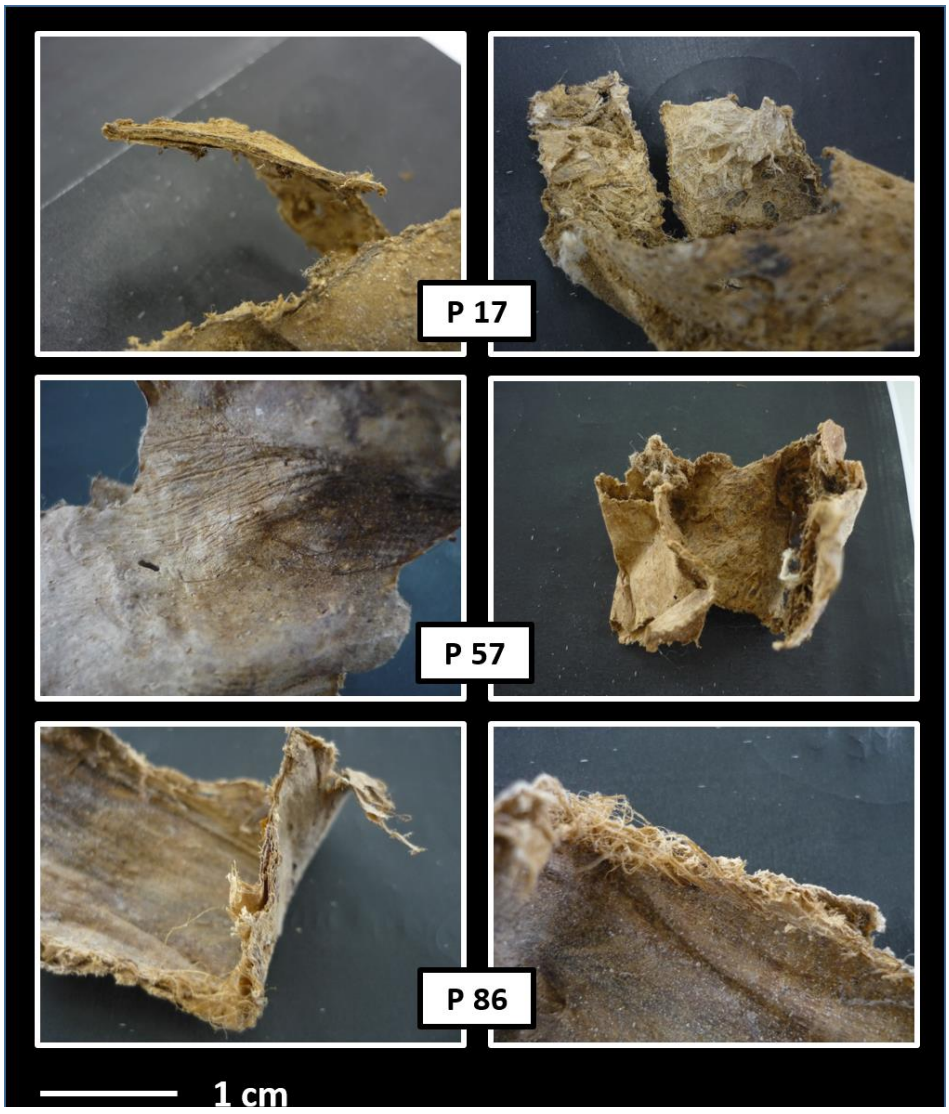

Figure 3.9: Mummified skin samples from Roccapelago

3.2.3 - Fossilised bones

Figure 3.10: Fossilised bone samples

Some samples of fossilised animal bones, with different dating, were analysed. The animal bones are:

- Sample **473/11**: metacarpus of *ovis aries* comes from Central Anatolia and it dates back to V millennium BC.
- Sample **92/9**: femur of *sus domesticus* comes from Central Anatolia and it dates back to between 3000 and 2800 BC.
- Sample **Ciuss**: it is a fragment of bone of unidentified animal species coming from Friuli, Italy and it dates back to the medieval period, between VI and VII century AD.

Chapter 4

Protocols and analytical techniques

4.1 - In vitro Procedures

4.1.1 - Dehydration and re-hydration of rat tail type I collagen

The rat tail type I collagen purchased from SIGMA-ALDRICH was used without any further purification. Aqueous and acid acetic 33 mM solution was prepared, deposited on a CaF_2 window and dried under ambient conditions.

The collagen film smeared of the IR-trasparent window was assembled in a home-built sample holder, equipped with a vessel, containing saturated salt hydrating solution, to avoid any contact of the sample with the external atmosphere and to adjust the desirable inner relative humidity. Different hydration degrees of the samples were obtained, by equilibrating the collagen film for 24 hours, directly in the inner ambient of the box. The CaF_2 window was assembled in the holder, over the vessel containing the suitable hydrating saturated salt solutions and finally inserted, all together, into the box.

Salt	a_w
KNO3	0.92
$BaCl_2$	0.90
KCl	0.84
NH4Cl	0.79
NaNO3	0.74
KI	0.69
Ca(NO)3	0.51
NaI	0.38
CaCl2	0.29
LiCl	0.11
KOH	0.09

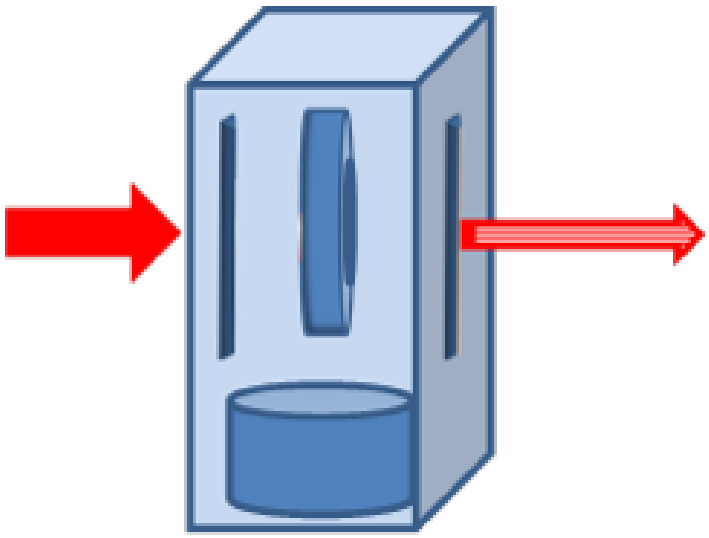

Figure 4.1: Sample holder for equilibrating of the collagen film at controlled activities a_w

In this way, the relative humidity was made to vary in the range 0.92 - 0.09% (desorption run) and backwards 0.09 - 92% (adsorption run). Table 1 lists the activities a_w provided in the desiccator by each salt solution and the salts employed. The sample prepared was vertically positioned in the box, that was placed in the FTIR spectrophotometer, to analyse the sample in transmission mode (§ 4.3.1.).

Table 4.2: Saturated salt solutions employed to obtain the controlled activities a_w (expressed as a fraction) in the box where collagen films was equilibrated before FTIR measurements

4.1.2 - Extraction of collagen from rat tail

In order to perform the extraction of collagen, the tail was washed in distilled water. The skin was removed and the tendons were exposed. The long white collagen fibers were detached from the vertebra and washed in ethanol 70% for 2 hours. The fibers were cut in small pieces (around 5 mm) and stirred in acetic acid 0.5 M for 48 hours at 4 °C. Collagen solution was centrifuged at 4000 rpm for 1 hour. The supernatant was separated and dialysed against distilled water for 3 hours, then frozen and lyophilised.

The lyophilised collagen was analysed by FT-IR spectroscopy in transmission mode (see paragraph…) and compared with rat tail collagen from SIGMA-ALDRICH.

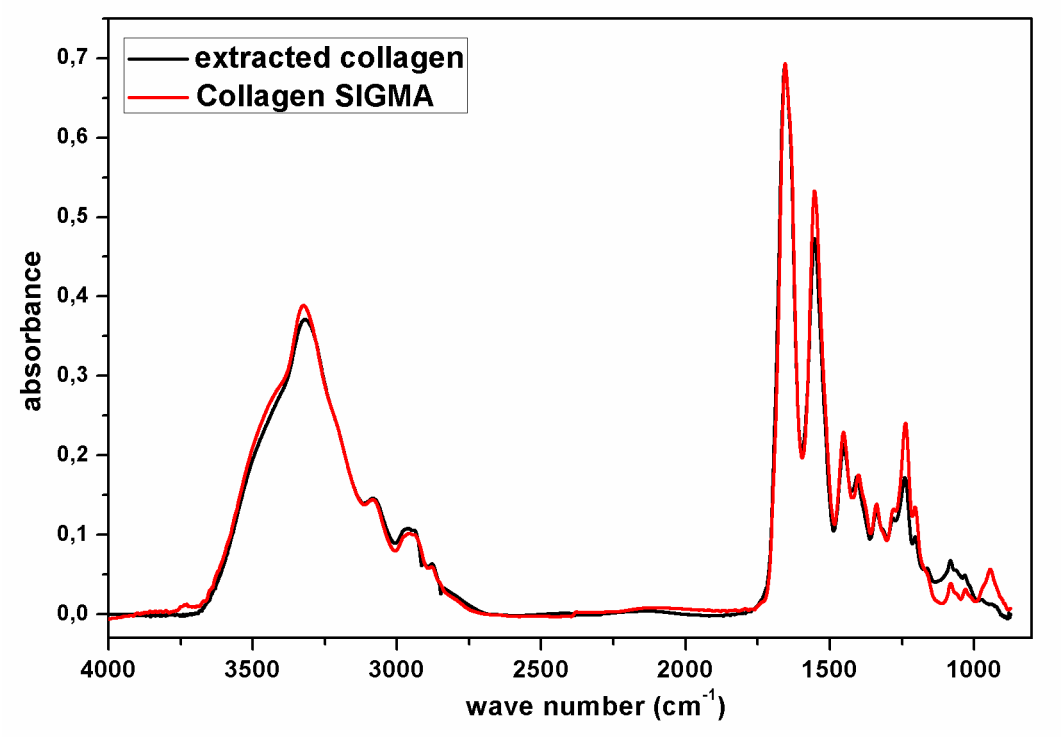

Figure 4.2: FTIR absorption spectra of the extracted collagen compared with collagen from SIGMA-Aldrich

As shown in figure 4.1, the spectrum of the collagen extracted in our laboratories did not show significant differences with of the collagen from SIGMA used as reference.

4.1.3 - In vitro glycation of type I collagen from rat tail with Glucose and Ribose.

The extracted collagen was subjected to the in vitro procedure of complexation with two different sugars, glucose and ribose.

It was dissolved in acetic acid 33mM and incubated at different time intervals (3, 5, 10 and 15 days) at 37° C with Glucose and Ribose (SIGMA-ALDRICH) at the concentration of both 5 and 50 mM each. A small quantity of sodium azide was added as biocide to inhibit bacterial

growth. The samples were dialysed against distilled water for 24 hours with three changes of the bath at the end of every temporal step, then frozen and lyophilised.
The samples obtained were submitted to FT-IR analysis and Circular Dicroism spectroscopy to monitor thermal denaturation kinetics. (§ 4.3.1. and 4.3.3)

4.2 - Archaeological samples preparations

All the archaeological samples were initially analysed by FT-IR spectroscopy prepared in different ways (§ 4.3.1).
Ancient collagen was extracted from some of specimens, skin or bone , and compared with the corresponding modern samples. The ancient tissues were morphologically studied and analyzed by means of Scanning Electron Microscopy and Histological Analysis.

4.2.1 - Low temperature collagen extraction from bone and skin

Bone

A first procedure of bones washing was done by immersing the samples in acetone for 24 hours. The bone were then mechanically cleaned with a scalpel to remove meat or tendon residues. The samples were frozen in liquid nitrogen and then reduced in small pieces grinding them in a mortar. The fragments were decalcified by HCl (0.5 N) treatment for 24 hours. The treatment was repeated 2 times and the organic fraction was separated from the inorganic one by centrifugation (4000 rpm for 30 minutes). The pellet was washed in acetic acid 0.5 M, centrifuged and suspended in acetone for 24 hours. The residue was then suspended again in acetic acid 0.5 M for 4 hours and centrifuged (10000 rpm for 5 minutes), frozen in liquid nitrogen and grinded in a mortar. This treatment was repeated three times. Finally the pellet, washed with acetic acid 33 mM, was centrifuged (10000 rpm for 5 minutes), frozen and lyophilised.

Skin

A similar protocol to extract collagen from the bone was used.
The skin was cleaned in acetone for 24 hours, then cut in small pieces by a knife, washed in acetic acid 0.5 M and suspended in acetone for 24 hours. Thereafter it was centrifuged and suspended in HCl 0.5 N for 24 hours in order to eliminate all the residues of inorganic materials deriving from the burial environment.

The HCl was eliminated and the sample was three times washed in acetic acid 33mM, then frozen in liquid nitrogen and grinded in the mortar. The powder was suspended in acetic acid 33 mM, centrifuged and the pellet was frozen and lyophilised.

4.2.2 – Histological sample preparation

Fragment of mummified skin underwent several treatments to prepare tissues for the inspection. Samples were rehydrated in distilled water and then fixed by a paraformaldehyde (2%)/glutaraldehyde (2.5%) fixative solution at 4°C for 12 h. Then they were dehydrated with grading series of ethanol and subjected to diaphonization with toluene. Then, they were immersed two times for several hours in paraffin, to obtain the total toluene elimination and paraffin infiltration and finally embedded in paraffin, until a complete wax hardening occurred. Sections of 6 μm thick were cut by a microtome. Tissue sections were mounted on the slides and deparaffinised with xylene, rehydrated in a grading series of ethanol, and washed with distilled and tap water and stained by Mayer's hemalum and eosin (some sections) and by Verhoeff-Van Gieson solution (other sections). The last staining technique is specific for the elastic fibers. Coverslips with resinous mounting medium were used to seal up specimens on the slides.

The residues of the sample treatments with water and ethanol were keeped and analysed by means of FTIR spectroscopy in ATR mode as described below (§ 4.3.1.)

4.3 - Analytical Techniques

4.3.1 - Fourier Transformed Infrared Spectroscopy

FT IR spectroscopy was applied in the MID infrared region of the electromagnetic spectrum, and the measurements were performed in various geometries, on samples prepared in different ways.

Transmission mode

Measurements were performed in transmission mode by a **Jasco 420** FT-IR Spectrophotometer, at RT, in the wave number range 4000 to 400 cm^{-1}, collecting 128 scans with a spectral resolution of 2 cm^{-1}. Samples were prepared by mixing ~1mg of sample with 100 mg of KBr, and the mixture was pressed at about 6 x 10^8 Pa to obtain thin pellets (diameter 13 mm and thickness 0.2-0.3 mm). Another way to run samples in this spectrometer is to smear small quantity of liquid samples on a CaF_2 window, in order to obtain a thin film.

Microreflection mode

FTIR Microspectroscopy measurements were performed by coupling a BOMEM DA8 spectrophotometer with an IR PLAN microscope. The microspectra were collected in reflection mode on small pieces of sample placed on a gold mirror (also used as a reflectance standard). The infrared light was focused onto areas of the sample as small as 0.4 x 0.4 mm^2. Reflectance (R) spectra were collected averaging over 500 scans and, in the following, are presented as absorbance [A, where A = Log (1/R)] spectra.

Attenuated Total Reflection mode

Some analysis on liquid extracts (§ 4.2.2) dried in thin films under ambient conditions were performed by means of a Nicolet – Nexus FT-IR Spectrophotometer. The spectra were acquired in ATR mode in the range between 650 and 4000 cm^{-1}, collecting 120 scans with a spectral resolution of 4 cm^{-1}.

4.3.2 - FTIR data analysis.

During the last years, the use of Fourier Transform Infrared spectroscopy (FTIR), to determine the structure of biological macromolecules, has strongly increased.

The three-dimensional structure of a protein at high resolution can be determined by X-ray crystallography or by nuclear magnetic resonance (NMR) spectroscopy. However, each one of these techniques shows some limitations. X-ray diffraction requires the molecule to form a well-ordered crystal which is not possible for all proteins. NMR, is able to determine the structures of the proteins in solution, but the interpretation of the spectra of large proteins is very complex, so the technique application is limited to small proteins (~15-25 kDa).

These limitations have led to the development of alternative methods able to provide structural information on proteins (especially on secondary structure). These methods include vibrational spectroscopies such as Infrared and RAMAN and circular dichroism (CD) spectroscopy.

FTIR spectroscopy has proved to be a powerful tool to investigate conformation of big proteins, such as collagen. This technique requires only small amounts of sample prepared in a large variety of conditions. In fact, the wide versatility of the technique allows to analyse proteins in liquid or solid state, pure or mixed with other substances thamks to the the spectral «linear unmixing» in this region of the e.m. spectrum. Therefore, high quality spectra can be obtained in a relative easy way, using a very small quantity of sample, without problems of background fluorescence and problems related to the size of the proteins. The water absorption can be

mathematically subtracted or it can represent, as in this work, an important information to understand the behaviour of the proteins in their *in vivo* environment. Nowadays, the availability of mathematical methods, enables us to separate subcomponents overlapping in the spectra of proteins, in order to obtain more detailed information on their conformational state.

A protein FT-IR spectrum is characterized by the typical amide vibrations, corresponding to the vibrational modes of peptide backbone. Peptide group, the structural recurring unit of proteins, in fact, gives rise to 9 characteristic IR absorption bands named Amide A, B, I, II, III …VII.

Amide A band (3300 cm^{-1}) originates from N-H stretching vibration. This mode of vibration does not depend on the backbone conformation, but is very sensitive to the strength of a hydrogen bond (between 3225 and 3280 cm^{-1} for hydrogen bond length from 2.69 to 2.85 Å).

Amide B band (3080 cm^{-1}) can be attributed to the Fermi resonance between the first overtone of Amide II and the N-H stretching.

Amide I and Amide II bands are the two major bands of the protein infrared spectrum.

Amide I band (peaked around 1660 cm^{-1}) is mainly associated with the C=O stretching vibration (70-85%) and C-N groups (10-20%). The exact band position is determined by the backbone conformation and the hydrogen bond pattern. It provides a great amount of information about protein secondary structure.

Amide II is peaking around 1550 cm^{-1} and is more complex than Amide I. It results mainly from in-plane N-H bending (40-60% of the potential energy). The remaining potential energy arises from the C-N (18-40%) and the C-C (about 10%) stretching vibrations. This band is conformation sensitive, as well.

Amide III band can even be attributed to C-N stretching and N-H in-plane bending.

The remaining Amide bands are very complex to study, as they result from the details of force field, the nature of side chains and hydrogen bonding. Their intensity is generally very low, therefore, they are of little use.

Deconvolution of the protein characteristic bands

The concept of Fourier deconvolution is based on the assumption that a single band could be the result of the overlap of a number of sub-bands that cannot be distinguished in the band envelope. A curve fitting procedure can be applied to Amide I band to estimate quantitatively the area of each component, that represents a type of secondary structure. The second derivative spectrum is used to determine the number and the position of the bands constituting the primitive band. The component band positions are revealed by the minima in the second

derivative spectrum. In their pioneer work Byler and Susi (Byler and Susi 1986) discussed the procedure of deconvolution of Amide I bands of several globular proteins by means of Gaussian curves, by an iterative curve fitting procedure. The conformational component amount were measured by the integrated areas of the respective peaks by assuming that the sum of the areas of the peaks represents the total amount of secondary structure in the protein.

The results obtained in this way agree with the structure data by X-ray analysis for a lot of proteins. This procedure was successfully applied to several globular proteins, but fibrous protein have to be carefully treated. The work by Payne and Veis (Payne and Veis 1988) can be considered a starting point for the application of the Fourier deconvolution method to collagen secondary structure. The spread of this analytical method during the last 20 years, pushed the researchers to apply it to several infrared spectral ranges, in order to obtain information on secondary structures of collagen, not only from the Amide I band, but also from Amide III band and OH stretching band in the high wave numbers region.

Amide I and III bands

Amide I region has been widely used, because it can provide a great amount of information about protein conformation. However, several problems of interpretation arise, in the attempt to use it for the secondary structure analysis, due to the water OH bending absorption falling within the same range.

Friess demonstrated that the analysis of the Amide III band can be related to the results obtained from Amide I deconvolution (Friess and Lee 1996). As suggested by DeOliveira (DeOliveira et al. 1994), OH vibrations from H_2O do not interfere with Amide III band. It was used by several researchers as a direct qualitative indicator for conformational changes in proteins. These properties ensure Amide III region analysis should be employed as a complementary, if not an alternative, method for protein structural analysis.

Several studies were carried out on the assignment of protein secondary structure using this band (DeOliveira et al. 1994; Cai and Singh 1999; Belbachir et al. 2009). However, the secondary structure attributions are controversial and no study, reporting the attribution of collagen secondary structures by means of Amide III band fitting, can be found in literature. As suggested by Belbachir, collagen Amide III band (1305 – 1175 cm^{-1}) is characterized by three main peaks centered at 1283, 1240 and 1204 cm^{-1} and can be deconvolved in 5 Gaussian sub-bands, peaking at 1284, 1260, 1243, 1234 and 1203 cm^{-1}; however he does not attempt any attribution to the secondary structure.

DeOliveira et al. and Cai and Sing applied the deconvolution procedure on several globular proteins and assigned the band at highest wave numbers to α-helix and the band at lowest wave number to β-sheet motif. The intermediate region of the band was attributed by DeOliveira et al. to unordered structures while Cai and Singh attempt an attribution to coil and turn structures. In this work, a first attempt to assign the component of Amide III band deconvolution to collagen secondary structure was carried out.

OH Stretching band

In a protein spectrum the band at highest wave number (3800-2600 cm^{-1}) is very important because it provides information on the hydration structure of the protein. When a protein is in solution, two main categories of water molecules can be identified interacting with it: bound internal water and the surface water. The internal water molecules, located in the internal cavities of the protein, play a structural role in the folded protein structure. The relationship between the structure of protein and the water plays a very important role in the assessment of the protein function.

Some studies were performed on this band by means of deconvolution procedures. After the paper of Onori et al. (Onori and Santucci 1993), recently Schmidt presented an alternative interpretation of the structure of the IR vibrational mode of pure water. The interpretation is based on the cooperative hydrogen bonding arising from a network of hydrogen bonds in the liquid. He suggested that the deconvolution of the OH stretching band of pure water by means of 6 sub-bands is directly related to the number of hydrogen bonds and the O-H bond length and that variations in this bond length are caused by the influence of the surrounding hydrogen-bonded network of water molecules (Schmidt 2007).

Mallamace et al. studied the same band to investigated the water structure of lysozyme at different temperatures and therefore at different hydration degrees. The deconvolution of the band was performed by means of three Gaussian sub-bands two peaking at 3100 cm^{-1}, 3220 cm^{-1} and one falling in the range 3540-3620 cm^{-1}. These bands were attributed to low-density-liquid phase (LDL), to the liquid phase with hydrogen bonds coordinating a number of water molecules close to four and, finally, to non-hydrogen-bonds (NHB) i.e. water molecules poorly connected with other environmental molecules, respectively (Mallamace et al. 2007).

Bridelli and Crippa, applied the study to melanin, a biopolymer responsible of the animal pigmentation. The deconvolution of the OH stretching band by means of three Gaussian sub-bands allowed to obtain information about the three water families associated to the bands called high- (HW), medium- (MW), and low- (LW) wavenumber components. They were

peaking at 3624 cm^{-1}, 3550 cm^{-1} and 3350 cm^{-1} and were corresponding to vapour water, liquid water and bulk water respectively (Bridelli and Crippa 2010a).

FT-IR bands were processed by means of Origin 7.0 software. All the spectra acquired were corrected for the baseline and slightly smoothed.

The procedure of multipeak fitting was applied, in order to study in detail the secondary structure of pure collagen and skin collagen, in the spectral range corresponding to Amide I and III bands, between 1750 to 1600 cm^{-1} and 1300 to 1180 cm^{-1} respectively. and to investigate the hydration structure in correspondence of the OH stretching bands in the range 3750 to 2600 cm^{-1}.

The same procedure was applied to the $\nu_1\nu_3$ phosphate band localised in the spectral range 900 to 1200 cm^{-1} of bone spectra in order to obtain information about the mineral matrix crystallinity and structural order of the analysed samples.

The most critical step of the deconvolution process is represented by the choice of the correct number of sub-bands to use in the iteration procedure of the multipeak fitting. It is essential to study deeply the band composition.

The absorption band of interest have to be isolated and a baseline has to be subtracted. Initial component peak positions can be obtained from second-derivative spectra of the raw data. Substantial attention has to be paid to obtain the best fit with the minimum significant number of component bands. The evaluation of the goodness-of-fit (GOF) can be attained by a least squares regression analysis through the R^2 and reduced χ^2 settlement. R^2 represents the coefficient of determination and is defined as:

$$R^2 = \frac{SS_{reg}}{TSS} = 1 - \frac{RSS}{TSS}$$

where SS_{reg}, the regression sum of squares, is the portion of the variation that is explained by the regression model; RSS is the residual sum of squares, a portion that is not explained by the regression model, and TSS is the total sum of squares. R^2 should vary between 0 and 1. A value close to 1 indicates that the fit is a good one.

Reduced χ^2 is defined as:

$$Reduced\,\chi^2 = \frac{\chi^2}{df_{error}} = \frac{RSS}{df_{error}}$$

and represents the residual sum of χ^2 divided by the degree of freedom. A value close to 0 indicates that the fit is a good one.

4.3.3 - Circular Dicroism spectroscopy

CD measurements were performed by means of a Jasco J715 spectropolarimeter in the range of wavelengths from 190 to 250 nm. A scan speed of 50 nm/min was used and the spectrum was obtained as average of 3 scans per each sample. Quartz cells of 0.2 cm path length were used. The spectropolarimeter was equipped with a Peltier system to accomplish the heating of the sample for the measurement of the thermal denaturation. The temperature was changed in the range from 20 to 48 °C with steps of 2 °C/min. The spectra analysis was performed by means of CDPro Software.

4.3.4 - Scanning Electron Microscopy

The samples were analysed without any specific preparation, just pasting them onto the double-side conductive tape. SEM images were acquired with Zeiss Supra 40-high resolution Scanning Electron Microscope, using low energy beam, in order to avoid a damage of the samples. Microanalysis was performed using an EDX Oxford Instrument.

Chapter 5

Results: In vitro experiments

5.1 - Study of hydration structure of type I collagen from rat tail.

Infrared spectroscopy is a very powerful technique to study water bound to biological macromolecules, as it is able to monitor changes in the structural features, such as changes in water spectral properties (Bridelli and Crippa 2010a).

The spectral ranges of OH stretching, and Amide I and III bands have been studied in order to have a complete knowledge about the conformational characteristic in collagen secondary and tertiary structure in relation to changes in the collagen hydration degree. The following works will shed light on the modification of the collagen secondary structure submitted to in vitro procedures of dehydration – rehydration, thermal denaturation and interaction with different types of sugars, applying the Fourier deconvolution methods described in great detail in Chapter 4.3.2.

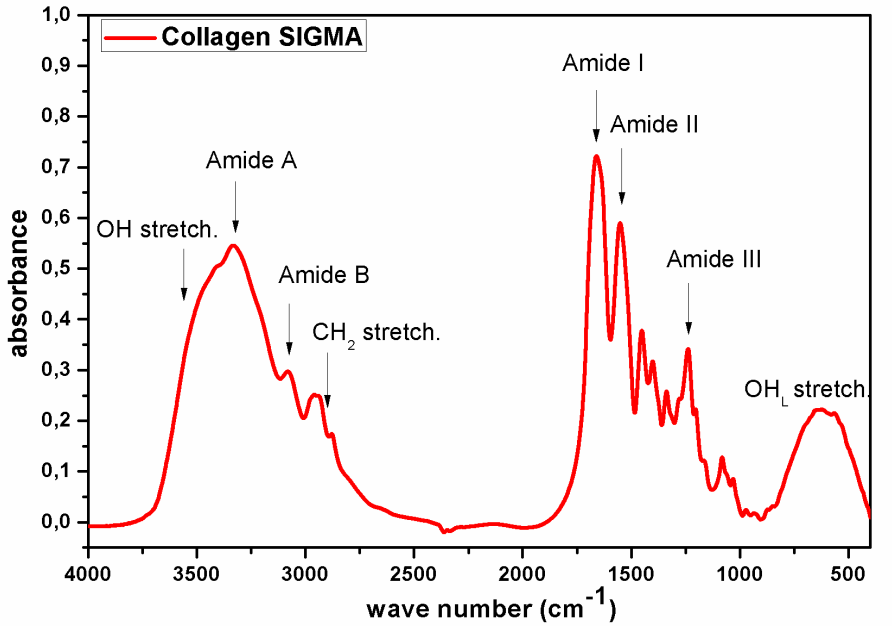

Figure 5.1 – FTIR spectrum of rat tail type I collagen from SIGMA – Aldrich

The typical IR spectrum of collagen is dominated by the bound water absorption bands: the broadest one between 3700 and 3000 cm^{-1}, due to the hydroxyl stretching vibrations (ν(OH)); the hydroxyl bending mode (δ(OH)) around 1640 cm^{-1} overlapped under the Amide I band; and the absorption band around 600 cm^{-1}, due to the OH librational modes.

The FTIR spectrum of collagen shows the typical Amide band absorptions. Amide A and B bands are peaked at 3300 cm^{-1} and 3080 cm^{-1} and fall within the same spectral range of the OH stretching giving rise to a broad band.

The Amide I, II and III bands, instead, are peaked around 1660cm^{-1}, 1550 cm^{-1} and 1240 cm^{-1}.

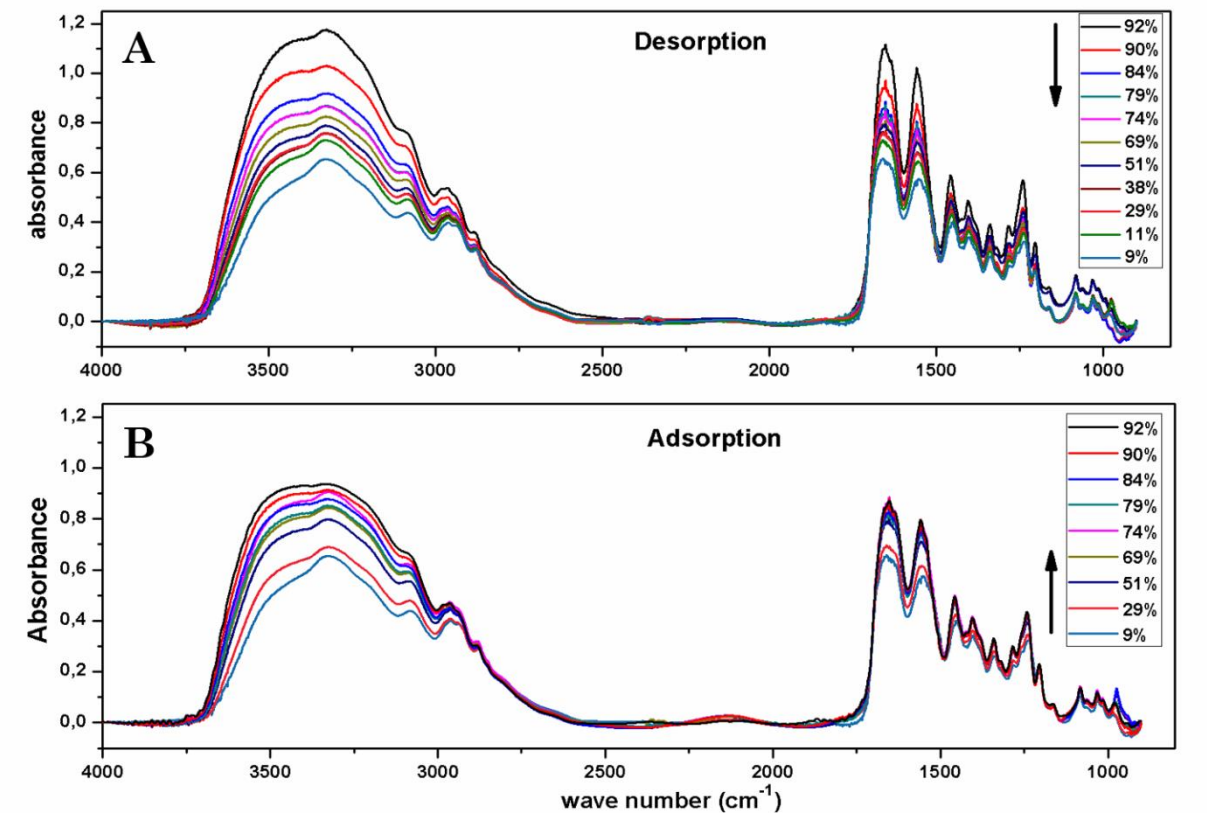

Figure 5.2: FTIR collagen spectra during the desorption (panel A) and adsorption (panel B) cycles

The spectra of the samples collected by decreasing (desorption run) and increasing (adsorption run) of a controlled relative humidity were compared and analysed.

Infrared spectra were collected on a collagen that was dehydrated from 92 to 9 % (desorption run) and then re-hydrated from 9 to 92% (adsorption run) of humidity as described in Chapter 4.1.1. To better understand the role of water in the collagen structure modifications, the spectra were divided in two region, one corresponding to the high wave numbers region, ranging between 3800 and 2600 cm-^{1} and one that can be called low wave number region spanning the spectral range 2000-500 cm^{-1}.

5.1.1. - High wave number region: OH stretching band deconvolution

In figure 5.3 the magnification of the spectral range 3800-2600 cm^{-1} was showed. This broad band represents the absorption of OH stretching vibrations overlapped with the characteristic absorptions of Amide A and B bands and aliphatic groups CH_3-CH_2.

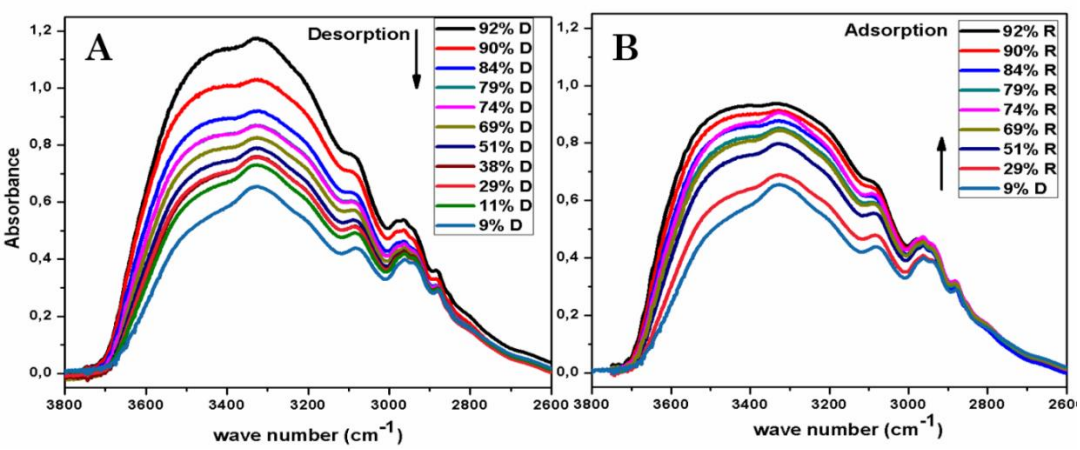

Figure 5.3: Magnification of the spectral region 3800-2600 cm^{-1}, during the desorption (panel A) and adsorption (panel B) runs

In order to study the water changes in relation to the collagen structure, the spectrum, obtained for the sample at the lower degree of hydration (9%), was subtracted from all the other spectra. In this way, any contribution to the band of N-H and C-H stretching vibrations, occurring in the same wavenumber range investigated was systematically eliminated.

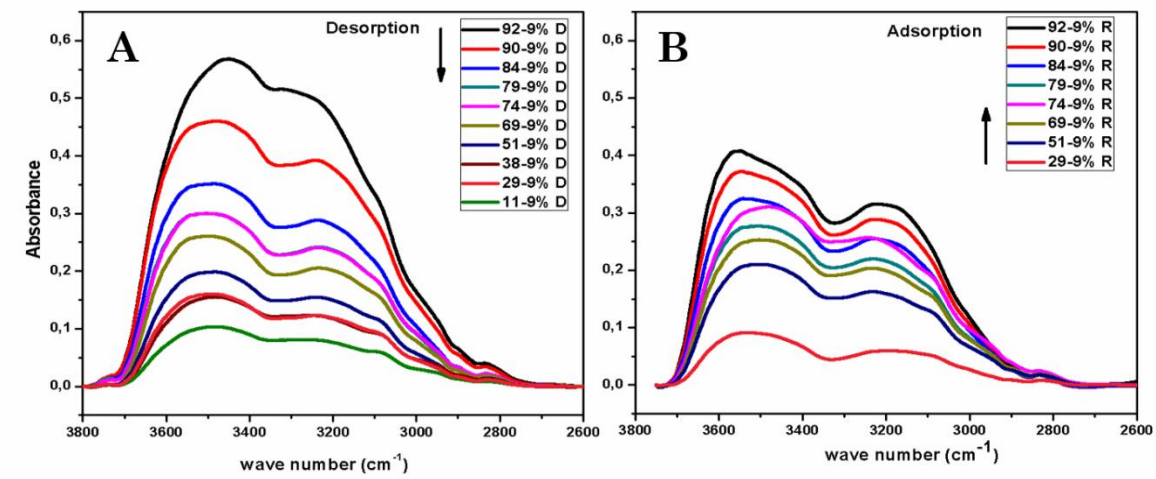

Figure 5.4: Difference spectra obtained from the subtraction of the spectrum at different hydration level and the spectrum at the lower hydration degree (0.09)

This way, the spectra represent the OH stretching vibration of the water bound to the samples. Changes in the water content resulted in the variation of the amplitude and the shape of the bands, as a consequence of a modification of the component sub-bands. They can be easily correlated to the structural changes occurring in collagen during the different dehydration-re-hydration treatments.

Figure 5.4 shows that the each band is strongly reduced in its amplitude if compared to the absorption band at a_w=0.92. The spectrum of band collected at the end of the desorption treatment (a_w = 0.11) is very different from the one at the start, in shape and amplitude, and the resolution into components testifies changes in the spectral contributions.

Assuming that the OH stretching band is due to the distribution of hydrogen bonds of variable strength, composing the shells surrounding the collagen molecules, each *ν*(OH) feature was resolved by means of a deconvolution procedure into three Gaussian components following the deconvolution procedure of the second derivative analysis and the literature (Mallamace et al. 2007; Bridelli and Crippa 2010a). The analysis is shown in Figure 5.5.

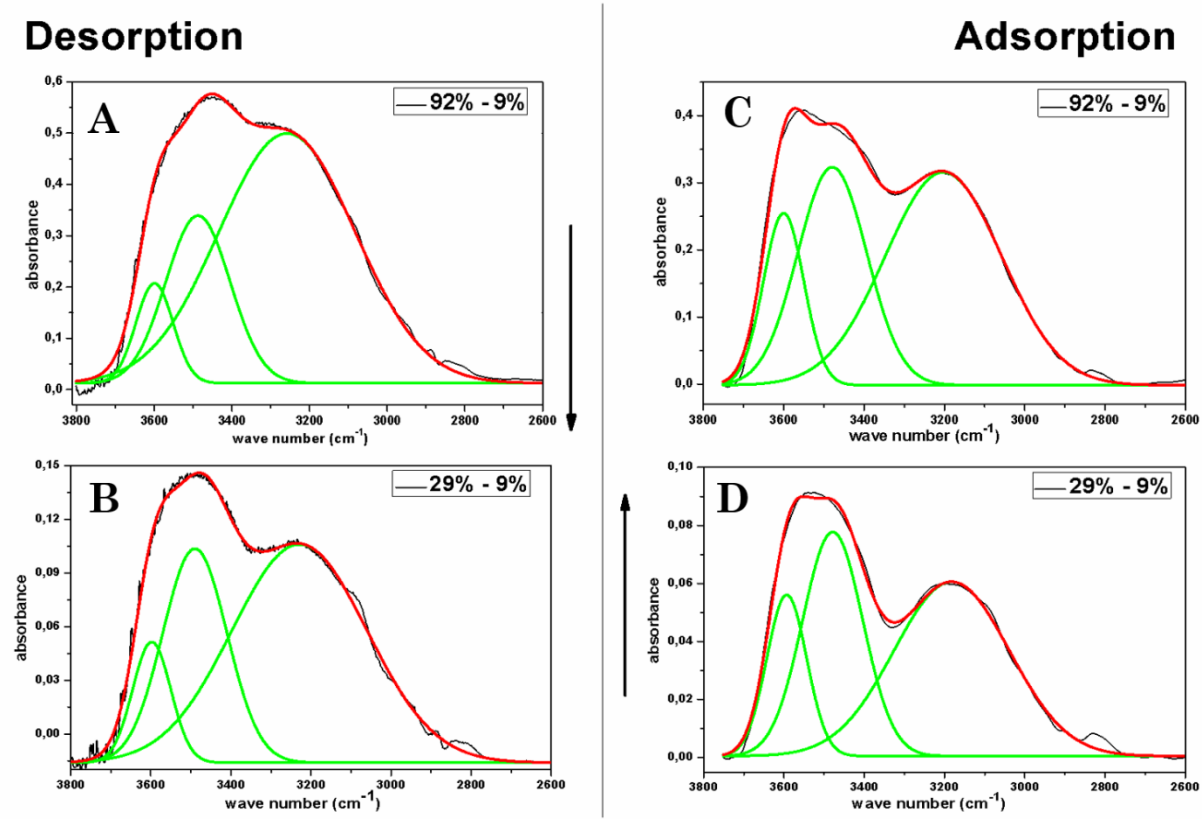

Figure 5.5: Deconvolution of the subtracted bands by three Gaussian bands. Panels A and B: desorption run (92% and 29%). Panels D and C: adsorption run (29% and 92%).

Following Bridelli and Crippa, the three bands obtained were defined as high- (HW), medium- (MW), and low- (LW) wavenumber components. (Bridelli and Crippa 2010a). They are peaked at 3598 ± 3cm^{-1} (HW), at 3480 ± 10 cm^{-1} (MW) , and at 3230 ± 20 cm^{-1}(LW)

From the vibrational frequencies, corresponding to the maximum of the component peaks, the H-bond distances (H · · ·OH lengths) were estimated, following Nakamoto (Nakamoto et al. 1955) at 3.02 Å for HW band, 2.9 Å for MW band, and 2.77 Å for LW band.

Following Popescu the H-bonds energies were calculated using the following formulae:

$$E_H = \frac{1}{k}\left[\frac{\nu_0 - \nu}{\nu_0}\right]$$

where ν_0 is the standard frequency of the OH (3650 cm^{-1}) monomer observed in the gas phase

while ν is the stretching frequency of OH group observed in the infrared spectrum of the samples, and k is a constant equal to 1/2.625 x 10^2 kJ (Popescu et al. 2010).

The values of hydrogen bonds energies were estimated to be 0.55 kJ for the HW band, 1.72 ± 0.05 kJ for MW and 4.50 ± 0.35 kJ for LW band.

The calculated values of hydrogen bonds distances and energies permit to attributed the HW band to single water molecules or bound in small clusters (such as dimers) as in the gas phase, whose structure oscillates between H-bonded and non-H-bonded. Some researchers, in fact, consider the hydrogen bond to be broken if the bond length is 3.10 Å. The MW band can be assigned to liquid water bound 3 to 5 water molecule and, in closing, the LW band can be attributed to bulk water bound to 6-7 water molecules (Schmidt 2007; Bridelli and Crippa 2010b). The deconvolved spectra (figure 5.5) show a decrease of the percentage areas of the three bands in the sample treated at a_w = 0.29. After the complete rehydration of the collagen at a_w=0.92 of the adsorption run, the shape of the total band is very different if compared to the shape of the band at the same hydration degree at the beginning of the desorption run. This effect may be attributed to the incapability for one of the water phase to be regained by the collagen structure.

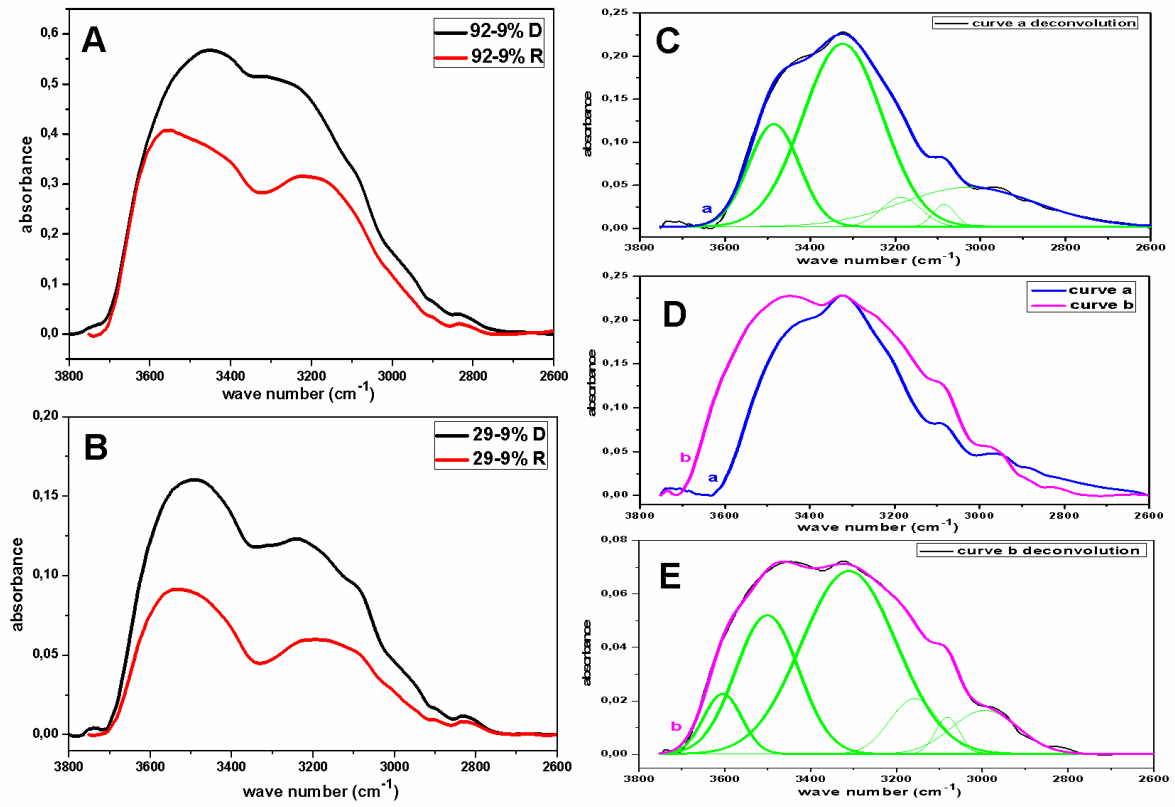

Figure 5.6: Panel A and B: superimposition of the OH stretching bands of the samples at the same hydration level (0.92 and 0.29 after desorption and adsorption runs).
Panel D: curve b (blue line): difference band as deduced from panel A; curve b (pink line): difference band as deduced from panel B.
Panel C and E: deconvolution of the subtraction bands a and b (blue and pink line respectively).

To better understand which one of the water phase have been lost and no longer soaked up by the collagen, the bands corresponding to the hydration level a_w = 0.92 of the adsorption run, (figure 5.6, panel A, red line) was subtracted from the same hydration level (a_w = 0.92) of the desorption run (figure 5.6, panel A, black line). The same mathematical treatment was performed for the hydration degree a_w 0.29 (figure 5.6, panel B, black line: desorption run; red line: adsorption run). The difference bands obtained were plotted in the same graph (figure 5.6, shown in panel D), and normalized at the maximum intensity of one of the two bands, in order to compare the band shapes. The difference in the shape is significant because it can represent the spectrum of the water that can no longer be soaked up into the sample after the dehydration treatment. This difference bands were analysed and decomposed into Gaussian components, as shown in the panels C and E. It was possible to resolve the subtracted bands into the three original components just for the 0.29. At 0.92, in fact, the HW band cannot be regained. The peaks at 3485 and 3322 cm^{-1} roughly fill the position of the original MW and LW peaks.

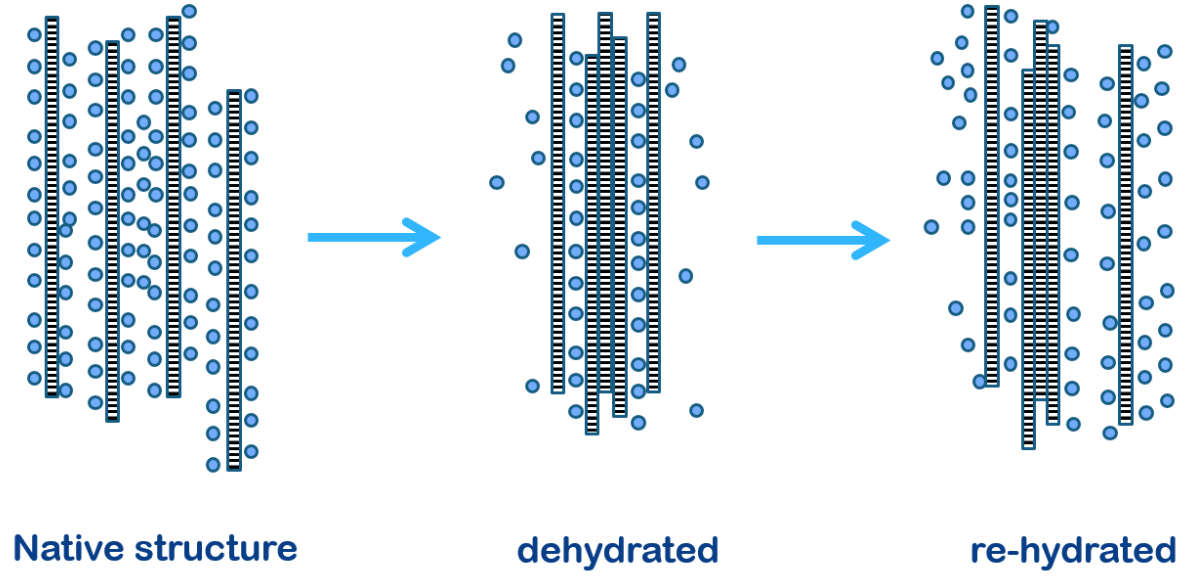

Figure 5.7: Schematic representation of collagen fibers surrounded by water molecules in the native state and after dehydration and re-hydration treatments.

The result emphasizes the hypothesis that the dehydration-re-hydration treatment results in an adsorption hysteresis effect, so that in the re-hydrated collagen a considerable inner water portion, once desorbed, cannot be re-adsorbed probably due to the tight aggregation of the collagen triple helices. The water molecules available during the re-hydration treatment reorganise themself all around the collagen triple helices but not all are able to reach again the inner space between the aggregate triple helices as shown in the schematic representation of figure 5.7.

5.1.2 - Low wave numbers region: Amide I and III band Deconvolution

The study of the Amide I band, by means of the deconvolution curve-fitting, can provide many information about the collagen secondary structure modification. These changes are strongly influenced by the variations in the shells of hydration wrapping the collagen molecules. The fitting multi-peaks procedure was applied both to Amide I and III band.

Following the second derivative spectrum, a good fitting of the collagen Amide I band was obtained by means of 6 main sub-bands peaking around 1690 cm^{-1}, 1674 cm^{-1}, 1660 cm^{-1}, 1642 cm^{-1}, 1630 cm^{-1} and 1614 cm^{-1}. Each band was assigned to a secondary structure and their shift toward higher or lower wave number regions is indicative of slight or significant modification of the collagen secondary structure. The component at 1690 cm^{-1} has generally been attributed to β-sheet. This secondary structure is not very well represented in collagen secondary structure, so it could be interpreted as an aggregation of collagen triple helices bounded very close to each other in a sort of β-sheet-like conformation.

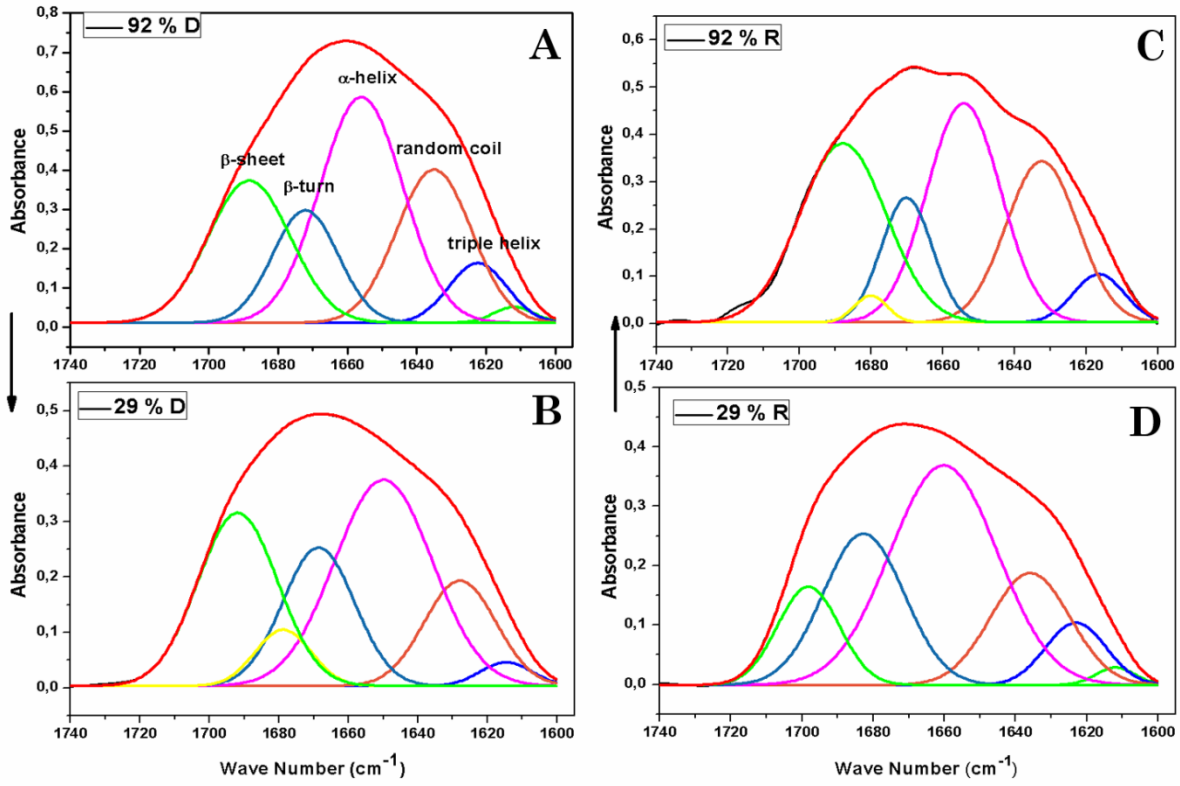

Figure 5.8: Deconvolution of Amide I bands in collagen prepared at different hydration degree: Panel A and B: a_w 0.92 and 0.29 after the desorption run. Panel D and C: a_w 0.29 and 0.92 during the adsorption run.

After dehydration (Figure 5.8, panel B), the area of this band increases. This observation suggests that dehydration of collagen leads to a modification of the hydration shells that arose an approach of the triple helices between them.

The band at 1674 cm^{-1} is attributed to β-turns of the C- and N-telopeptides in collagen (Rabotyagova et al. 2011). The β-turn conformation is important because it can be related to the accessibility of lysine for hydroxylation and subsequent cross-links formation. Even the area of this band increases after dehydration, and this could confirm a cross-link formation between triple helices.

The peak at 1660 cm^{-1} is generally assigned to α-helix. It represents the triple helix motif of collagen in the native state. In the samples at a_w = 0.29 (after dehydration treatment) it undergoes slight shift toward lower wave number. It is indicative of an increase in the structural disorder of the triple helix, leading to a helix-coil transformation. The band around 1640 cm^{-1}, in fact, represents the random coil structure. It increases especially after the complete rehydration of the sample (a_w = 0.92 during the adsorption run). This could suggests that original conformation of the collagen triple helices cannot be completely recovered, because the water molecules cannot reorganize the H-bonding set as before the desorption run started. The peak around 1630 cm^{-1}, according to some authors (Bryan et al. 2006; Mary et al. 2009), can be assigned to polyproline in triple helix conformation. In our samples, there is not a significant modification of this band. This is indicative of a good preservation of the collagen structure. Probably, the dehydration treatment changes the mechanical properties of the collagen triple helices and their way to aggregate each other, but do not cause a proper modification of the collagen secondary structure.

	% Band Areas				
Secondary structure	**β-sheet**	**β-turn**	**α-helix**	**Random coil**	**Triple helix**
Samples					
92% D	22	14	35	22	6
29 % D	25	18	36	14	2
29 % R	11	22	42	16	7
92 % R	29	12	30	22	5

Table 5.3: percentage areas of the amide I sub-band components

The spectrum shown in Figure 5.8 panel D represents one of the first step of the adsorption run. At this stage, water molecules begin to be re-adsorbed by collagen. The collagen conformation described by the deconvolution spectrum is difficult to be interpreted, probably because in this

step the organization of the water molecules around the collagen triple helices did not attain an equilibrium configuration.

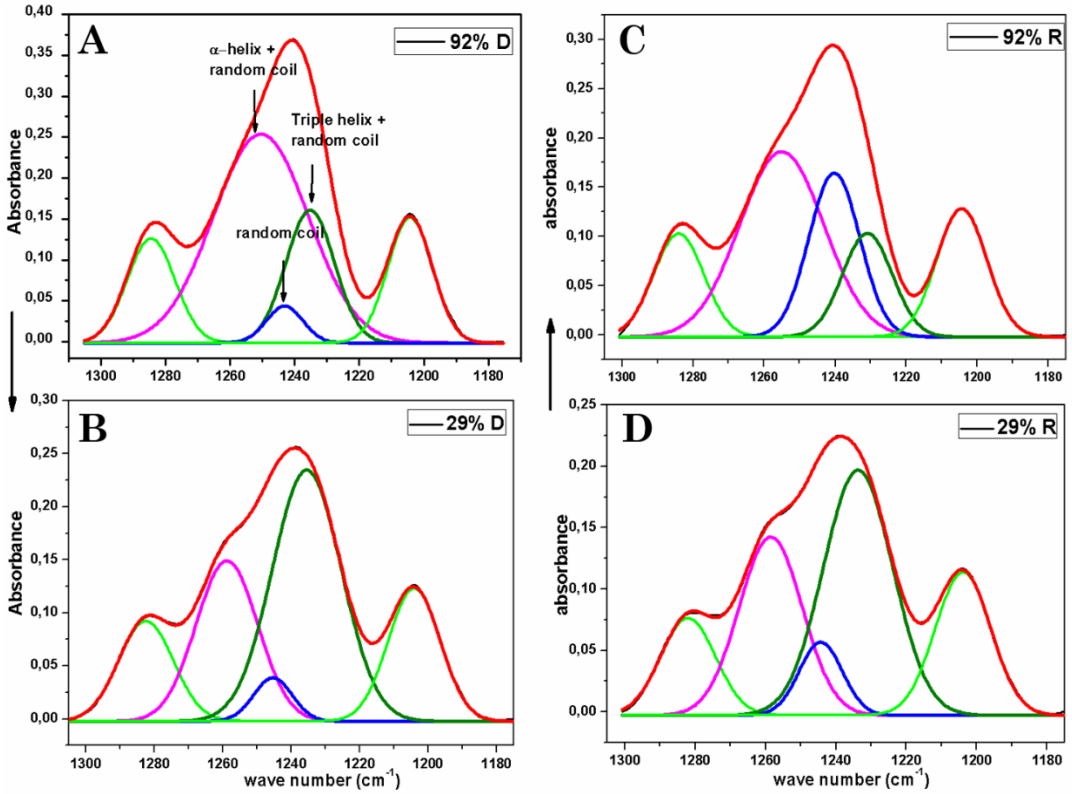

Figure 5.9: Deconvolution of the Amide III bands: Panel A and B: a_w 0.92 and 0.29 desorption run. Panel D and C: a_w 0.29 and 0.92 of the adsorption run.

The fitting multi-peak of the Amide III band was carried out following the few references found in the literature, as describe in detail in Chapter 4.3.2 and by means of the second derivative spectrum analysis.

The collagen Amide III band was cut in the spectral range 1305 to 1175 cm^{-1}, baseline-corrected and deconvolved in five Gaussian sub-bands following Belbachir as shown in figure 5.9. The five obtained Gaussian bands are peaking at 1284, 1250, 1243, 1235 and 1204 cm^{-1}. As shown in figure 5.9, the bands peaking at 1283 and 1204 cm^{-1} do not show significant differences in shape, amplitude and percentage areas. Following DeOliveira et al. and Cai and Singh, the band at 1284 cm^{-1} was assigned to collagen α-helix in the native state while the band at 1204 cm^{-1} was attributed to the aggregation of collagen triple helices in a β-sheet-like conformation.

The intermediate region of the band (from 1270 to 1215 cm^{-1}), deconvolved by means of three sub-bands, shows the most significant variations of the percentage areas. An attribution of these sub-bands to collagen secondary structures was attempted. The band peaking at 1250 cm^{-1} was assigned to α-helix, in association with β-turn or random coil; the band at 1243 cm^{-1} is associated with the random coil structure and, in closing, the band centered around 1235 cm^{-1} could be indicative of an association between random coil and triple helix. Thus, this region

may describe a transition from α-helix to triple helices in aggregated strand through a slight state of disorder. As shown in figure 5.9, panel B, the decrease of the humidity degree of the collagen sample causes an increase of the area of the band peaked at 1235 cm^{-1}, related to the aggregated triple helices. This result was already highlighted in the study of the Amide I deconvolution. The slight increase in the area of the random coil band, in the spectrum of the collagen at a_w= 0.29, during the adsorption run accounts for the changes in band shape monitored in the Amide I band analysis as above shown. In the sample at aw= 0.92 during the adsorption run, the Amide III band (Figure 5.9, panel C) shows an increase in the area of the band related to random coil structure. Thus, the results support the hypothesis that a not complete re-adsorption of the total amount of water might cause a modification of the collagen structure, leading to a partial aggregation of the collagen helices.

5.2 - Influence of non-enzymatic glycation on collagen conformation.

Non-enzymatic glycation is the process by which reducing sugars post-translationally crosslink proteins, such as collagen. Glycation has been studied primarily as associated with aging phenomena. The accumulation of advanced glycation end products has been shown to change the mechanical and biochemical properties of collagen and consequently of living tissues.

The mechanism of nonenzymatic glycation, characterized by the Maillard reaction, has been deeply illustrated in Chapter 1. In vitro glycation has been documented to decrease the degradation rate of collagen (Roy et al. 2010).

In order to have a better comprehension of the aging mechanism of collagen, and to understand how actually modification of the mechanical properties of the protein could preserve it from the degradation, changes in the secondary structure of collagen, when exposed to the Glycation reaction were investigated. The results obtained from this in vitro study will be useful and will be applied to better understand the mechanism of preservation of the archaeological remains.

The results obtained on collagen forming complexes with glucose 50 mM after 10 days and with ribose 50 mM after 3 days were showed in figure 5.10. FTIR spectra were recorded for pure collagen, glucose and ribose to determine if there were isolated peaks that could be used to distinguish the presence of glucose or ribose in the collagen.

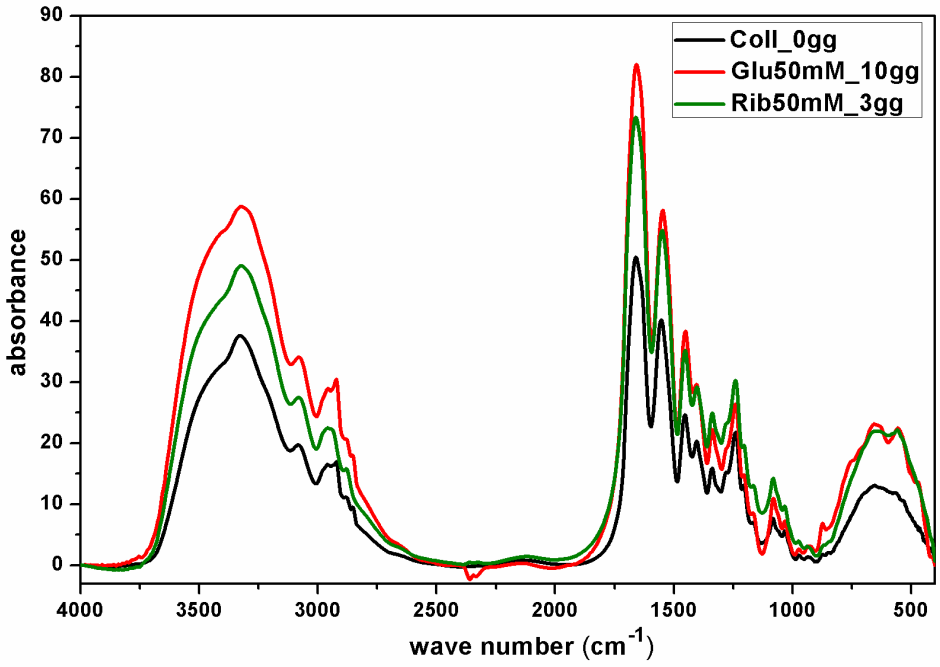

Figure 5.10: Native collagen (black line), collagen + glucose 50 mM after 10 days of treatments (red line), Collagen + ribose 50 mM after 3 days of treatment (green line).

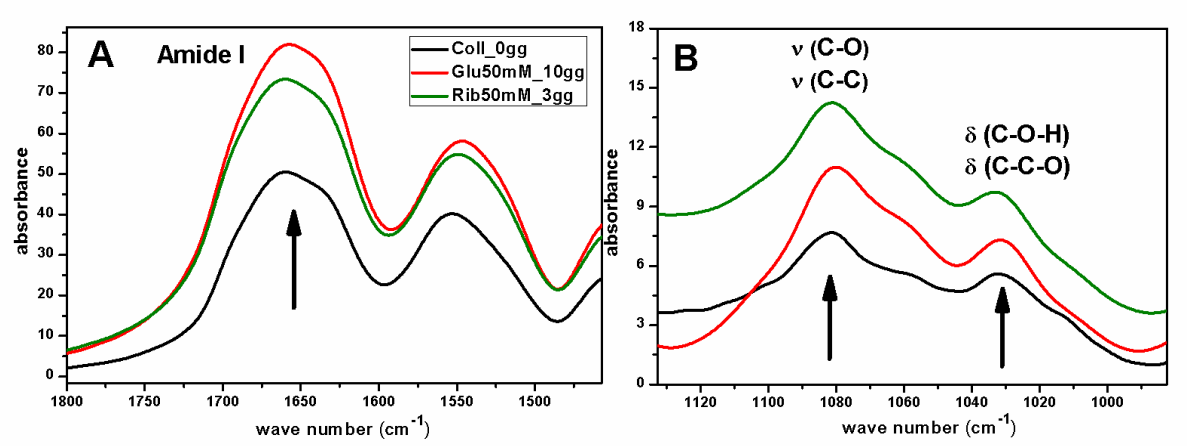

Figure 5.11: Panel A: Magnification of the Amide I and II band region (1800 – 1450 cm^{-1}) Panel B: magnification of the spectral range assigned to carbohydrates absorption bands (1200 – 900 cm^{-1})

As shown in figure 5.11, the spectra of the samples were analysed in the ranges of Amide I band and carbohydrates absorption bands.

The main absorption bands for glucose and ribose were detected in the range 990 - 1120 cm^{-1} as shown in figure 5.11, panel B. The peaks around 1080 and 1032 cm^{-1} corresponding to C-O and C-C stretching vibrations and the C-O-H and C-C-O bending vibrations respectively can be assigned to the accumulation of glycation products.

All the spectra were normalized to the amplitude of the Amide I band (around 1600 cm^{-1}). This mathematical treatment allowed to calculate the ratio of the band areas 1032cm^{-1}/1660cm^{-1} . This parameter relating the band area assigned to the accumulation of AGEs product with the area of the Amide I band, permits to quantify the amount of sugars attached to collagen. The values obtained by means of this parameter were correlated with the ribose and glucose concentrations (5mM and 50 mM) as shown in figure 5.12 (panel A and B). In the glycated collagens, the increase in the amount of glucose and ribose bound to collagen was correlated with the increase of the sugars concentration in the samples.

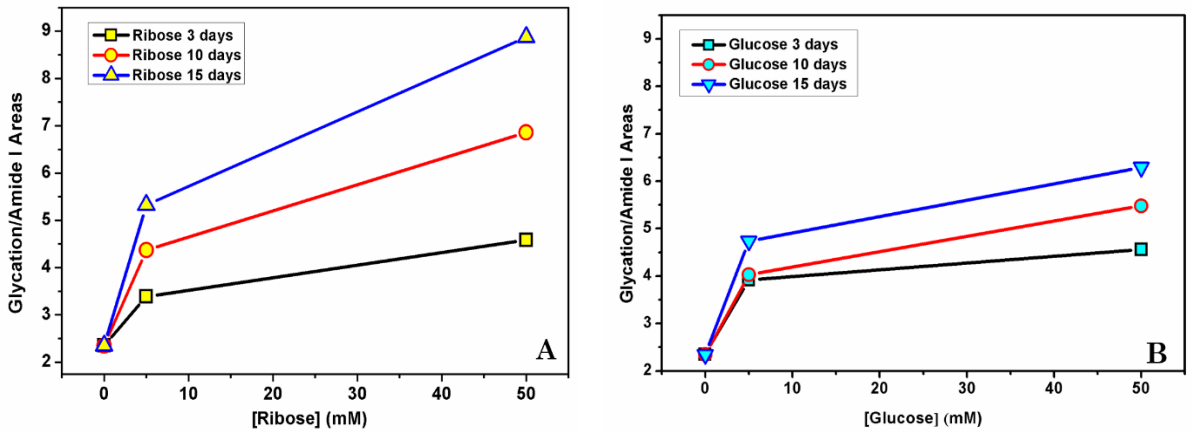

Figure 5.12: Panel A: Effect of ribose concentration on Glycation/Amide I band Areas ratio. Panel B: Effect of glucose concentration

As shown in figure 5.12, panels A and B, the glycation reaction depends on the sugar concentration increase in the solution, and the accumulation of glycation products increases with time (figure 5.13). As shown in figure 5.13, ribose shows a higher efficiency in the formation of the complex with collagen than glucose.

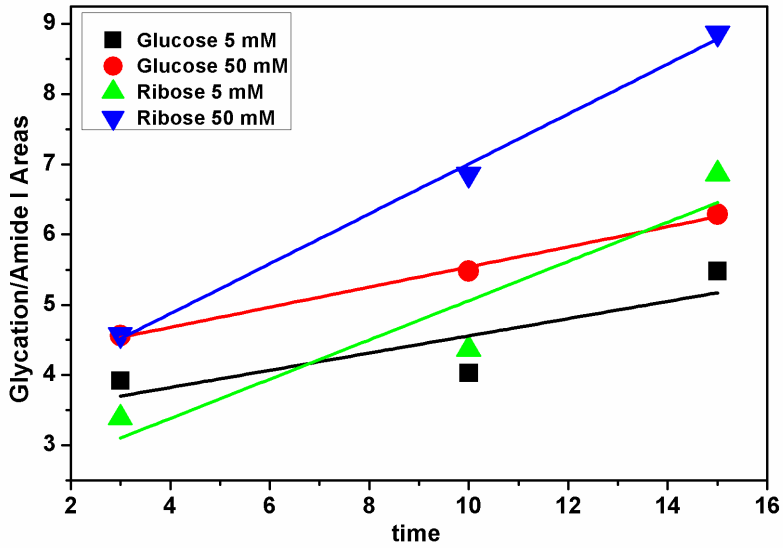

Figure 5.13: Temporal dependence of the area ratio for the glycation reactions produced on collagen by the two sugars at different concentrations.

In figure 5.14, panel A, the Amide I bands belonging to the spectra of the analysed samples were compared after normalization of the maximum amplitude to compare the shape of the bands. The Amide I bands were analysed by means of a multi-peak fitting to determine if there were conformational changes in collagen structure, as a consequence of glycation. The Amide I bands of collagen, treated with glucose and ribose, showed just slight differences in the shape, but through the fitting procedure small differences of the relative secondary structures were pointed out. The treatment of collagen with glucose causes an increase in the percentage areas

of β-turn and random coil structures. The slight denaturation of collagen may has been caused by the treatment of the sample at high temperature (37 °C) for 10 days. The treatment of collagen with ribose, instead, causes an increase in the percentage areas of the β-sheet. (Figure 5.14 and Table 5.2), suggesting an increase in the amount of the cross-links between the triple helices enhanced in the complexes collagen-ribose.

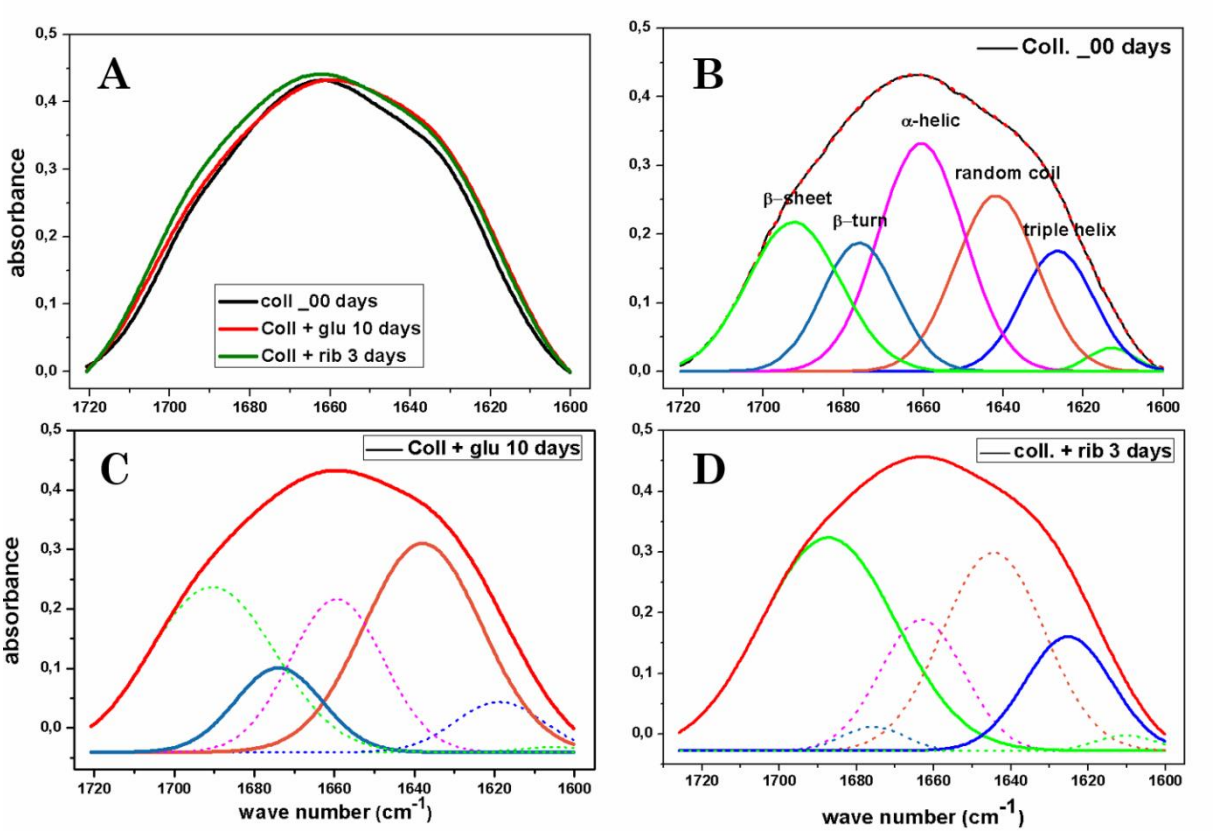

Figure 5.14: Panel A: Comparison of the shape of the normalized Amide I bands of native collagen (black line), collagen + glucose 50 mM after 10 days (red line), Collagen + ribose 50 mM after 3 days of treatment. Panel B, C and D: Deconvolution of the Amide I bands for untreated collagen, collagen + glucose and collagen + risose respectively

	β-sheet	β-turn	A-helix	Random coil	Triple helix
Coll (0 days)	20	10	30	21	13
Coll. + Glucose (10 days)	30	12	20	35	2
Coll. + Ribose (3 days)	40	2	15	28	14

Table 5.4: percentage areas of amide I sub-band components

In addition, all the samples were analysed by means of Circular Dichroism during the treatment of thermal denaturation as described in Chapter 4.3.3.

Collagen adopts the polyproline II-like helical conformation as shown by the characteristic CD spectrum, displaying a negative minimum dichroic band around 190 nm and a weak positive maximum one at 210-230 nm as reported in literature (Zhang et al. 2006)

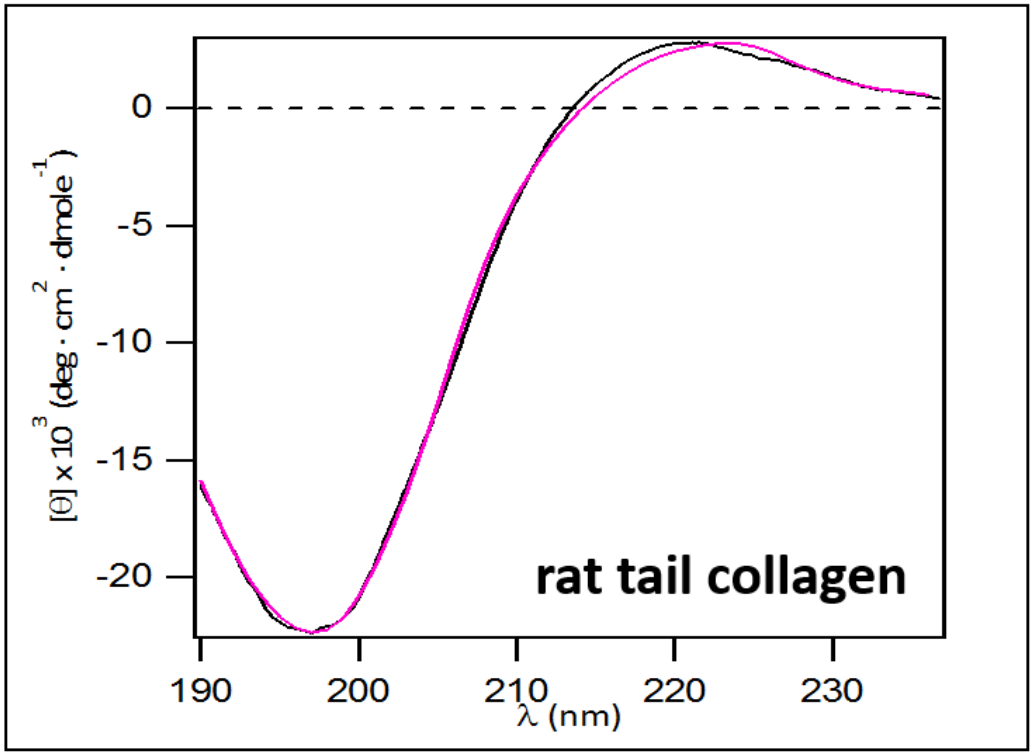

Figure 5.15: CD spectrum of a native type I collagen from rat tail.

In figure 5.15, the CD spectrum of rat tail collagen (SIGMA) is displayed: it shows a positive maximum peak at around 221 nm and a negative minimum peak at 196.4 nm, suggesting a typical triple helical conformation.

As shown in figure 5.16, the thermal treatment from 20 to 50 °C leads to a weakening of the two bands in the CD spectrum. Around 37 °C the negative peak shifts towards higher wave number. At 40 °C the positive peak is completely flattened. Above 40 °C no more changes occur in the CD spectrum. The modifications of the characteristic features of the CD spectrum of the collagen are indicative of the protein denaturation.

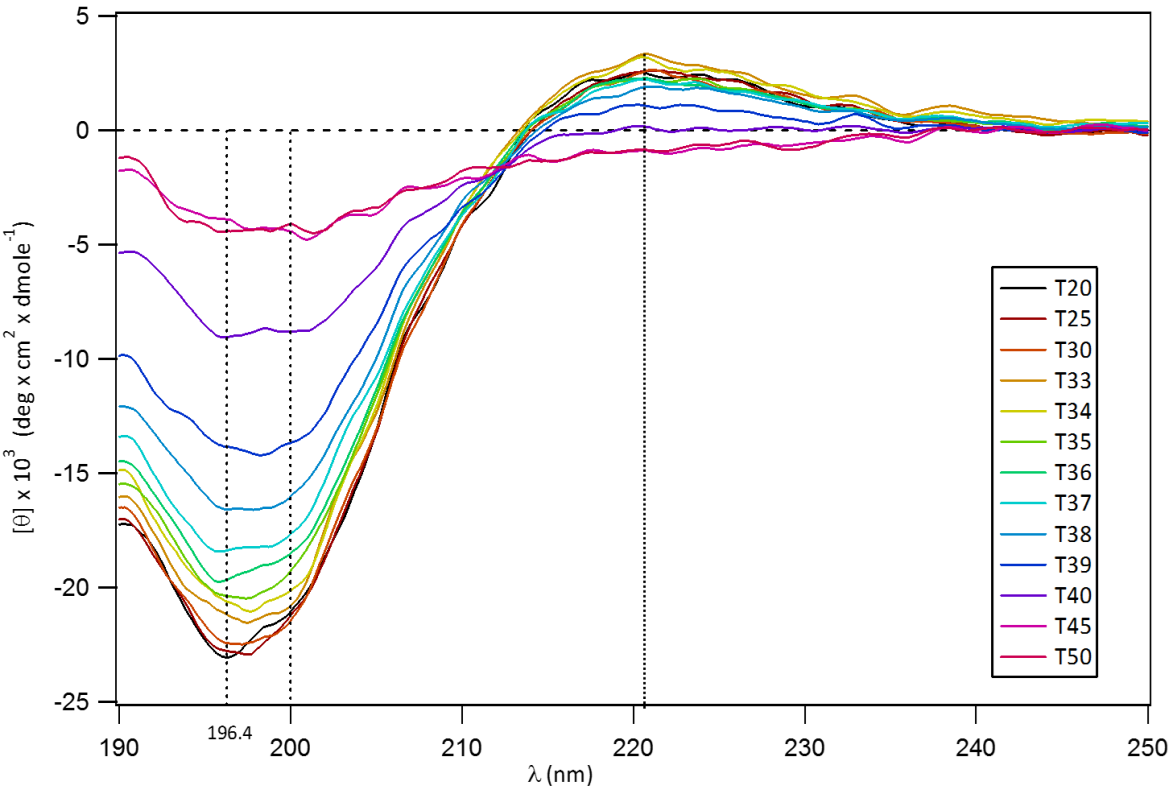

Figure 5.16: CD spectrum of a untreated collagen in its native state submitted to thermal denaturation from 20 to 50 °C.

As suggested by many authors (Tiffany and Krimm 1972; Zhang et al. 2006) and observed for our sample, the denaturation temperature of a collagen in its native state is around 37.5°C. Experimental studies on model compounds show that the CD spectra of rigid molecules are, in general, more intense than those of flexible ones. Theoretical studies of CD spectra suggested that the binding of water to the imide group tends to stiffen the chain. On the contrary, the heating of a solution of PP II leads to a weakening interaction between the chain and the bound water, thus, elevated temperatures also contribute to enhance the chain motion and flexibility (Tiffany and Krimm 1972).

The triple helix of the native collagen tends to achieve a more flexible conformation when it is heated above the denaturation temperature. This happens because, during the denaturation process, the physical properties of the protein such as viscosity, solubility and optical activity change, due to the collapse of the triple helical structure. The helix-coil transition of collagen involves the breakage of hydrogen bonds between the adjacent polypeptide chains of collagen molecules (Zhang et al. 2006).

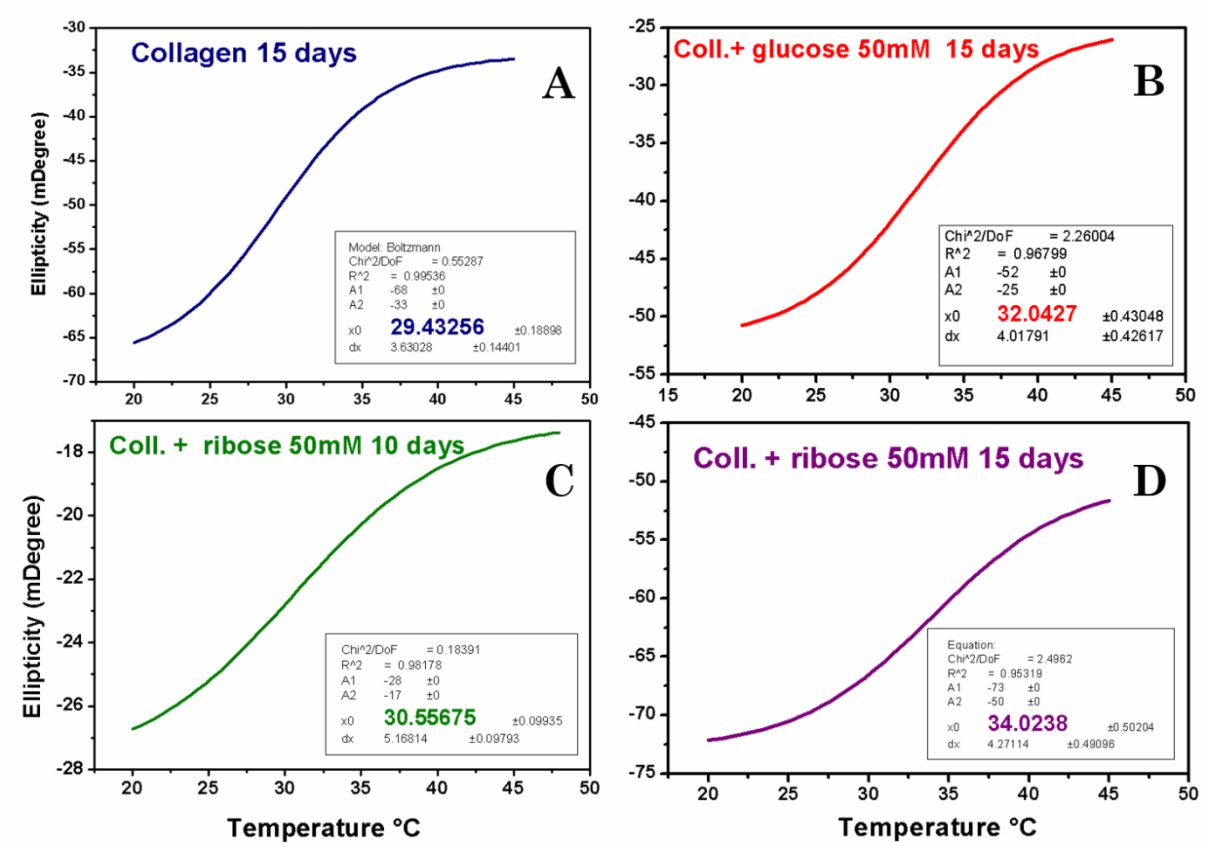

Figure 5.17: Denaturation temperature for pure collagen after 15 days of treatment (panel A), collagen + glucose after 15 days of treatment (panel B) and collagen + ribose after 10 and 15 days of tretament (panels C and D respectively).

In the CD spectra of the samples treated with sugars, some differences are recognizable. First of all, the collagen used as reference sample shows a denaturation temperature (29.4 °C, figure 5.17, panel A) lower that of the native collagen. It has to be taken in consideration that the samples underwent several treatment phases (see chapter 4.1.3). These procedures could probably slightly modify the triple helical structure lowering the denaturation temperature of the samples. However, the figure 5.17 (panel B, C and D) shows a very important result. The denaturation temperature of the collagen samples, treated both with glucose and ribose increases, in particular with ribose after 15 days. This result supports and confirms the results obtained by FT-IR spectroscopy. The glycation reaction increases the rigidity of the collagen secondary structure, avoiding a destabilization of the triple helices, as a consequence of the heating treatments. Thus, the sugars interacting with collagen really play a very important role in the preservation of the protein.

Chapter 6

Results:
Archaeological cases of study

6.1 - Preservation of the mummified remains

The taphonomic modifications of the body after death is a mixed process that, varying in dependence on the decomposition way, involves autolysis, putrefaction, infestation by insects, adipocere formation up to, in particular conditions, the mummification.

In these cases, factors such as the period of time before the body was buried (allowing putrefaction to begin), the environmental temperature, the presence or absence of oxygen, the burial depth of the body, the topography of the soil and its composition, and the type of coffin used, considerably affect the speed and the types of modification of the body.

The formation of adipocere is a natural preservation process that has been known for centuries (Ubelaker and Zarenko 2011). The process begins immediately after death, with the hydrolysis (mediated by enzymes) of the triglycerides, which cleave the fatty acids from the glycerol molecules, producing a mixture of unsaturated and saturated fatty acids. Free fatty acids may bind sodium and potassium ions of the interstitial liquid and cellular water, and later on, to calcium ions, forming fatty acid salts. This process, known as saponification, was improperly considered as a part of putrefaction. Actually, it inhibits putrefaction, increasing acidity and dehydration of the tissues, and, as a consequence the growth and spread of putrefactive organisms is reduced.

Mummification is a process of natural or artificial conservation, involving the dehydration and exsiccation of soft body tissues. It may be complete or partial and it may coexist with other forms of conservation and/or putrefaction. It is common to find slight traces of adipoceres in mummified bodies (for example, in Similaun mummy, Otzi). Indeed, there is a close interconnection between these two processes; the water lost by the body during the exsiccation of tissues may contribute to the fat hydrolysis reaction and to the adipocere formation.

As expected, mummification is achieved in dry, ventilated environments and generally, favourited by, warm climates where the body loses fluids through evaporation. More extensive and complete mummification occurs in desert environments. (Schmitt 2006)

Although the most famous mummies in the world are, with no doubt, the embalmed ones, during the most ancient period of the Egyptian history, a type of natural mummification was accomplished. In fact, during the pre-dynastic period (from 6000 BC to 3100 BC approximately), that corresponds to the Neolithic age, that means before the Pharaonic dynasties began, the bodies were buried in desert soils, on the borderline of cultivable lands, in order to preserve the necropolises from the Nile floods. The tombs, usually circular or quadrangular, were directly excavated in the soil. The bodies were laid down in foetal position,

with the head pointing to the South and the face turned to East, wrapped in wickers or canvas and in some cases, surrounded by precious grave goods. In this way, the bodies mummified naturally, thanks to high temperature, incoherence and chemical composition of the soils, which all allowed a quite fast dehydration of the buried bodies. In the Pharaonic ages, the monumental tombs such as mastabas and pyramids, did not guarantee the same micro environmental conditions of the desert soils anymore. So the necessity to preserve the body after death leaded to the setting of the embalming procedures which evolved and were refined during the historical ages (Donadoni Roveri 1988; Cimmino 1994; Dunand and Lichtenberg 1997).

Mummification also takes place in icy environments, thanks to the dryness of the air and to the low growth of bacteria at such temperatures. (Schmitt 2006)

The mummification process, both in case of natural or embalmed mummies, even though it induces modification in the skin structure and morphology, it preserves tissues from decaying, providing a preservative aging" of the bodies, which are able to resist to degradation over thousands of years (Bridelli et al. 2011).

6.1.1 - Case I: Natural and embalmed Egyptian mummies.

One natural pre-dynastic mummy and ten heads of embalmed dynastic mummies were studied. In Figure 6.1, the spectra of three mummified skin samples, collected from a naturally mummified pre-dynastic mummy (red line), and two Egyptian embalming mummies (9092: green line and 996: blue line) were superimposed with the spectrum of a modern skin sample, to observe their main features. The spectra show the main absorption bands of Amide (A,B, I, II, III) characteristic peptide bonds of proteins.

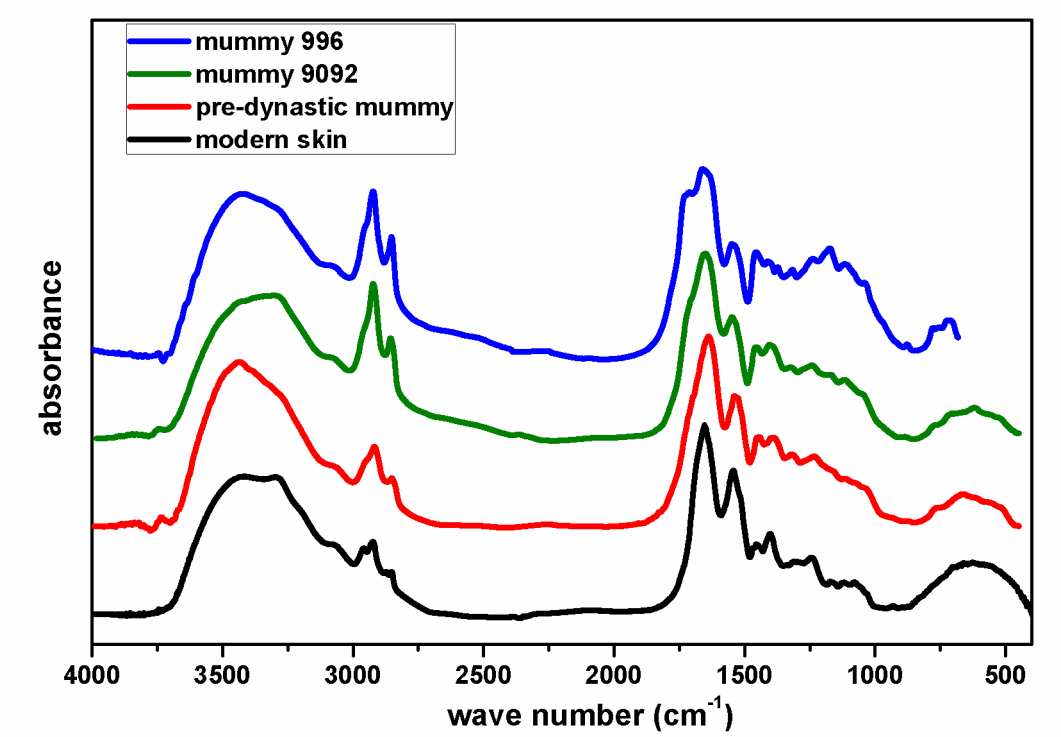

Figure 6.112: FTIR Spectra of skin of Egyptian mummies (embalmed mummies 996 and 9092: blue and green lines; Pre-dynastic mummy: red line). The black line is the spectrum of a modern skin sample assumed as reference

With the aim to investigate the protein structure, the attention was focused on the amide I band region, submitting the bands of the four spectra to a fitting multi-peaks procedure. The deconvolution analysis on FTIR Amide I bands for the mummified sample spectra shows a differences of the conformation of collagen structure, if compared to modern skin sample, as shown by Bridelli et al. (2011; 2012) (Stani et al. 2014).

Following the second derivative spectrum, the Amide I bands of the modern skin sample was deconvolved by means of 5 Gaussian sub-bands. The sub-bands obtained are peaking around 1690, 1660, 1640, 1630 and 1610 as displayed in Figure 6.2. A lengthen of the Amide I bands of the mummified samples towards high wave number was detected.

For this reason, it was necessary to deconvolved the spectra by means of 7 sub-bands. The percentage areas of the bands are listed in table 6.1.

The pre-dynastic sample shows a decrease of the percentage amount of α-helix (22%), compared to the content detected in 9092 and 996 ones (respectively 27% and 39%) and in the modern skin (40%). The low α-helix content, accompanied by an increase of the triple helix in the disordered state (22%) might be interpreted as a partial uncoiling effect of the native collagen structure in the naturally mummified remain (Payne and Veis 1988; Bryan et al. 2006; Rabotyagova et al. 2011; Vidal and Mello 2011) .

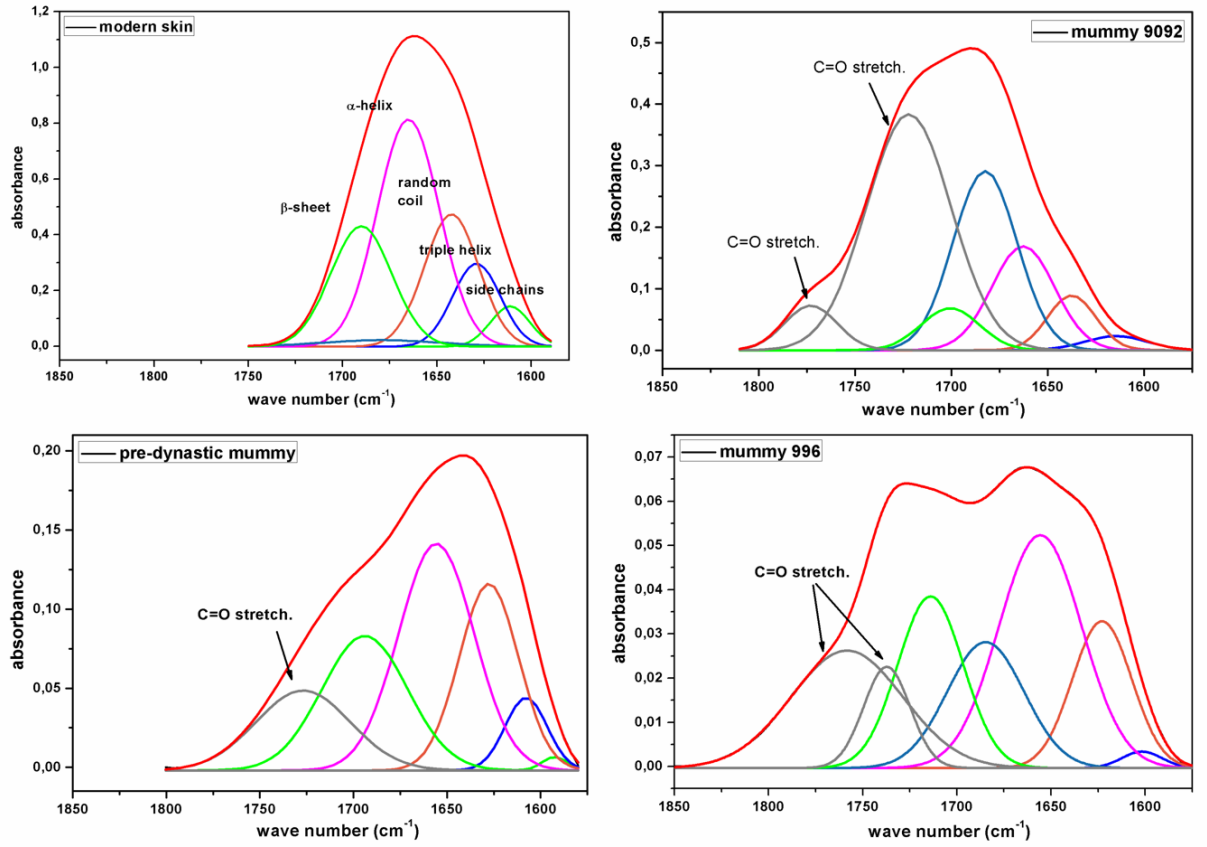

Figure 6.213: Amide I band deconvolution of modern, mummy 9092, pre-dynastic mummy, mummy 996 skin samples

In the amide I bands of the two embalmed mummies, the increase of the percentage amount of the β-sheet and β-turn motifs was recorded. It could be related to the increase of cross-link formation among triple helices consequent to the aggregation of collagen triple helices, which associate forming β-sheet-like structures, and which are indicative of the formation of aging products.

	Secondary structure (% area)				
	β-sheet	**β-turn**	**α-helix**	**Random coil**	**Triple helix**
Modern skin	21	2	40	20	11
Pre-dynastic mummy	15		22	15	22
Embalmed Mummy 9092	10	48	27	11	4
Embalmed Mummy 996	22	20	39	18	1

Table 6.5: Percentage areas of the sub-bands obtained by the deconvolution procedure in respect to the total area of the band.

All the three samples of mummified skin show some additional bands in the high wave number side of the Amide I band: it can be assigned to the C=O stretching vibrations and it can be considered due to the carbonyl moieties of lipids.

The presence of lipids in the embalmed skin samples may be explained in relation to the use of oils and balms during the several steps of the embalming procedure. In the pre-dynastic mummy spectrum, this band cannot be attributed to this, due to the lacking of any treatment of this mummy, but its presence can be justified as the trace of as a first step of the adipocere formation (Cotte et al. 2005; Forbes et al. 2005; Stuart 2007).

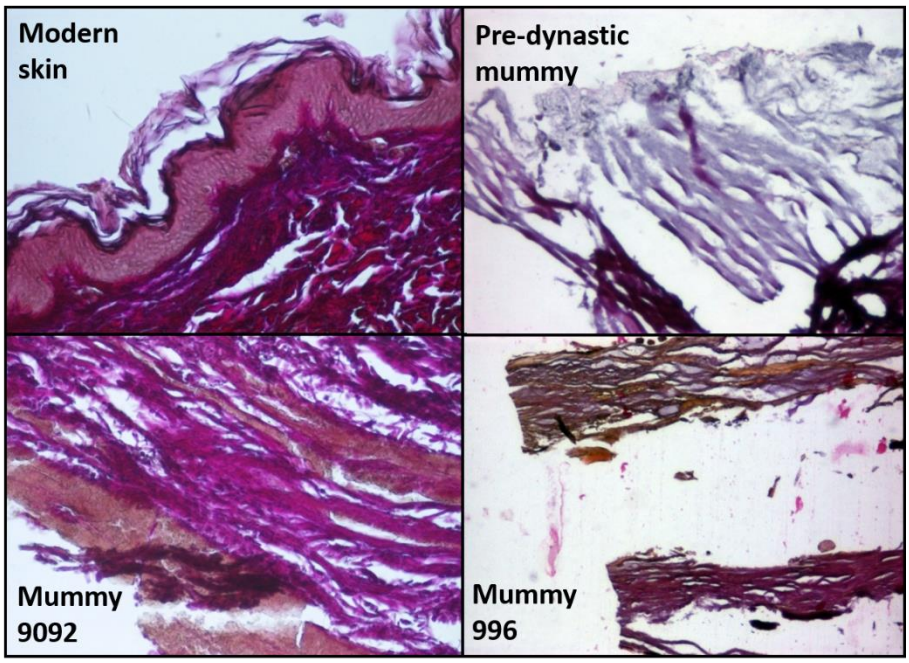

Figure 6.3: Histological sections. a) Modern skin (EE x120); pre-dynastic mummy skin (EE x60); mummy 9092 skin (EE x120); mummy 996 skin (EE x30)

Histological analyses confirm the results of spectroscopical measurements. Dynastic and pre-dynastic samples exhibit remarkable differences in the general architecture of the skin. In all the samples neither epidermis nor other types of cells can be observed and, although derma collagen fibers are well recognizable in both kind of samples, they display different appearance in the various specimens. In the pre-dynastic mummy, sample collagen fibers are bluish-purple stained and show a liquid-like appearance, due to the gelatinization phenomena indicative of an unfolding of the protein structure (Figure 6.3) (Stani et al. 2014).

In the dynastic sample n° 9092 they are deeply pink stained and show features resembling those in modern skin (Figure 6.3) (Stani et al. 2014). In the 996 dynastic sample, two layers of collagen bundles are clearly discernible, separated by an empty space (Young et al. 2007). The first one displays a brownish-yellow colouration, which may be attributed to the embalming substances soaked into the collagen fibers. The balms penetrated through the skin surface deeply in the tissue. In the second layer, collagen fibers are deeply pink stained and show a thinner structure than the fibrils in the first layer. Considering that the sample was collected from the mummy scalp, this second layer could represent *galea capitis* layer (Ottaviani 2008) and the optically empty space might be the space originally occupied by hypoderm, which is degraded.

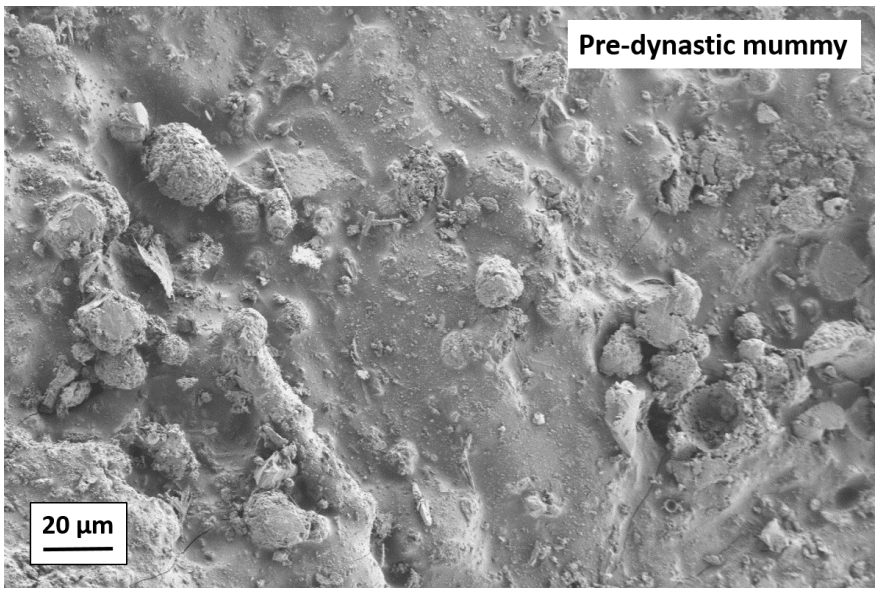

Figure 6.4: SEM image of the skin surface of the pre-dynastic mummy. No skin structures are recognizable.

Figures 6.4 and 6.5 represent the SEM images taken respectively on the pre-dynastic mummy skin and the embalmed one, for different mummy remains. In the SEM image of the pre-dynastic mummy (figure 6.4) no type of skin structures are recognizable. The small circular

objects on the skin surface could probably be identified as sand or dust grains, due to the soil where the mummy was buried (Do Seon et al. 2008).

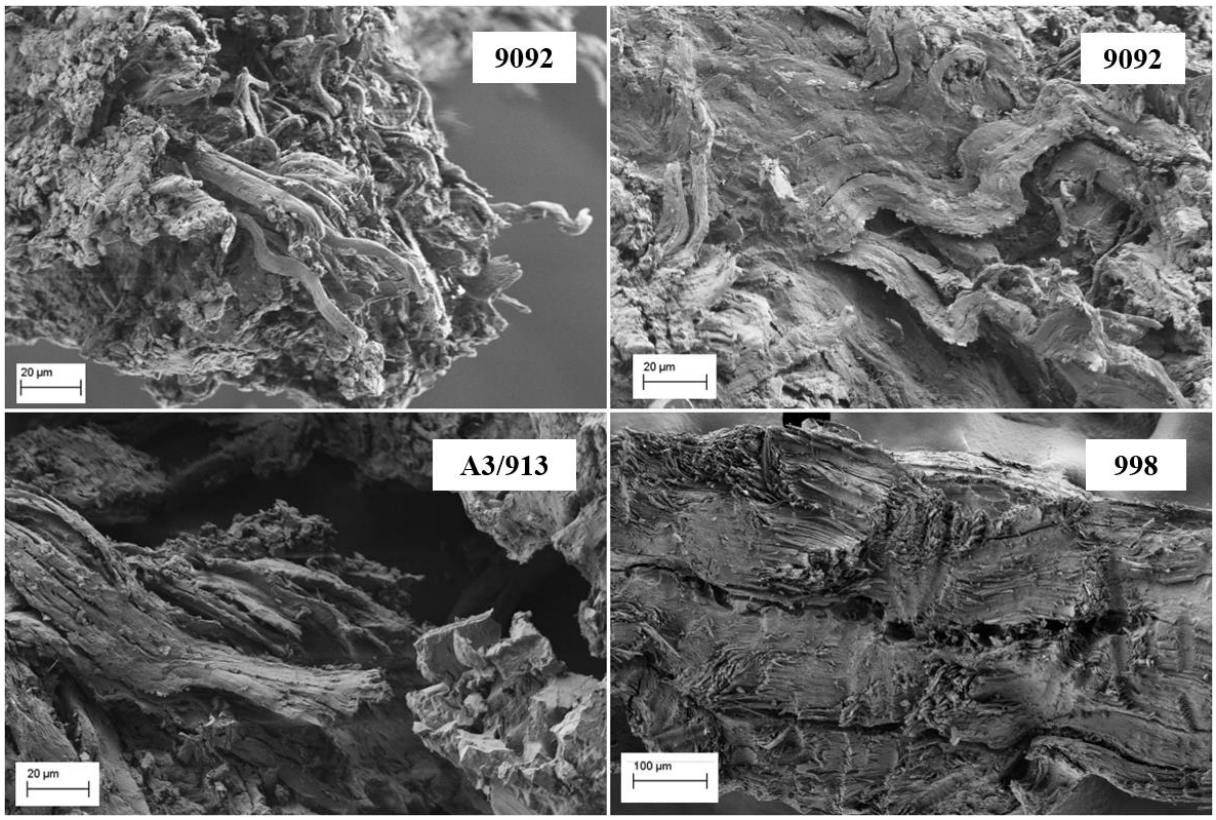

Figure 6.514: SEM images of the embalmed skin samples of the mummies 9092, A3/913 and 998

SEM images of samples taken from embalmed remains (figure 6.5), instead, show very well preserved collagen fibers and big bundles of fibers, exhibiting a strong dehydrated and stiffened appearance. The close packing of the fibers could be indicative both of the cross-linking increase and of the soaking of the tissue by the embalming agents.

Thus, it is possible to assert that the pre-dynastic mummy skin appears in a worse state of preservation, if compared to the skin of the dynastic mummies. In the pre-dynastic mummy, in fact, strongly degraded and gelatinised collagen fibers were detected, whereas in the embalmed mummies they still exhibit very well preserved features, even though dehydration and aging could have produced protein conformational alterations, as shrinkage and/or lengthening of the triple helix. This fact suggests that the embalming process is indeed more successful in preserving tissues from deterioration than natural mummification.

6.1.2 - Case II: Modern natural mummies from Roccapelago

Three samples of mummified skin belonging to Roccapelago mummies were analysed by means of Scanning Electron Microscopy and FTIR Spectroscopy.
Figure 6.6 shows several SEM images of the samples P17, P57 and P86.
In panel A, sample P17 exhibits a multi-layered epidermis, that is several microns thick, completely detached from the dermis. The layers show a stiffened and dehydrated appearance, no cells are observable. In panel B, instead, it was possible to recognise some of the epidermal layers, which are still attached to the dermis (indicated by an arrow and a star respectively) (Do Seon et al. 2008). The dermis layer shows an amorphous appearance and no structures are visible.

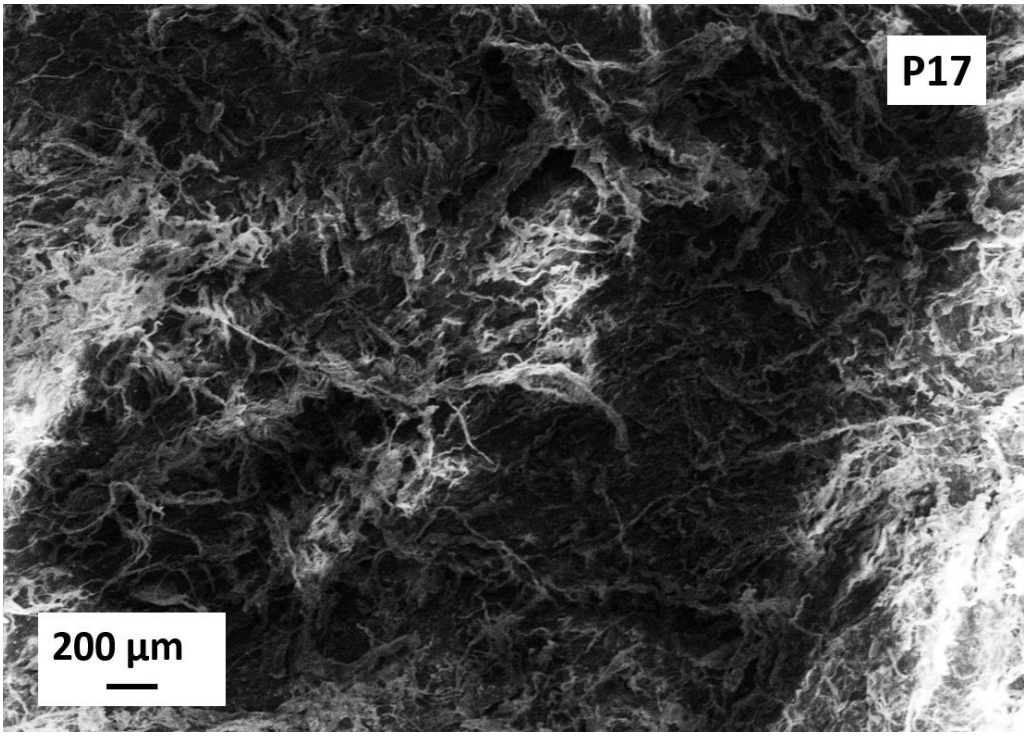

Figure 6.6: Thin collagen fibers in an irregular arrangement

Another image of this sample shows very thin collagen fibers in an irregular arrangement (figure 6.6). These could represent the collagen IV fibers constituting the basal lamina, the layer that interconnect epidermis and dermis layer (Do-Seon et al. 2008) .

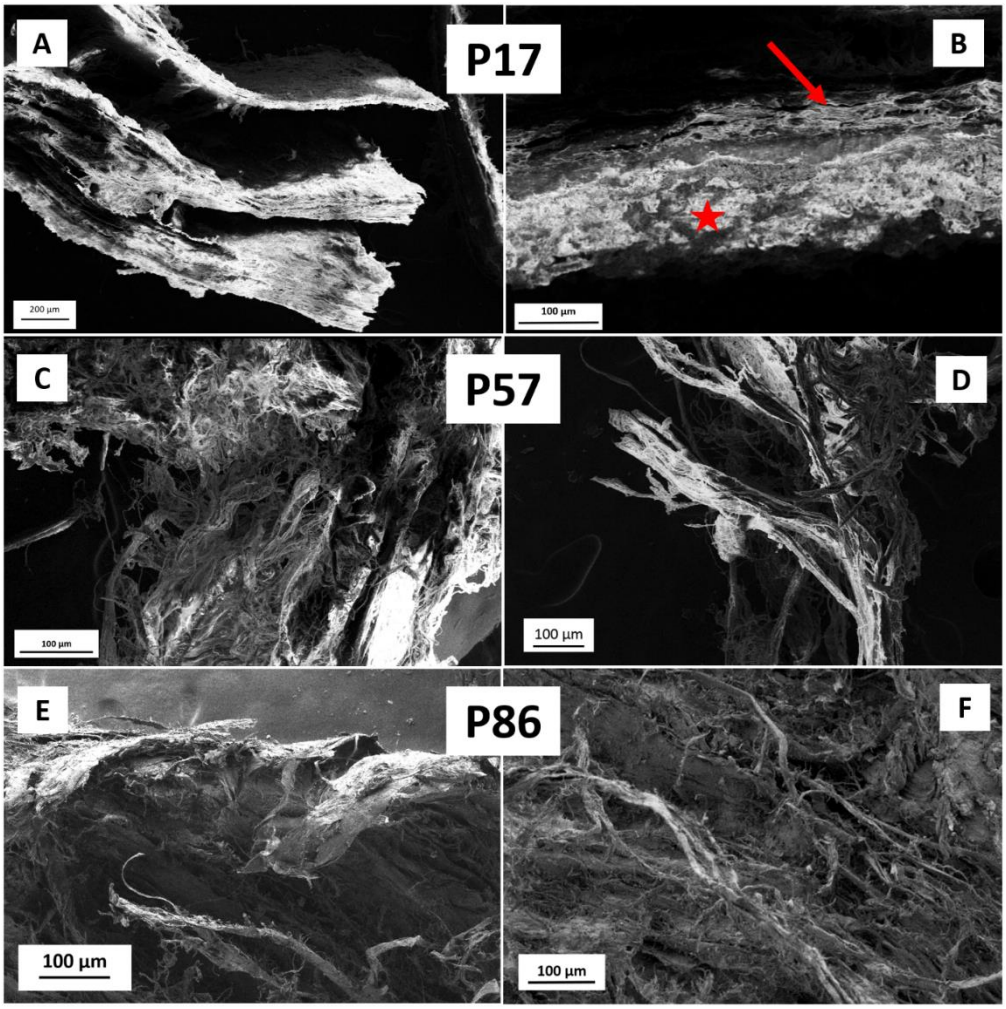

Figure 6.7: SEM images of mummified skin samples from Roccapelago. Sample P17: isolated epidermal layers (panel A) and epidermal layers still attached to dermis layer (panel B). Sample P57 and P86: collagen fibers in an irregular arrangement (panel C), unrolled and broken collagen fibers (panels D, E, F).

Panels C, D, E and F of Figure 6.6 display different regions inspected of samples P57 and P86. They show collagen fibers both in big bundles and in an irregular arrangement. The bundles appear strongly dehydrated and stiffened, and this is due to the aging processes. In some points, the collagen fibers are strongly unwrapped and broken, showing a great state of disorder. These features are indicative of a remarkable damage of the collagen structure.

Figure 6.8 represents a magnification (5,500x) of the image shown in Figure 6.7, panel F (sample P86). In this picture, collagen fibrils are observable. A striated motif of these structure s is recognizable. Due to the low image resolution, it was not possible to measure the length of each striation, but we can hypothesize that this motif could represent the typical collagen D-period. The result supports the assumption that collagen, although exposed to highly damaging conditions, however preserves its secondary structures.

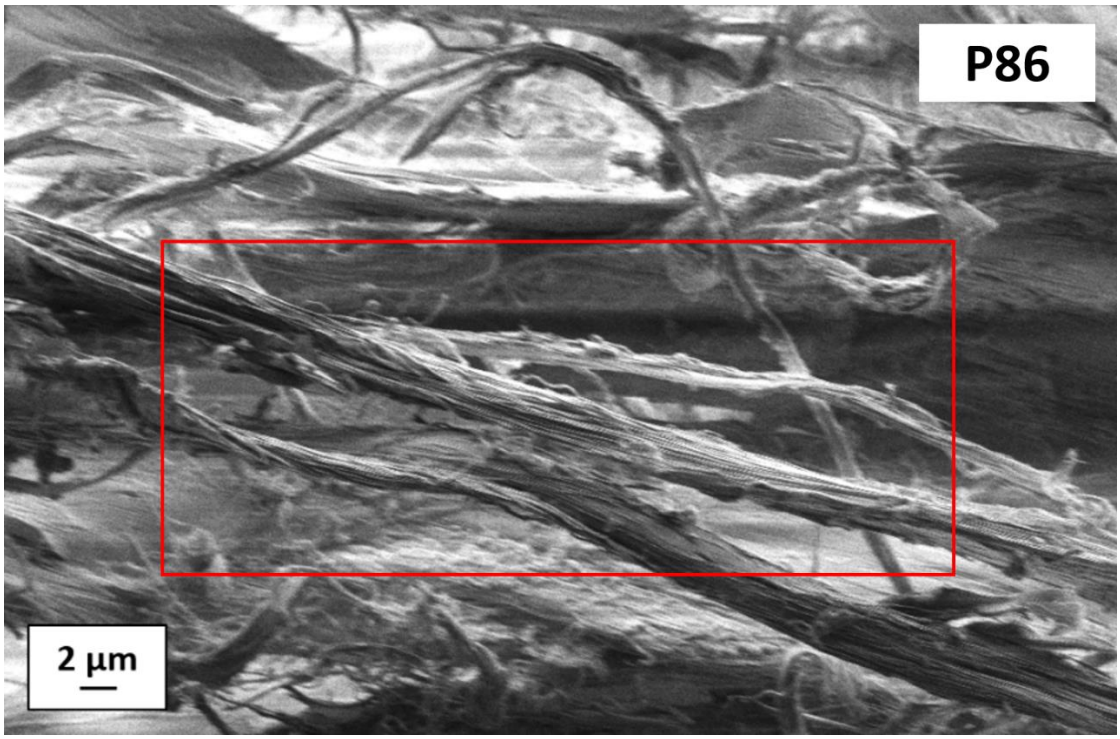

Figure 6.8: SEM image of P86 sample. Magnification (5,500x) of the panel F, figure 6.6. Collagen fibrils can be recognized. An interesting banding pattern is highlithed by a rectangular selection.

Figure 6.9 shows two images collected in different points of the sample P57. As indicated by the red circles and the arrows, some spherical structures can be seen. These structures are present in a great amount almost in every image collected on this sample. The evaluation of the shape and the size of these structures suggest that they could be some kind of leucocytes. Leucocytes are usually located in the lymphatic system, but in case of skin inflammatory diseases, they could cross the vessels and spread into the connective tissue. Since anthropological and medical studies revealed these mummies show alterations caused by several diseases (affecting also the skin) and infestantions by insect and parasites, we can suppose that leucocytes may be related to some kind of pathological state. Further studies, such as histological and immunocytochemical analyses would be necessary to confirm this hypothesis.

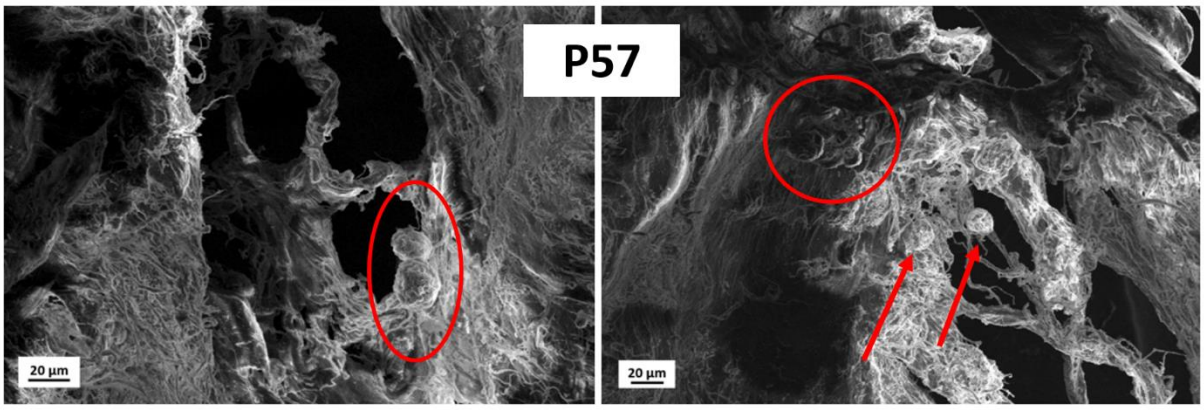

Figure 6.9: SEM images of sample n° P57. Spherical structures, maybe leucocytes, spreading among the collagen fibers are indicated by red circles and arrows

As a general consideration, SEM images of the samples showed different degrees of preservation of the tissue components, not only in the various samples, but even in the different scanned areas within the same sample. Epidermal layers and collagen fibers, and some kind of cells, were identified.

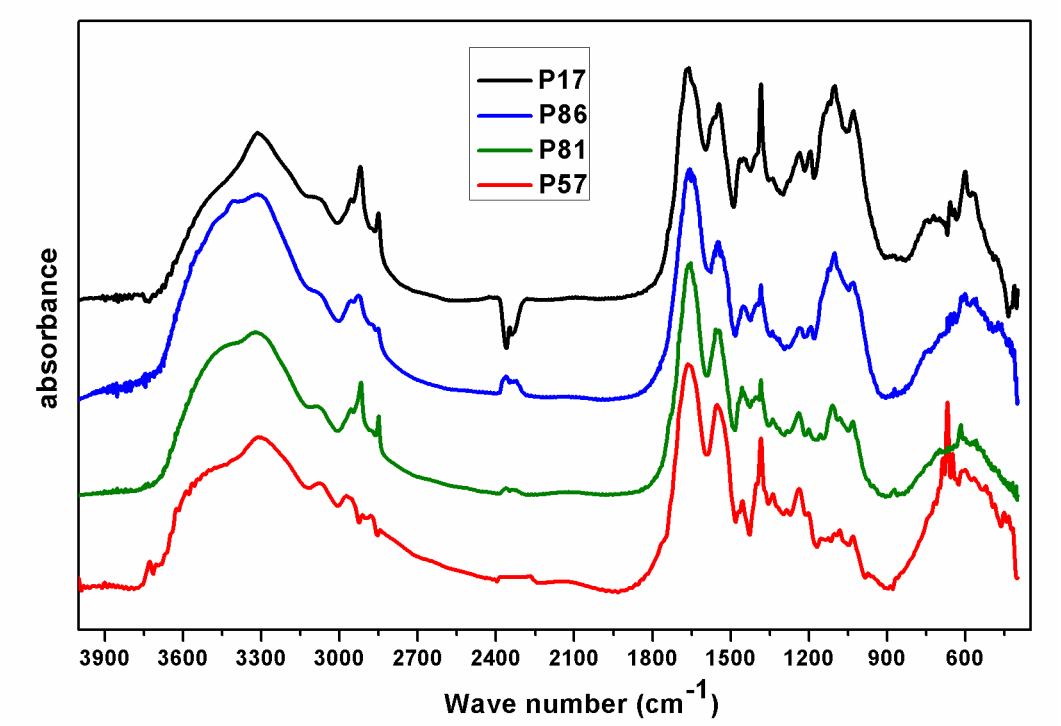

Figure 6.10: FTIR spectra of mummified skin samples from Roccapelago: P17 (black line), P86 (blue line), P81(green line), P57 (red line).

Small fragment of skin taken from the different specimens were studied by means of FTIR spectroscopy. The obtained spectra are displayed in figure 6.10. The spectra exhibit several characteristic absorption bands and different amplitude ratios among the main peaks reveal diverse structural alterations of the tissue, which can be related to the different preservation degree of the remains.

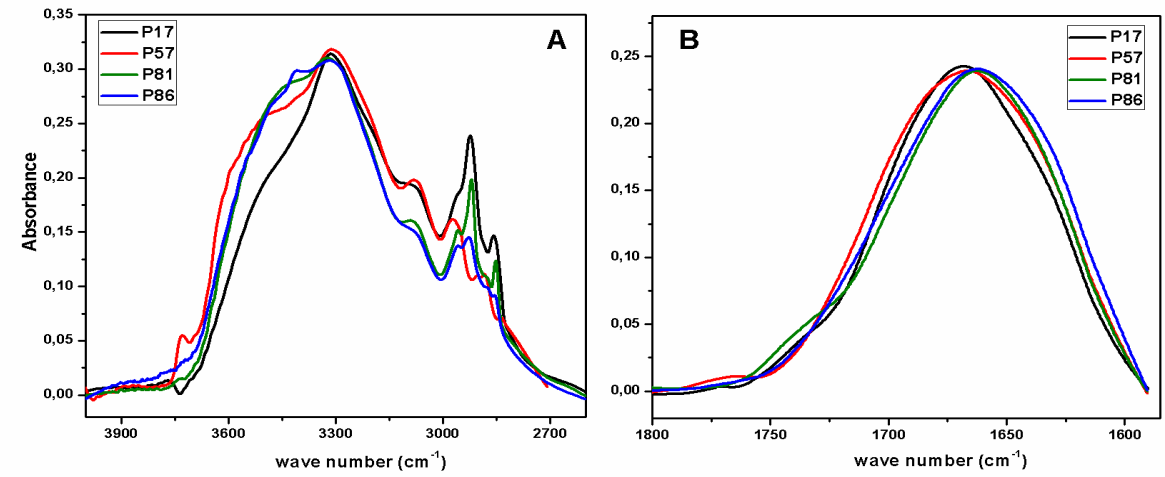

Figure 6.15: Roccapelago mummified skin samples. Panel A: OH stretching band (4000-2600 cm^{-1}); panel B: Amide I band region (1800-1600 cm^{-1})

The water bands in the high wave numbers region show different profiles among the samples, demonstrating they possess a different hydration degree as shown in figure 6.11, panel A. The sample P17 seems to have undergone the more intense dehydrated process if compare with the other samples. In the other samples, we can hypothesize that the water fraction (around 3400 cm^{-1}) corresponds to the free water component. This water does not interact directly with the macromolecule structures of the subcutaneous tissue, but it represents just the ambient humidity absorbed by the mummified skin. The identification of this water component confirms that collagen, after a severe dehydration, cannot restore at all its complex molecular hydrogen-bonds pattern with water, but these molecules are just stored in tissue layers.

The amide I bands of the samples show a modified band profile that indicates a modification of the collagen structure, due to the aging processes. The amide I bands display a shoulder around 1735 cm^{-1} which can be assigned to C=O stretching vibration. This band together with the bands in the spectral regions 3000-2800 cm^{-1} and 1400-1200 cm^{-1}, lead towards the hypothesis of an accumulation of lipid species constituting adipocere (Stuart et al. 2000). The sample P17, together with the sample P81, they show the highest amount of these substances if compared to the other samples as shown in figure 6.11, panel B.

The spectra of the samples P17 and P86 show very intense bands in the spectral interval 1000-1100 cm^{-1} corresponding to the characteristic C-O-C groups vibrations which reveal the accumulation of advanced glycation end products (Roy et al. 2010). The increase of the amount of these substances in the tissues causes a modification of the mechanical properties of the skin namely a decrease of elasticity and flexibility.

The presence of keratin, the main component of the epidermal layers (observed by SEM analysis) is proven by the presence of the band around 540 cm^{-1} due to the disulfide bridges stretching vibration. The band changes its shape in the different samples examined and shifts

towards higher wave number, with respect to the feature recorded in a modern epidermis sample (see the spectrum of modern skin in figure 6.1, black line).
The change of the band is indicates that keratin still shows its own structure mainly characterized by α-helical motif, even though the shift of the band, which can be related to a decrease in the S-S bridges amount, suggests local structural modifications.

In the light of the results obtained by SEM and FTIR spectroscopy, it is possible to affirm that the sample P17 exhibits the highest level of damage. FTIR spectrum shows very intense absorption bands of lipids suggesting adipocere formation, and the accumulation of a great amount of AGEs products is testified both by the strong bands between 1100-1000 cm^{-1} and indirectly by an altered shape of the amide I band. These data suggest heavy structural modifications of collagen and keratin, also proven by the SEM analyses that showed the stiffened epidermal layers, the impossibility to reveal dermal structures in some areas of the sample and very disordered collagen fibers in other ones. The low level of hydration of this sample, if compared to the others can be a consequence both of the role of barrier against humidity, played by adipocere, and of the close packing of the collagen molecules caused by the accumulation of the aging products.
The extensive macromolecular alteration processes to which the sample was subjected could be explained by two hypothesis. The first one suggests that the body was collocated in the middle of the stratigraphic unit partially or completely covered by some other bodies. The percolation of the decomposition body fluids of the surrounding bodies, coupled with the insufficient exposition of the body P17 to the cold air-flows, may have triggered the decomposition process, testified by the initial stage of the adipocere formation stopped and replaced by the mummification process. The second hypothesis, instead, is that the decomposition/mummification processes of the bodies may have been influenced by the fluctuations of the climate conditions inside the crypt. These phenomena could have caused a different level of conservation of the soft tissues, in relation to the season when the bodies were buried.

As a general consideration, all the bodies found in the crypt show great differences in the preservation degree. Some bodies are completely mummified, some others only partially.
Both the variations of temperature and humidity inside the crypt, and the proximity with other bodies, which were in different stages of decomposition, could have caused such a heterogeneous state of preservation of these archaeological remains.

6.2 - Fossilised bones

Skeletal tissue is a complex material composed by a mineral phase (constituted by hydroxyapatite) and an organic phase represented by collagen, non-collagenous proteins, lipids and water. The relative amount of each component depends on the organism age, the health and the diet during life. The study of the archaeological bones can provide a great amount of information, not only about the life of the individual, but also on the burial rituals and climate conditions and the aging processes, which the ancient remains underwent to. The severe modifications that the bone undergoes during the burial are named diagenesis; it can evolve following three ways of deterioration: deterioration of the organic fraction, degradation of the mineral fraction, biodegrade.

Damages of the collagen lead to a change in the structural organization, followed by gelatinization and loss of collagen. The protein loss produces an increase of the bone porosity. If secondary minerals coming from the burial soils fill the micro interconnected pores, the bone undergoes a structural modification, called fossilisation, which allows the bone to be preserved for thousands of years. The rate at which collagen is lost, depends on time, temperature and environmental pH. Extreme values of pH can also cause collagen swelling and an accelerated hydrolysis. Collagen is particularly sensitive to alkaline soils.

Bone in the burial environment is exposed to processes of dissolution/re-precipitation of the constituting minerals, as they interact with the soil minerals. The hydrology of the site plays a key role in bone survival. Mineral transformations (caused for example by low pH) expose the collagen to an accelerated chemical and biological degradation.

Finally, microbial degrade, is the most common mechanism of bone deterioration. It is optimized at near neutral pH and can influence the collagen damages when the mineral matrix has already been degrade consequently to the burial environment interaction. It could lead to a complete destroying the bones remains. (Collins et al. 2002).

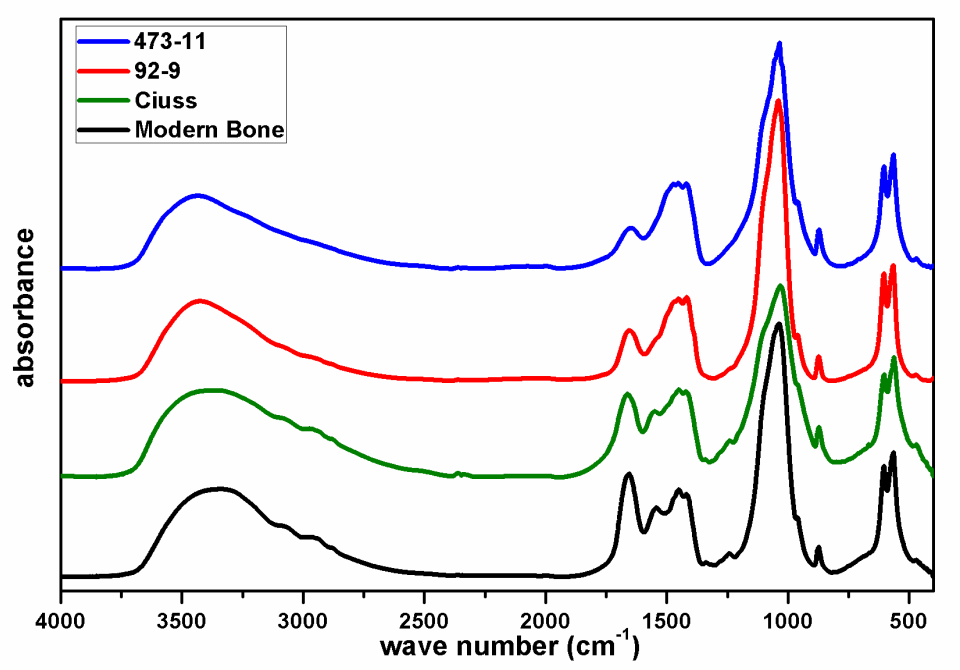

Figure 6.12: FTIR spectra of fossilized bone samples 473/11 (Central Anatolia, V millenium BC, blue line), 92/9 (Central Anatolia, 3000- 2800 BC, red line), CIUSS (Friuli, VI – VII century AD, green line) compared with the spectrum of a modern bone.

In figure 6.12, the spectra of the ancient animal bones from Central Anatolia and Friuli (See Chapter 3) are shown. They are compared with the modern bone spectrum used as reference. The main characteristic bands of the organic and inorganic fractions of the bone were detected. The organic fraction is represented by the amide bands (A, B, I, II and III) peaking respectively at 3300, 3080, 1650, 1550 and 1230 cm^{-1}.

The inorganic fraction exhibits the typical absorption bands of phosphates and carbonates. Phosphates show a broad band at 1035 cm^{-1} ($\nu_1\nu_3(PO_4^{3-})$: symmetric and asymmetric stretching vibration) and the double peak at 604-565 cm^{-1} ($\nu_4(PO_4^{3-})$: asymmetric bending mode). carbonate bands are peaking around 1415 cm^{-1} arising from the asymmetric stretching vibrations ($\nu_3(CO_3^{2-})$) and at 870 cm^{-1} due to the out-of-plane bending mode ($\nu_2(CO_3^{2-})$) (Wright and Schwarcz 1996; Lebon et al. 2010a).

6.2.1 - Mineral matrix.

Through the mathematical treatments of the areas or amplitude of the main bands (Amide I, carbonate and phosphate bands), some indices such as mineralization, carbonate/phosphate ratio, mineral maturity and crystallinity can be obtained from the FTIR spectra. These parameters provide useful information to understand the processes of aging and diagenesis, and thus, the state of preservation of the fossil bones.

The mineralization index is defined as the amplitude ratio 1035/1660 cm^{-1} and it indicates the amount of the mineral fraction relating to the organic one.

The carbonate/phosphate ratio (C/P) is evaluated as the band area ration at 1415 cm^{-1} and 1035 cm^{-1}: it provides information about the relative carbonate and phosphate contents.

The mineral maturity parameter is developed from the ratio of the band areas at 1035 cm^{-1} and 1110 cm^{-1} obtained by means of a deconvolution process of the $\nu_1\nu_3(PO_4^{3-})$ band. The sub-bands are assigned to the mature and immature apatite fractions respectively. It measures the transformation of immature surface-hydrated domains into a more stable apatite lattice, during organism growth (Pleshko et al. 1991; Farlay et al. 2010).

The crystallinity index (CI) is evaluated from the $\nu_4(PO_4^{3-})$ peak splitting and calculated as CI = (A565 + A605)/A595, (where A is the absorbance intensity at the frequencies indicated in the brackets) as reported by Shemes (Shemesh 1990). It expresses the mineral order, in relation to the size of the apatite crystals.

The indices were measured for the fossilized bones analysed and the values are listed in table 6.2.

Sample	Age	Mineralization	C/P	Mineral maturity	CI
473/11	V millenium BC	2.3	0.45	8.8	3.3
92/9	3000-2800 BC	5.6	0.38	8.7	3.3
CIUSS	VI-VII century AD	5.5	0.30	6.1	3.2
bovine	Modern	2.4	0.33	6.2	3.1

Table 6.6: Mineral indices

The value of protein content in the modern bone is around 40%, while the values decrease at 20% and 17% for the samples 92/9 and CIUSS respectively. The sample 473/11, the most ancient bone, shows a percentage value comparable to that calculated for the modern bone.

This could be indicative of a complete modification of the sample that interested both the organic fraction and the mineral one giving a result comparable with that one of the modern bone.

The values of the C/P ratio show slight differences, if compared to the modern bone value. An increase of the values of the sample 473/11 and 92/9 can suggest a modification of the mineral matrix due to the burial environment.

The mineral maturity parameter increases for the most ancient samples (473/11 and 92/9), confirming that the immature apatite component was reduced, while the mature one increases, as a consequence of the bones aging mechanisms.

No remarkable differences were detected for the crystallinity index, suggesting that the crystal order and sizes of the ancient samples are comparable with the modern one. Usually, samples showing a CI in the range 2.8-3.9 can be considered in a good state of preservation.
All the results agree with each other, confirming a general good state of preservation.

6.2.2 - Collagen modifications

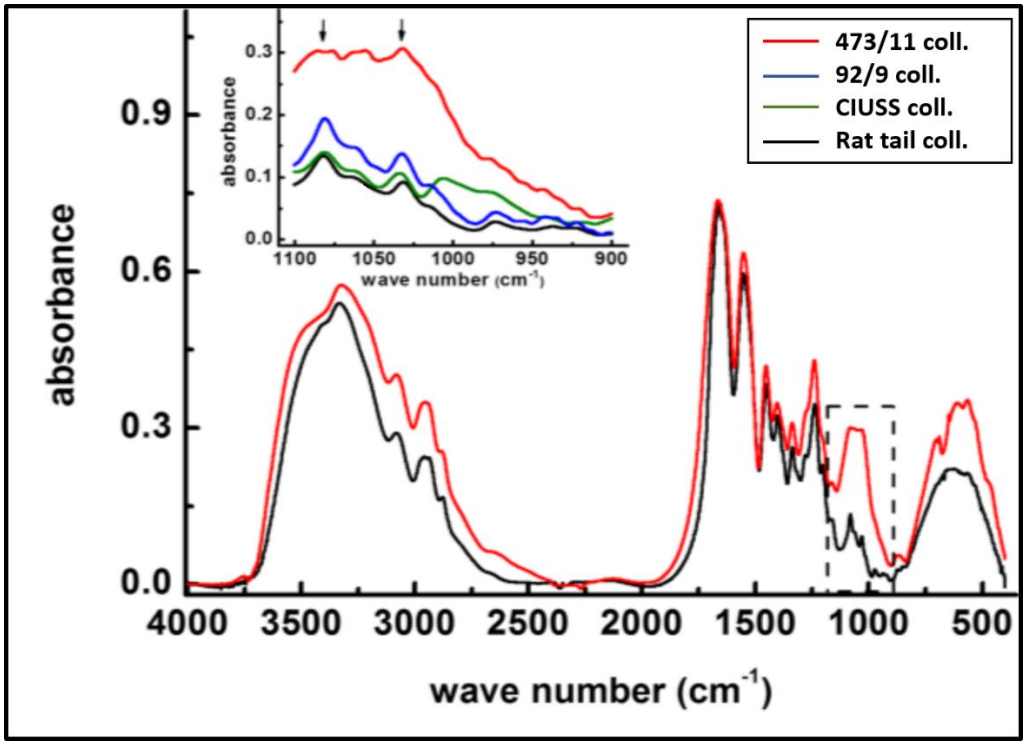

Figure 6.1316: FTIR spectrum of collagen extracted from the sample 473/11 (red line) compared with rat tail collagen (SIGMA). Inset: Spectral range 1100-900: characteristic absorption bands of carbohydrates. Sample 473/11 (red line), 92/9 (blue line), CIUSS (green line), rat tail collagen (black line).

In figure 6.13 the spectrum of the collagen extracted from the sample 473/11 was compared to the rat tail collagen (SIGMA) used as reference. The spectrum of the collagen extracted was normalised at the intensity of the amide I band of the reference sample.
The characteristic band of alkyl groups CH_3 - CH_2 at 2960 and 2850 cm^{-1} and the amide bands were detected as previously described. The bands in the spectral range 900-1100 cm^{-1} in particular, can be assigned to the carbohydrates moieties vibrations. It is known that matrix carbohydrates form a complexes with collagen, as a consequence of the glycation processes. These bands appear more intense in the collagen extracted from the bone 473/11 than in the reference sample as shown in the inset of figure 6.13.
The two main absorption bands are peaking at 1082 cm^{-1} and 1032 cm^{-1} and they correspond to C-O and C-C stretching vibrations and to C-O-H and C-C-O bending vibrations of carbohydrates. As suggest by Roy et al., the amplitude if this band increases with the

accumulation of the advanced glycation end products as a consequence of the collagen aging (Roy et al. 2010).

In order to evaluate the glycation level of collagen for every sample analysed, two glycation indices were measured. They are listed in table 6.3.

The first one was obtained by the calculation of the band amplitudes ratio 1032/1660 cm^{-1}.

It shows a strong increase of the amount of the AGEs in the sample 473/11 with respect to the reference sample and the other ancient bones.

The second one represent the values of the band area ratio corresponding to the α-helix and β-sheet fractions evaluated as A(1655 cm^{-1})/A(1690 cm^{-1} + 1610 cm^{-1}) and calculated from the data obtained by means of the Amide I band deconvolution.

	FTIR Results	
Sample	$\frac{I_{1032}}{I_{1660}}$	$\frac{A_{1655}}{A_{1690+1610}}$
473/11	4.2	4.3
92/9	0.19	3.6
CIUSS	0.15	7.1
Rat tail	0.12	8.8

Table 6.7: Glycation Indices

Shape and position of the amide I bands were compared as shown in figure 6.13, panel A. The bands shift towards lower wave numbers for the samples 473/11 and 92/9.

The amide I band deconvolution procedure was applied to all the amide I bands shown in figure 6.14, panel A. Panel B of the same figure reports the amide I band deconvolution of the sample 92/9 as an exemplificative sample. In this sample, even though the portion of α-helix is still well represented, an increase in the percentage of triple helix and random coil was detected if compared to the amide I band deconvolution of a modern skin (figure 6.2). The increase of triple helix motif could be attributed to an increase in the L-polyproline imino carbonyl groups absorbance caused by the exposition of these groups, as a consequence of a modification of the collagen tertiary structure (Mary et al. 2009). These changes can be followed by a molecular fragmentation with formation of AGEs products.

The calculation of the second parameter provides similar information about the aging of the samples. The increase of the β-sheet percentage areas, with respect to a decrease of α-helix, is indicative of covalent cross-links among triple helices due to the accumulation of AGEs products. This parameter suggests a stiffening of the collagen secondary structure, as a

consequence of the bone aging. The values, in fact, decrease with the increase of the remain age.

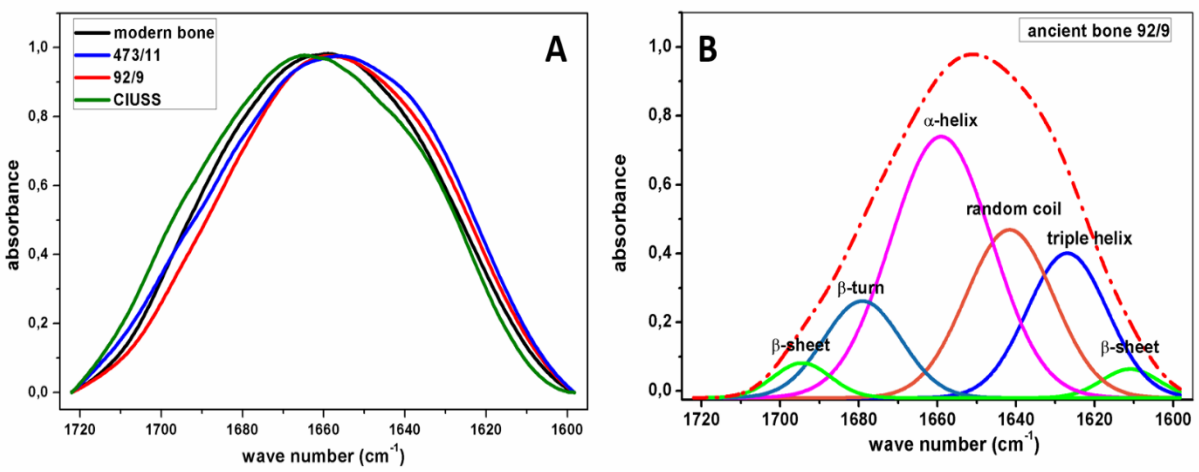

Figure 6.14: Comparison of the Amide I bands shape (panel A). Amide I band deconvolution of the ancient bone 92/9 (panel B)

The results obtained from this parameter are in good agreement with the age of the sample showing the low values form the oldest bone (473/11 and 92/9). The lowest value of the sample 92/9 could be indicative of strong diagenetic medication due to the burial environment.

The samples were also analysed by means of Circular Dichroism. The results obtained by this technique agree with those collected by FTIR Spectroscopy, taking into consideration that the samples were analysed in different phases (liquid and solid respectively). The CD spectra of the reference sample and of the sample 473/11 are shown in figure 6.15 (panels A and B respectively).

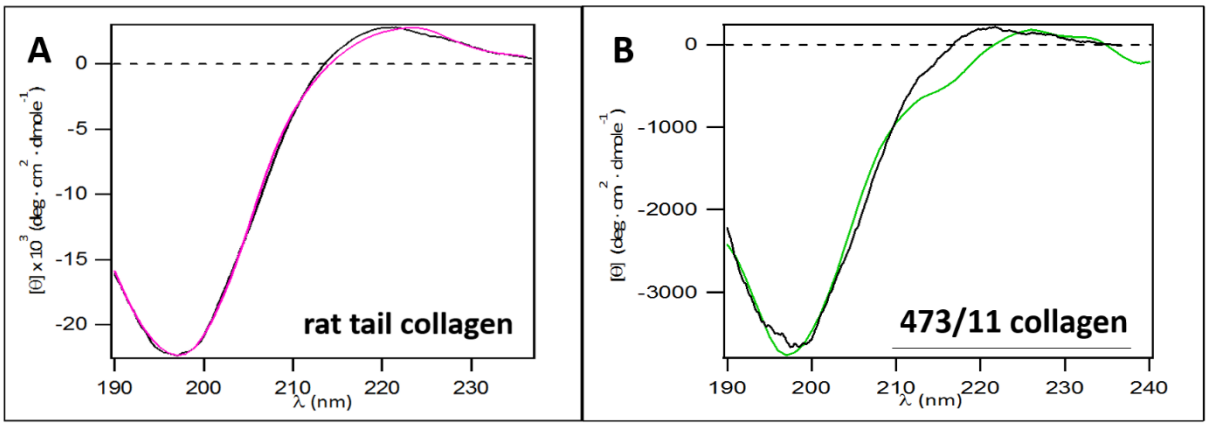

Figure 6.1517: CD spectra of rat tail collagen (reference sample, panel A) and extracted collagen from ancient bone 473/11 (panel B)

The data obtained by the deconvolution of the CD spectra, reported in table 6.4, highlight a decrease in the fraction of α-helix balanced by a slight increase of the polyproline structure and

a decrease of the random coil motif, which indicate a reduction of the collagen fibers size in the ancient samples compared to the reference one.

On the contrary, the increase of the β-sheet structures could be interpreted as the cross-links formation among the collagen fibrils as a consequence of dehydration and formation of aging products.

	CD results				
Sample	**α-helix**	**β-sheet**	**β-turn**	**polyproline II**	**random coil**
473/11	1.4	30.9	12.1	12.8	42.8
92/9	1.6	30.6	12.4	13.1	42.4
CIUSS	1.2	30.8	11.9	12.8	43.3
Rat tail	5.8	18.3	16.0	11.5	48.4

Table 6.8: Results of the deconvolution procedure applied to the CD spectra of collagen extracted from the ancient bone samples and to rat tail collagen (SIGMA), as reference sample.

In conclusion, it is possible to affirm that the combined use of the two techniques applied both on the bone tissue and on the extracted collagen, allows to monitoring the changes occurred in ancient bone as a consequence of both the natural aging of the biological tissue and the diagenetic modifications, which affected the archaeological remains during burial.

The extraction of collagen from the ancient remains, by means of a protocol based on the use of low temperatures and solvents compatible with the collagen structure, allows us to obtain collagen samples reflecting the real conditions of the molecules at the moment of the digging up. The results obtained, in fact, suggest that the procedures of collagen extraction did not add any further modifications to the ancient collagen structure.

Thus, the revealed damages to collagen molecules can be ascribable exclusively to the aging of the archaeological remains. However, the slight changes detected with respect to the modern samples and concerning mineral and protein matrices revealed a general very good state of preservation of the ancient bones analysed.

Chapter 7

Results:

Egyptian embalming agents and biodegrade of the mummified skin

7.1 - Preliminary characterization of the embalming agents

In Ancient Egypt The embalming procedure consisted of several important steps such as brain ablation, evisceration and wash of the body with Nile water, palm wine and spices, dehydration of the body with natron salt, ointment with balms, natural oils and resins, vegetal gums, wrapping and sealing of the wraps with bitumen (only from the XVIII dynasty onwards).

7.1.1 - Natron

The dehydration of the body with natron represented the most important phase of the whole procedure avoiding the decomposition of the body and allowing the start of the mummification process. It was collected from ancient salty lakes. The most important source in the ancient Egypt was the Wadi Natrum lake.

As reported in literature Natron is composed by a polyphasic mixture of carbonates, sulphates and sodium chlorides.

By means of the Scanned Electron Microscopy wide salt concretions were observed on the mummified skin samples of some dynastic mummies (mummies XX6 and A3/913) as shown in figure 7.1. The crystals showed different crystalline habits and peculiar growth indicative of the presence of different minerals phases.

They were further analysed by means of microanalysis EDX (sample XX6) and revealed to be composed by elevated amount of sodium (Na), chlorine (Cl), carbon (C), oxygen (O) and low amount of sulphur (S) and calcium (Ca). The chemical analysis confirm the typical composition of natron. Thus, it is possible to conclude that the concretions really represent traces of the natron used during the embalming procedures.

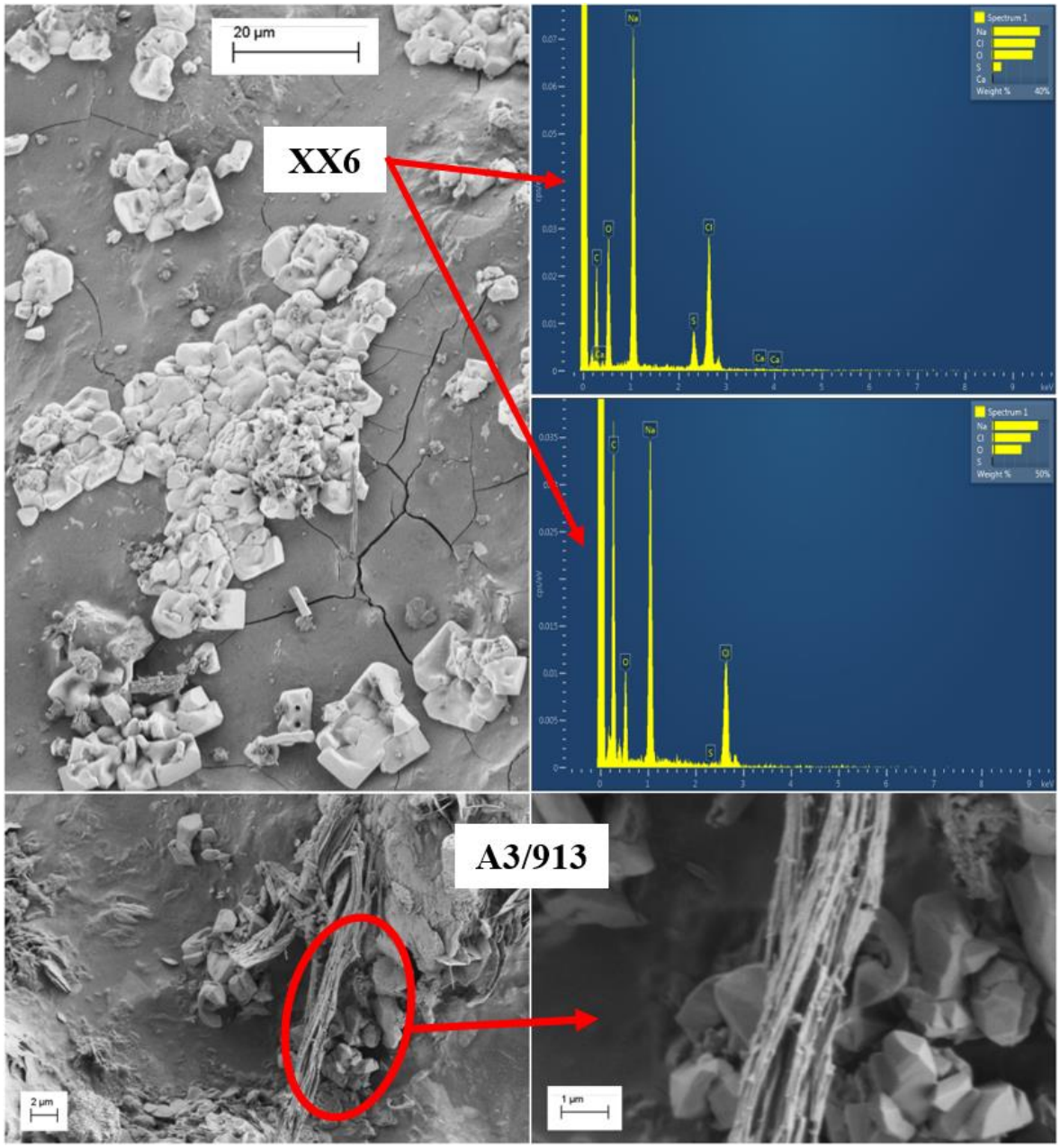

Figure 7.118: Natron crystals on the skin surface of the samples XX6 and A3/913. The crystals of the sample XX6 were analysed by means of Microanalysis EDX. Sodium, Chlorine, Carbon, Oxigen, Sulphur and Calcium were detected as the main chemical elements composing the crystals.

7.1.2 - Balms, oils and resins

The study of the natural substances used during the embalming procedures represent a very interesting field of research. It can provide several information not only on the chemical properties of the embalming agents which allowed the preservation of the bodies during time, but even about the high technological level reached in this practice by the embalmers. During the preparation of the sample 9092 for the histological analysis, some extracts of water and ethanol (see the protocol in chapter 4.2.2) were recovered and analysed by means of FTIR

spectroscopy in ATR mode. All the collected spectra were compared with the spectra of the mainly known substances used during the embalming procedures deposited in the private database of the Chemistry Department of the University of Parma.

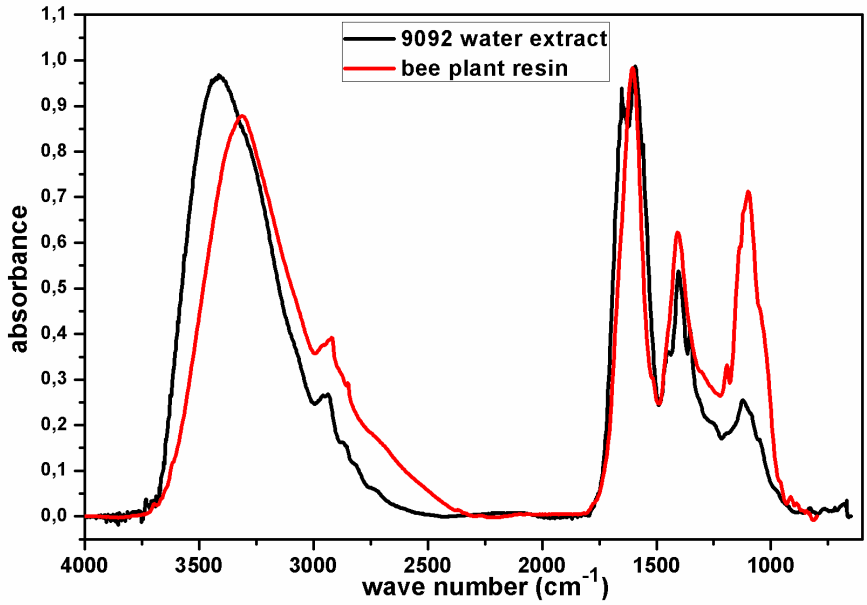

Figure 7.219: Spectrum of the water extract of the sample 9092 (black line) compared to the reference spectrum of a bee plant resin (red line).

The spectrum of the water extract of the sample 9092 showed three broad absorption bands around 1595 cm^{-1}, 1400 cm^{-1} and 1090 cm^{-1}. The absorption bands correspond to the asymmetric stretching of C=O, to the asymmetric vibration of C=O and C-N of amines group and to the C-C, C-H stretching vibrations. It was possible to attribute the extract to bee plant resin. The detected bands, in fact, correspond to the typical infrared signals of alcohols, acids, esters and aliphatic amines of which the bee plant resin is composed (Kothi and Jayanthi 2014).

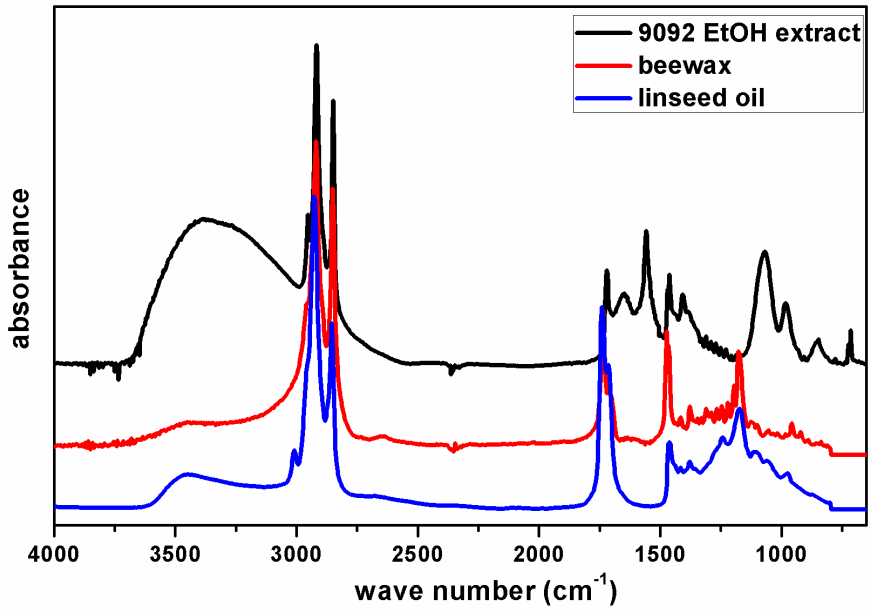

Figure 7.3: spectrum of the ethanol extract of the sample 9092 (black line) compared to the reference spectra of beewax (red line) and linseed oil (blue line).

Comparing the ethanol extract with the database, a possible attribution to bee wax or linseed oil was suggested. Some of the characteristic absorption bands of lipid such as the C=O stretching vibrations at 1740 cm^{-1} and the wagging mode of CH_2 around 1400 cm^{-1} were recognized, as shown in figure 7.3.

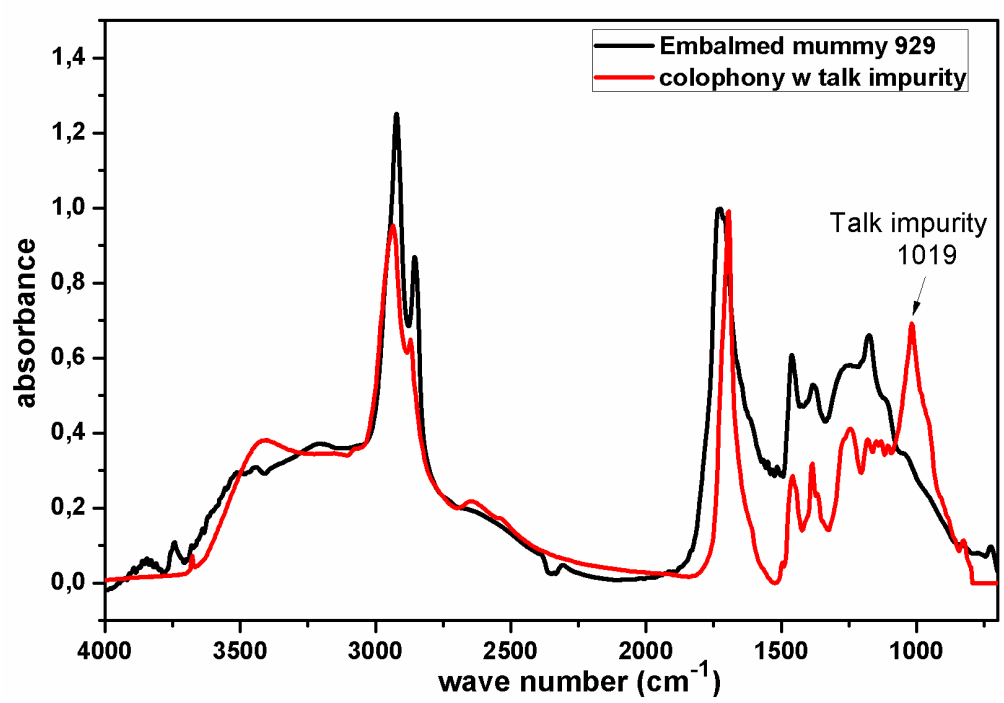

Figure 7.420: spectrum of the sample 929 (black line) compared to the reference spectrum of a colophony resin (red line).

Figure 7.4 shows the spectrum of the mummified skin of the sample 929 compared with a reference spectrum of a colophony. The spectrum of the mummified sample exhibits a broad shoulder in the range 2600-2500 cm^{-1} and the characteristic peak around 1730 cm^{-1} which can be attributed to the ketone C=O stretching vibration. The shoulder at 1620 cm^{-1} is due to C=C stretching mode. The bands at 1467 and 1379 cm^{-1} were assigned to C-H and C-O bending vibrations. The characteristic bands assigned to ketone compounds are considered, in literature, as markers of the presence of the colophony resin (Azémard et al. 2014).

The use of the substances described above for the ancient embalming procedure is attested not only by the ancient sources (Koller et al. 2005) but even by many studies already carried out in this field (Buckley et al. 1999; Buckley et al. 2004; Koller et al. 2005; Colombini et al. 2011; Łucejko et al. 2012).

7.2 - Biodegrade of mummified skin

Fungal colonization and infestation by insect can represent two of the more important phenomena correlated to degrade of the organic archaeological remains.

Fungal deterioration can lead to very fast deterioration of organic materials displayed in the museums, such as mummified remains. Resins, ointment and waxes represent organic substances highly susceptible to fungal deterioration because there are good nutrient sources for the fungal growth.

Improper environmental conditions of storage of the ancient remains can promote a fungal infestation. High humidity accompanied by a lack of ventilation in storage rooms also enhances fungal growth. Fungal deterioration can cause changes in the properties of the mummified remains such as loss of strength, general durability, and discolouration. Furthermore, many fungi contain coloured substances that can cause stains and spots on the ancient biological tissue. The best method to prevent fungal growth in the museums would be the control of the environment in storage rooms in order to protect remains surfaces from contamination, keeping the relative humidity low and avoiding treatments, which may activate germination.

The remains of the Marro Museum collection, unfortunately, do not have these controls available. The mummified head, for example, are stored in cardboard boxes wrapped and acid-free papers and collocated in big wardrobes. The humidity level of the storage rooms, anyway, is not controlled and, probably, subjected to level variations.

The SEM analysis carried out on the mummified remains pointed out in some cases the presence of fungal colonisations as shown in the four pictures of figure 7.5. Both on the natural mummified skin of the pre-dynastic mummy and on the embalmed skin of the dynastic mummies, fungal hyphae were identified. In the pre-dynastic mummy and XX6 mummy the hyphae seems to be septate . The hyphae are long tubular structures constituted by several cells. Every cell is separated from the following by means of an internal cross-wall called septum. In the sample XX6 it is possible to observe that some cell shows a pore (see magnification of the sample XX6, rectangular selection). In all the samples, hyphae exhibit a different aspect. In some areas of the samples they shows the characteristic tubular appearance. In some other region, the tubules seem to be broken, opened or completely degraded (magnification of the pre-dynastic sample, rectangular selection). On the surface of the sample XX11 a very intricate set of aseptate hyphae was detected. This could indicate that the several samples were infested

by different species of fungi. Anyway, the hyphae structure are very simple and no conidiophores were found, suggesting that fungal colonisation could be at the first development stages.

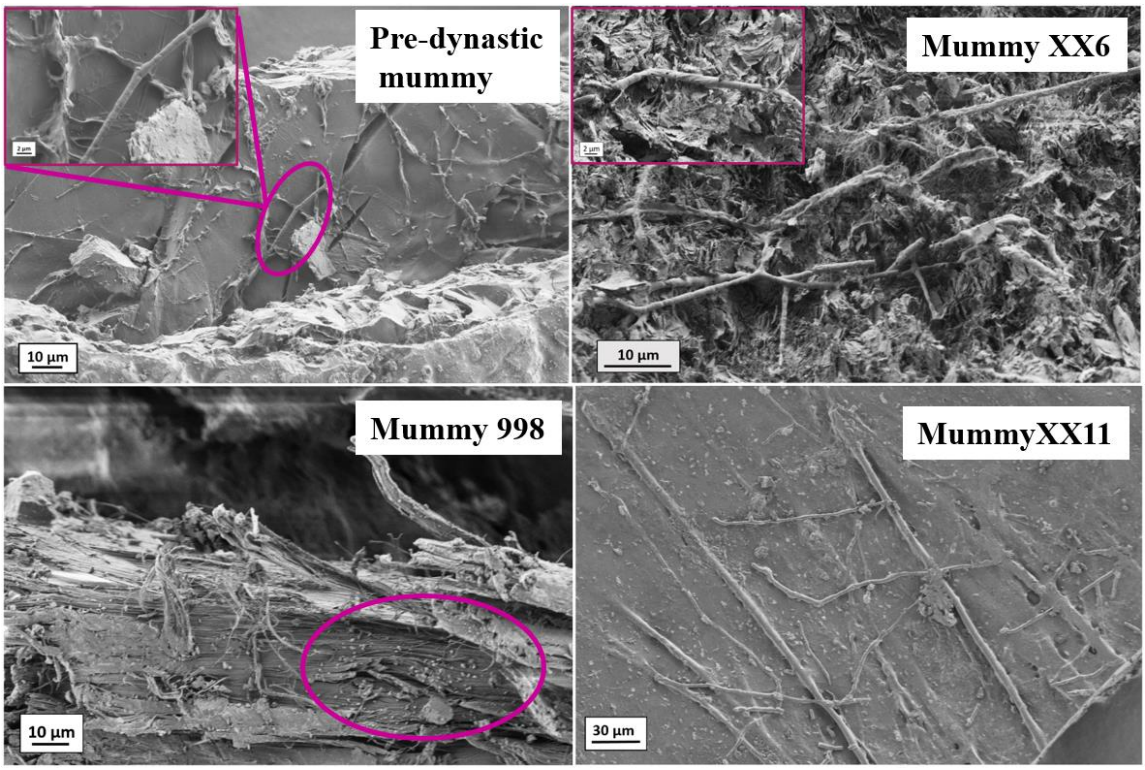

Figure 7.521: SEM images of mummified samples: pre-dynastic and embalmed no XX6, 998 and XX11. Fungal septate hyphae and spores were recognized.

On the skin surface of the sample 998 some very small spherical objects (diameter about 1 µm) were observed. They could represent spores of *Aspergillus* as suggest in literature (Abdel-kareem 2010a; Abdel-kareem 2010b).

Roccapelago mummies, were extensively affected by infestation of a lot of insects attracted by the miasmas due to the decomposition of bodies. A number of entomological studies were performed to analyse this problem which can be related to the life and death conditions of the community . The sample no 57 revealed a very particular finding. The exoskeleton of a very small insect was identified. The evaluation of the anatomy and size suggests the presence of a mite (figure 7.6).

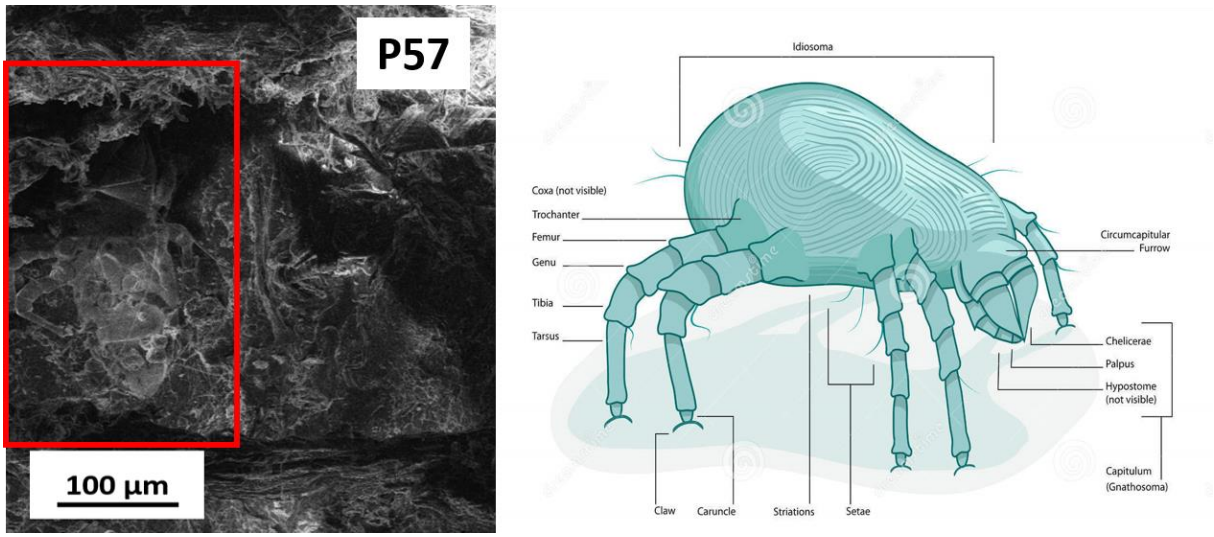

Figure 7.6: SEM image of the skin sample P57 from Roccapelago (left side). The presence of a microscopical insect, maybe a mite, was detected (highlighted by a rectangular selection). An anatomical model of a mite was reported for comparison (right side).

PART II

Chapter 8:

Experimental Archaeology: 2 cases of study

8.1- Case 1:

Deterioration patterns in pigskin subject to wet and dry alkali treatment.

The essential step in the embalming process was the dehydration of the dead body. Egyptians used to employ a natural salt, that is natron, which gathered in crystalline deposits in ancient lakes - now dried out - in the area of Wadi Natrun (Wâdi El Nâtrun, which means in Arabic "Valley Of Natrun"), located 64 km north-west from El Cairo.
The first finding of solid natron, in an archaeological site of the Badarian Period is dated 1937, and it was found out by Brunton, in Mostagedda. In 1925, at Giza, however, small quantities of solution of natron have been found inside some canopic jars. These rare finds have been discovered mostly in jars, vases, packets, which were placed inside tombs of the Dynasty XVIII. They were also placed inside mass graves with other finds, which were scraps from embalming chemicals, which belonged to Dynasties XI, XII and XVIII: for example, some of the scraps were deposits on wood mortuary tables of Dynasty XI or even on the bodies of some mummies of the Middle Kingdom, and of Dynasties XII, XVIII, XX, XXI and XXII (Sandison 1963; Shortland 2004).

Many studies have been done on these salts, and the samples, which were collected and analysed with different techniques, show that the chemical composition changes from sample to sample, depending on where the salt was originated. In general, it is possible to say that the natron salt that was used during the embalming process was made by a polyphasic mixture of carbonates, sulphates and sodium chlorides (Shortland 2004; Edwards et al. 2007; Marchesini and Barresi 2009). This is confirmed by the analyses made on samples taken in the area of Wadi Natrun and by some studies done, in the first half of the 19th Century, on salt finds discovered in tombs.

There are not Egyptian sources which explained the steps of the embalming process, and the use of natron, as the art of preparing the dead bodies was secret and it was passed down from one generation of embalmers to another only orally.

The only information about the use of natron comes from written works of some famous Greek and Latin historiographers. Pliny the Elder, in Book XXXI of Naturalis Historia, lists the countless characteristics of this natural salt: among these qualities, natron is a strong desiccant agent and it is able to prevent bodies from rotting.

Herodotus of Halicarnassus, after a journey to Egypt dated around 450 B.C., in Book II of Histories gives information about Egyptian mortuary rituals. He confirms that the body was "immersed in natron" for 70 days and that natron was able to disintegrate the flesh and to keep the bones and the skin intact. The word "immersed" used by Herodotus suggests that the body was placed inside a tank full of solution of natron. This operation was never proved, actually, and it is strongly questioned by many researchers, who affirm that the dead bodies were placed on some "embalming tables", made of a slightly inclined table, with a drainage draw in the underside, and they were covered by dry natron. Many objects of this kind have been found out while digging out. On the contrary, no tanks and jars made for dehydrating the bodies in solutions of natron were discovered. Archaeologist Joann Fletcher, from University of York, is convinced that some stone sarcophagus were used for that purpose.

Different translations of ancient texts, moreover, call into question even the duration of the salt treatment. Herodotus said it last 70 days, whereas Diodorus Siculus, in Book I of Bibliotheca Historica, say the treatment last around 30 days, without telling more about how natron was used. So, it is more likely that what has been written by Herodotus is the duration of the whole mummification process: from desiccation to entombment.

From the findings of Egyptian mummies to nowadays, many researchers tried the basic technique of the mummification process used in Ancient Egypt, just to confirm the steps of the process, as there are different theories. Many studies focused on the need to clarify which was the real use of natron, if that was used dry or as a solution of natron.

Sandison went through a series of experiments, both trying dry natron or solutions with a different concentration. He affirm that the immersion in liquid natron causes the softening and the embrittlement of the skin, so that it is impossible to bind the body with bandages: however, this is proved wrong from some histological studies on a mummy's skin done by M.A. Ruffer, who denied the formation of a soft mass in the subcutaneous layer.

Both of them, though, confirm that the liquid process causes stink, and even putrefaction, in case the solution is not that concentrated. In the experiments with dry natron, on the other hand, there are not foul odours, as salt neutralise the rests of decompositions and fatty acids.

In 1994, American Egyptology Robert Brier lead the first experiment in human mummification, following the techniques used in Ancient Egypt and using dry natron, with excellent results.

Recently, Stephen Buckley, researcher of University of York, together with Archaeologist Joann Fletcher, after some studies on royal mummies of the tomb KV35 of the Valley Of The Kings, they insisted that there has been an evolution, throughout the centuries, of the embalming

technique, whose peak was reached with Dynasty XVIII, as bodies were treated with solution of natron.

Through X-Ray scans it has been possible to recognise a huge number of salt crystals in mummified tissues. The british researchers affirm that only a body treated with a solution could have allowed the penetration and the crystallisation of salt in the deepest layers of the skin. In 2010, Dr. Buckley and Dr. Fletcher together with a team of anthropologists and paleo-pathologists, they made a new experiment of human mummification on Alan Billis, a British taxi driver, a terminally ill with cancer, who decided to donate his own body for the sake of scientific research.

Figure 8.1: Dr. Buckely and his team – 2010. Mummification of the Alan's body using natron solution and following the XVIII dynasty procedures.

In order to strengthen their theory, Buckley and his colleagues followed the whole embalming procedure as it was in Ancient Egypt, but this time they dehydrated the body in liquid natron. After an internship done in the BioArCh Department of the University Of York, the collaboration between Dr. Buckley, Dr. Fletcher and Professor Collins continued with an archaeological experiment on the pigskin. The skin, treated with both dry natron and a solution of natron was analysed by Fourier Transformed Infrared Spectroscopy, in order to understand which were the main changes of the biological tissue and the structure of collagen, after the two different treatments. The last part of the project had the possibility to analyse, with the same technique, some samples of Alan Billis' skin.

8.1.1 Material and Methods

Natron solution

Due to the unavailability of Natron salt (Wadi Natrun lake is a restricted military area) the salt was prepared following Sandison (Sandison 1963): four saturated salt solutions were prepared and mixed.

The homemade natron mixture was composed with six parts of sodium carbonate (Na_2CO_3), three parts of sodium chloride (NaCl), and half a part of sodium sulphate ($NaSO_4$) and sodium bicarbonate ($NaHCO_3$) each. The pH was 10.93.

Six Falcon tubes (50 ml) were filled with natron solution. The remaining solution was dried out on a heated plate at 40°C to obtain natron salt.

Pigskin samples

The pigskin was purchased from a local factory. After a wash by hot tap water, the skin was washed in a bath of water and Marsiglia soap for 15 minutes. Several washes by tap water and deionized water were performed to eliminate dirt and soap completely. Thirteen small pieces of pigskin (approximately 2.0 cm x 1.5cm, 0.3cm thick) were cut. One of these was untreated and analysed as reference sample.

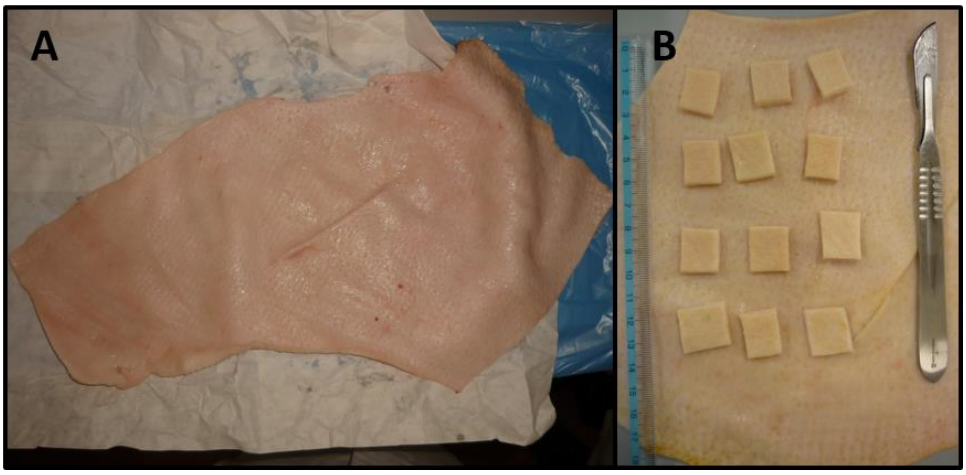

Figure 8.222: Pigskin before (panel A) and after the washes (panel B). The pieces used for the trial.

Six of the sample were put in glass vessels on a layer of dry natron and they were completely covered with a thick layer of salt. The remaining six samples were put into the Falcon tubes previously filled with the natron solution. The tubes were sealed with parafilm to avoid the evaporation of the solution.

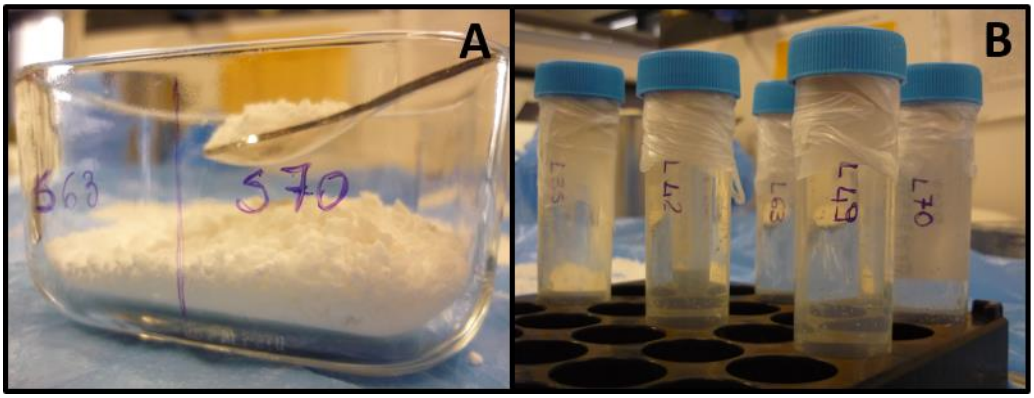

Figure 8.3: the pigskin samples in dry (panel A) and liquid (panel B) natron.

The samples were maintained in an oven at 40 °C to simulate the Egyptian climate condition. All the treated samples were analysed from the 35th to the 70th day after the starting day of the treatment, at different time intervals.

The samples are listed in table 8.1

	Treatment	
Time intervals (days)	**Dry natron**	**Liquid natron**
35	S35	L35
42	S42	L42
49	S49	L49
56	S56	L56
63	S63	L63
70	S70	L70

Table 8.1: List of the samples and time intervals

At the end of every treatment step the samples treated with dry or liquid natron showed a different appearance as shown in figure 8.4. The dry treatment give rise to samples characterized by stiffness and browning appearance, while the wet treatment seems not to change the colour and the natural softness of the pigskin. The samples treated with liquid natron were dried in oven at 40 °C for 3 hours, to eliminate water excess.

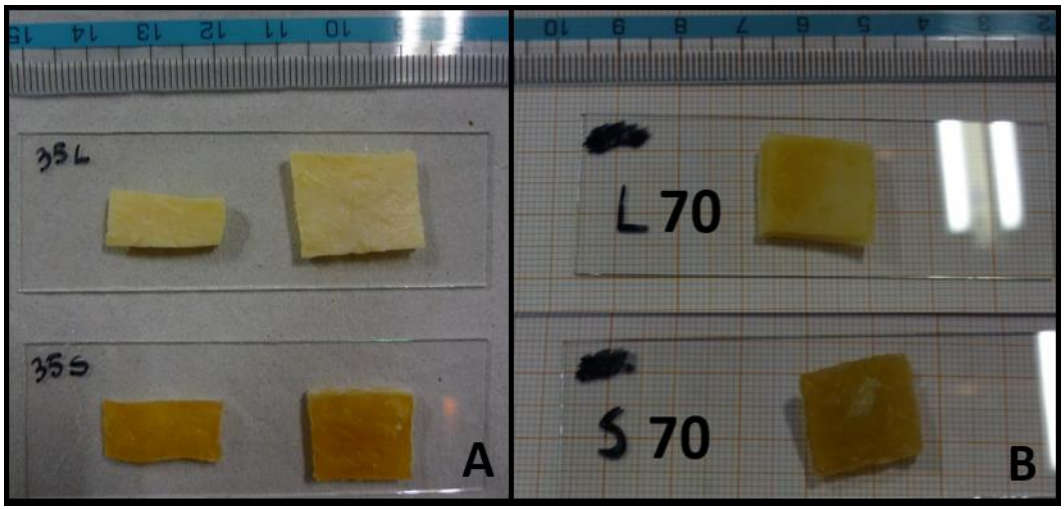

Figure 8.4: Different aspect of the samples treated with dry and liquid natron after 35 days of treatment (panel A) and 70 days of treatment (panel B)23

All the samples were analysed by means of a **VERTEX 70** FT-IR spectrometer in ATR mode equipped with a diamond crystal. The spectra were acquired in the range between 4000 and 600 cm^{-1}, collecting 28 scans with a spectral resolution of 2 cm^{-1}. A background against air was registered and automatically subtracted from the sample spectra by the OPUS FT-IR software. Moreover, applied advanced ATR correction function relating to the ATR accessory used were applied by means of the same software: refractive index of the ATR crystal (diamond = 2.4), the angle of incidence (45 degrees), the number of reflections (nominally 1).

Effect of high pH on collagen.

Collagen is very sensitive to pH variations. A weakly acid pH represents the optimal condition for the preservation of the collagen structure. Variations of the pH towards too much low or high pH can alter the collagen structure until the complete denaturation of the protein. To better investigate the action of the natron solution on collagen, a sample of pure type I collagen from SIGMA-Aldrich was treated with natron solutions at different concentrations.

The natron solutions were prepared at concentration 0.1M, 0.2M and 0.3M.

Collagen was dissolved in each of them at concentration 5mg/ml. About 200 µl of each solution were smeared on a CaF_2 window, dried in air in order to obtain a thin film. The samples were then analysed in transmission mode by means of a **Jasco 420** FT-IR Spectrophotometer.

Skin samples from Alan Billis.

The last part of this work is represented by the study of skin samples from Alan Billis.

Figure 8.5: Alan's arm and foot after the complete mummification procedure.

The samples were collected from Alan's upper left arm and the heel left foot. The samples were prepared by mixing 1mg of sample with 100 mg of KBr, the mixture was then pressed at 6 x 10^8 Pa to obtain thin pellets (diameter 13 mm and thickness 0.2-0.3 mm).

All the measurements performed by the **Jasco 420** FT-IR Spectrometer were collected in transmission mode, at RT, in the wave number range 4000 to 400 cm^{-1}, collecting 128 scans with a spectral resolution of 2 cm^{-1}.

8.1.2 - Results

Figure 8.6 shows the spectra of the untreated sample (black line) and of the samples treated with liquid (blue line) and dry (orange line) natron after 56 days of treatment.

All the spectra show strong absorbance bands peaked at 2927 - 2853 cm^{-1} and 1746 cm^{-1} assigned respectively to the CH_2-CH3 stretching and C=O stretching vibrations of lipids.

The spectra of the samples, subjected to the alkali treatment, show differences in amplitude and shape of the band, relating to OH stretching vibration, in the region of the spectrum at high wave number (3800-3000 cm^{-1}). This is due to the dehydration of the skin tissue caused by natron both in dry and wet treatments.

Amide I, II and III in the spectrum of the untreated pigskin are peaking at 1660, 1545 and 1238 cm^{-1} respectively.

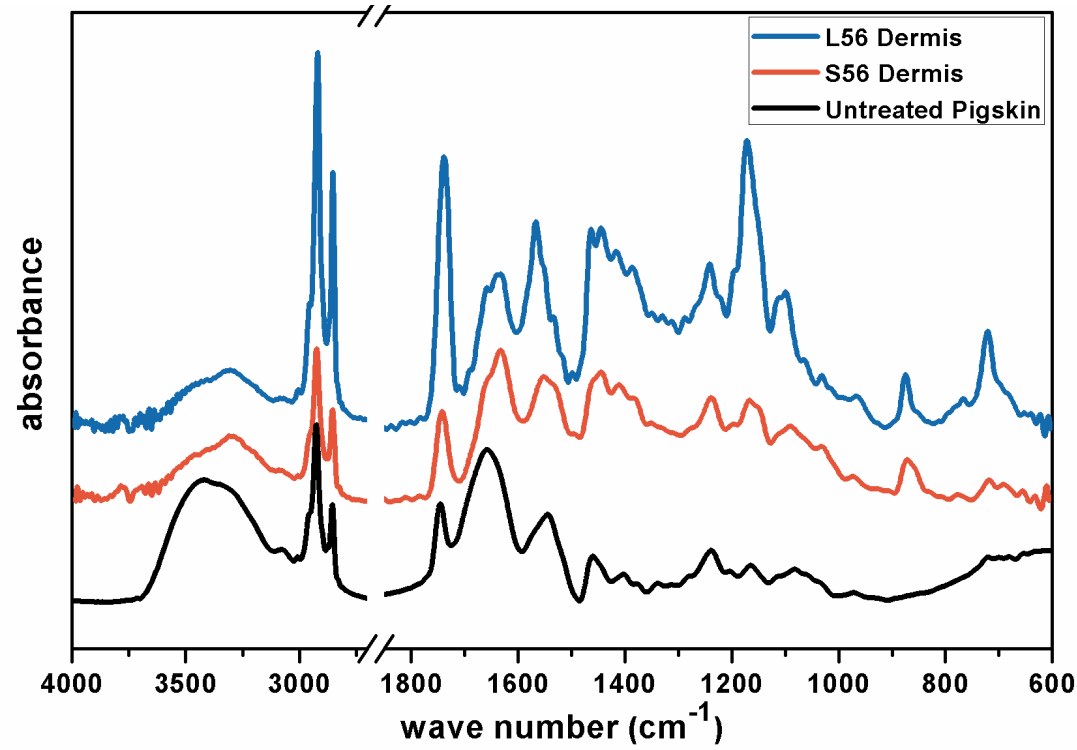

Figure 8.6: Spectra of the untreated sample (black line) used as reference and of the pigskin samples after 56 days of treatment: pigskin treated with dry natron (orange line), pigskin treated with liquid natron (blue line).

In the spectrum of the sample, treated with dry natron, slight but significant differences were identified with respect to the reference sample. The Amide I band is shifted at 1633 cm^{-1} with a shoulder at 1659 cm^{-1}. The shift of the band towards lower wave number is indicative of a modification of the collagen secondary structure, leading to a disordered state. In addition, the band is narrower, if compared with the Amide I band of the untreated sample. This modification could be explained by a decrease of the component related to OH bending vibrations of water, enveloped under the Amide I band. This is caused by the strong dehydration of the sample, already recognized by the observation of the OH stretching band at high wave numbers (Payne and Veis 1988; Habermehl et al. 2005; Rabotyagova et al. 2011).

The spectrum of the sample treated with liquid natron, on the contrary, shows very strong differences in the shape and amplitude of the absorbance bands. These differences are probably due to a higher interaction of the salty solution with the tissue, recognizable in some natron characteristic peaks at 1465 cm^{-1} and 1415cm^{-1}, assigned to the asymmetric stretching vibrations of carbonate (ν_3 (CO_3^{2-})) and at 867 cm^{-1} due to the carbonate out-of-plane bending (ν_2 (CO_3^{2-})).

Moreover, even the shape of Amide I and II band are very different. The Amide I band is narrower and peaked at lower wave number than in the spectrum of the sample treated with dry

natron. A relevant change was monitored in the Amide II band, instead. In the untreated sample, this band was characterized by a broad and smooth feature and peaked at 1545 cm^{-1}. In the spectra of the samples treated in natron solution, on the other hand, it narrows and shifts towards higher wave number showing the highest peaks at 1565 cm^{-1}. This absorbance range is usually assigned to the asymmetric stretching vibrations of the carboxylate groups ($\nu_{as}(COO^-)$) (Barth and Zscherp 2002). Generally, the Amide II band amplitude almost corresponds to the 2/3 of Amide I. In the spectra of the pigskin samples, treated with liquid natron, from day 49 to the end of treatment, on the contrary, the amplitude of Amide II band increases compared with the relating Amide I band amplitude, even if after the third sampling a decrease is recorded. No similar changes were detected in the pigskin samples treated with dry natron.

To better clarify the presence and behaviour of this band in the FTIR spectra of the pigskin samples, rat tail collagen (SIGMA) was treated with salt at increasing concentration (see Chapter 8, Materials and Methods) and its spectrum was compared with some of the spectra of the pigskin samples, treated with natron solution.

As shown in figure 8.7, the same behaviour was revealed. The changes showed by this band can be attributed to changes in collagen tertiary structure. The deep penetration of the salt in the skin, facilitated by the liquid phase, induces the initial deprotonation of the carboxylic residues of the aminoacidic lateral chains (responsible of the amplitude increase of the Amide II band). Gradually, the interaction of the carboxylate residues with salt counterions produces the decrease of the band intensity, when salt concentration further increases, as in the last phases of treatment. This process could be responsible of local enrollments of the collagen triple helices.

Collagen structure is heavily modified and can re-absorb an additional water amount, but it leaves the secondary structure almost unchanged, as testified by the Amide I band profile.

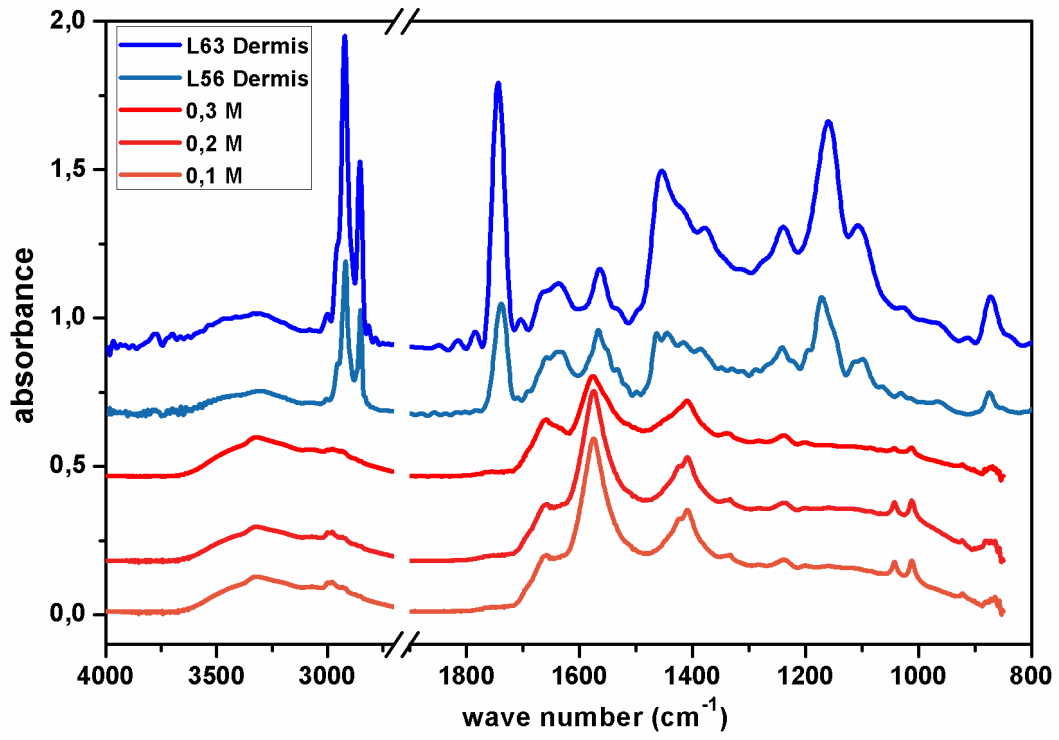

Figure 8.724: FTIR Spectra of the three collagen + natron solutions at increasing concentration (red shade lines) compared with the spectra of two pigskin samples (after 56 and 63 days of treatment) treated with natron solution (light blue and dark blue lines).

In the last stage of this work, the analysis of skin samples from Alan Billis was carried out. The spectra are shown in figure 8.8.

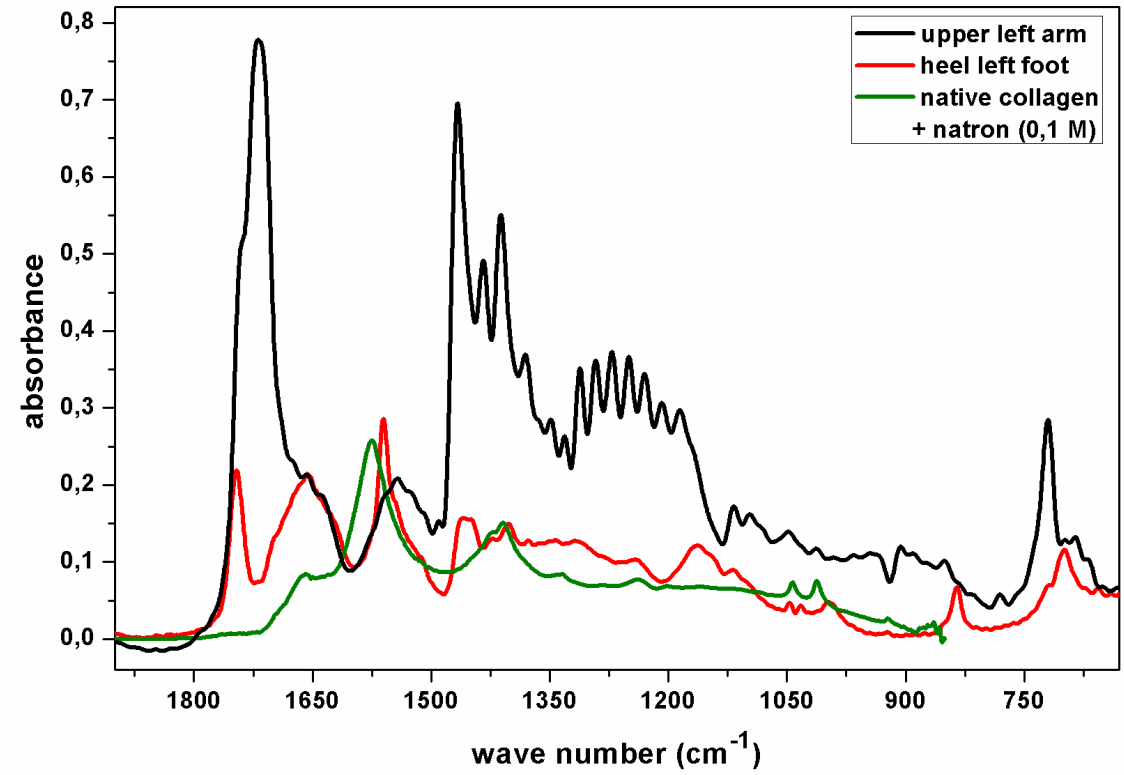

Figure 8.825: FTIR Spectra of the skin samples from Alan Billis (black line: upper left arm; red line: heel left foot) compared with the spectrum of collagen (SIGMA) treated with natron solution (0.1 M)

The spectrum of the upper left arm (black line) exhibits a complex profile. It is probably due to the mixture of substances used for the embalming procedure. In fact, the very intense peak at 1720 cm^{-1}, with a shoulder at 1740 cm^{-1}, could be assigned to the C=O stretching vibrations of lipids. The Amide I is overlapped to this huge band and is represented by a shoulder around 1655 cm^{-1}. The Amide II band is peaking at 1544 cm^{-1} and its intensity is almost comparable to that of the Amide I. Instead, in the foot skin, the Amide II band increases in amplitude and shifts towards higher wave number, showing the same behaviour observed in the pigskin and pure collagen, treated with the liquid natron.

8.2 - Case II:

Photometric Scanner Imaging (PSI) and FTIR Spectroscopy to characterise colour and structure of bones cremated following the Ancient Veneti population uses.

Cremation is a funerary ritual used in the Veneto area from the Bronze Age onwards. Later it became the predominant rite of the Ancient Veneti population during the Iron Age, as documented in the numerous necropolises. While the funerary cremation rites of the ancient Greek aristocracy are described in great detail (in particular, in the texts of Homer the funeral pyres of Patroclus and Hector are well described), the lack of historical information about these rituals in the ancient Veneto region makes their archaeological interpretation still very difficult. In the famous works of Homer, the description of the ritual is emphasized to underline the social prestige and the heroic dimension of the dead. The rituals described in addition to the pyre are practices very difficult to document through the archeological records, such as lamentations and ritual libations. However, particular attention is directed to the extinguishing of the pyre through the use of wine, a practice about which archeologists are still debating today.

In this light, the present work was planned with the aim of proposing a hypothetical reconstruction of a Veneti funeral pyre, whose bone remains were analyzed after cremation, to separately test only the alterations by fire and extinguishing procedures and with the aim to identify some changes which could be distinguished from the other diagenetic modifications.

As extensively suggested in the literature (Stiner et al., 1995;Thompson et al., 2009), the bone fragments were preliminarily considered in terms of their chromatic variability (Canci and Minozzi 2005; Duday 2006; Schmidt and Symes 2008; Mays 2010) by visual inspection. However, this technique displays two main critical points, related 1) to the subjective identification of the absolute colour degree of each bone fragment and 2) to the judgment of the differences of average colour of a collection of remains deriving from the same site or archaeological environment. Therefore the colourimetric analysis of the remains was performed by means of a Photometric Scanner and the results were matched with the FTIR (Fourier Transform InfraRed) spectrophotometric measurements supplying information about charred bone structural features.

8.2.1 Materials and methods

Pyre combustion experiment set-up

The three pyres were reconstructed on the basis of the information provided by the ancient sources, as well as following the results of recent experimental reconstructions (Marshall 2011). The pyres were built in a quadrangular shape (60x65x40cm) and were made by slotting the logs at right angles and filling the spaces with dried weeds and straw mattresses. Following the studies on the anthropological necropolises of Este and Padua, Veneto, Italy (Montella De Carlo 1998), 30 kg of beech, hornbeam, vines and fruit trees were used.

Three fresh legs (500 gr. each) of domestic pig (*Sus scrofa domesticus*) were placed directly on each pyre (Chen et al. 2007). The pyres burned for almost two hours from the beginning of the experiment and three different methods were then used to extinguish them: one was extinguished by means of 2 liters of a mixture of water and red wine (natural and without additives) composed of equal parts of both components (following the directions of the Homeric sources), one was put out by 2 liters of water; from the last pyre the bones were removed after complete spontaneous extinguishing of the fire.

Figure 8.9: Pyres combustion

The cremated bones were collected from the pyres after extinguishing and prepared for colourimetrical and spectroscopic analyses.

In order to simplify sample identification, the samples will hereafter be named as:

- **NE**, sample from pyre spontaneously extinguished,
- **W**, sample from pyre put out with water,
- **W-W**, sample belonging to the pyre put out using the water/wine mixture.

Colourimetric measurements

Samples

The bone fragments collected from the three pyres were considered in terms of chromatic variability to assess the degree of combustion, following the visual method described in the literature as shown in figure 8.10, panel A (Canci and Minozzi 2005; Duday 2006; Schmidt and Kazushi 2007; Mays 2010).

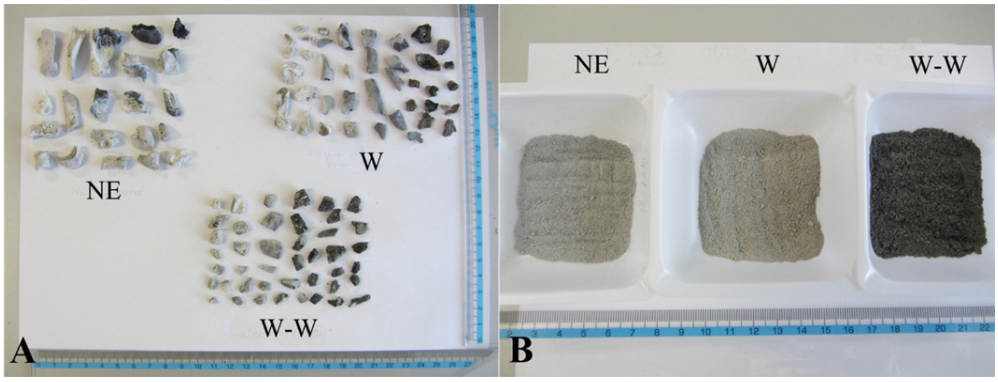

Figure 8.1026: Panel A: Bone fragments collected from the three pyres, spontaneously extinguished (NE), burn out by means of water (W), and by water-wine mixture (W-W); Panel B: bone powders submitted to PSI analysis.

For the colourimetric measurements an amount of about 4.00 g of bone pieces were gently fragmented in a mortar to favor the exposure of their interior. The three powdered samples were stratified in three square white holders to obtain a flat square surface (5 cm x 5 cm) (figure 8.10, panel B) to submit to Photometric Scanner measurements. A white tile (National Physical Laboratory (UK)) with certified spectral radiance factors at 0°/45° geometry was taken as white reference sample.

The Photometric scanner

The Spectrophotometric scanner employed to take the spectral images of the samples, was assembled in the Optics Laboratory of the Department of Physics and Earth Sciences of the University of Parma. The optical arrangement of the scanner is described in detail by Antonioli et al. (Antonioli et al. 2004). It is made up of a transmission spectrometer (Inspector V8E manufactured by Specim, Finland) designed for a 1 inch CCD sensor and equipped with an entrance slit (13 μm). It spans the 400÷780 nm spectral range with a spectral resolution of about 2 nm. The spectrometer is coupled to a monochrome 1 inch CCD matrix digital camera (Basler A2000) while a collecting lens for a 1 inch CCD, (Fujinon CF50HA-1) focalizes the sample surface on the plane of the entrance slit. The illumination is obtained by means of two 150 W halogen lamps whose light is filtered in order to prevent the illumination of the surface with a light of wavelength greater than 750 nm. The light enters into two optical fibers with

blade termination about 30 cm long. The blades are oriented at 45° with respect to the optical axis of the scanner to obtain a slightly homogeneous horizontal stripe of light of about 3 cm high and an illuminance of about 30000 lux. The reflection is taken perpendicular to the sample surface just to realize the CIE 45°/0° standard geometry measurement.

All the data taken by the Scanner are managed by means of an acquisition program "*SpectralScanner750*", supplied by DV Optics (Padova, Italy).

The uniformity of the CIEL*a*b* colourimetric space enables the evaluation of the difference between two colours as the Euclidean distance between the related CIELAB coordinates calculated as

$$\Delta E_{ab} = \sqrt{(a_2^* - a_1^*)^2 + (b_2^* - b_1^*)^2}$$

Two colours are perceived as different by the human eye if $\Delta E > 1$.

FTIR measurements

Samples

Small amounts of calcined bones were ground in an agate mortar. The samples deriving from the two pyres extinguished by liquids displayed a wet and doughy texture, very different from the dry feature of the powders obtained from the bones recovered in the naturally extinguished one. Therefore they were analyzed both in the humid form and after dehydration treatment by maintaining them in an oven at 80 °C for 3 hours, to eliminate residual humidity. A small fragment of a fresh untreated bone was also ground and used as a reference sample. 1 mg of every specimen was mixed with about 100 mg of KBr, and the mixture was pressed at ~ 6 x 10^8 Pa to obtain thin pellets (diameter 13 mm and thickness 0.2-0.3 mm). A thin layer of the red wine used to extinguish one of the pyres was smeared on a CaF_2 window and dried in air.

FTIR spectrophotometer

All the measurements were performed in transmission mode by means of a Jasco 420 FT-IR Spectrophotometer.

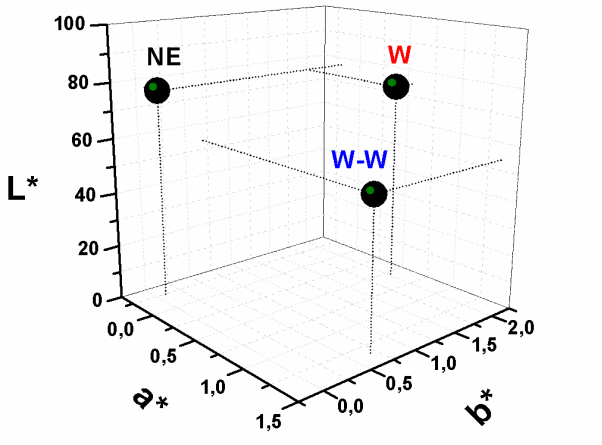

Figure 8.11: Average colour of the three samples examined, represented in the colourimetric space CIELab.

8.2.2 Results

Colourimetric results

The primary analysis of the specimens was performed on the perceived colour of the records, with the aim of distinguishing the different bone damage produced by the fire following the different extinguishing procedures. As shown in figure 8.10, panel A, all the three sets of bone pieces show the presence of differently coloured fragments, turning from white to black, through a grey series. No apparent difference can be detected among the three bone collections. However, once pulverized (see § Materials and Methods), the samples prepared for the Photometric Scanner measurements displayed different colour shades (Figure 8.10).

Colour of the bone powders, was obtained as average value in the colour space L*a*b*. From the L*a*b* coordinates related to each pixel, L* average, a* average and b* average were calculated for each sample examined, together with the colour difference (ΔE^*_{ab})

	L*	a*	b*		ΔE^*_{ab}
NE	77.07 ± 0.08	-0.21 ± 0.01	0.06 ± 0.02	**NE - W**	2.1
W	74.61 ± 0.09	0.54 ± 0.01	2.03 ± 0.03	**NE - W-W**	1.7
W-W	54.00 ± 0.11	1.37 ± 0.01	0.67 ± 0.06	**W - W-W**	2.1

Table 8.2: Chromatic coordinates and Euclidean distance between the chromatic coordinates

The tridimensional plot reveals that the samples have different chromatic coordinates, showing NE and W samples to have comparable L* values (~ 77 and ~75 respectively) and the W-W powder a slightly lower value (~ 54). Following the CIEL*a*b* reference system, the samples may be defined as:

- **NE** → "grey",
- **W** → "grey tending towards yellow",
- **W-W** →"grey tending towards red".

The three colours are chromatically perceived as different, being $\Delta E^*_{ab} > 1$ for each couple of samples, as displayed in Table 8.2. The colour differences may be related to differences in the microscopic texture of the mineral component of the burned bones and in the size of the microcrystals formed after cremation interacting with the light. In particular, it can be indicative of the formation in the NE sample of larger microcrystals, of non-uniform dimensions, able to reflect/scatter the light on a wide angle distribution and therefore responsible for the detected neutral colour. The quenching action produced by the liquids extinguishing the fire produced

W and W-W sample crystals exhibiting lower and more uniform sizes, giving rise to light emission on a relatively narrower and more confined wavelength range.

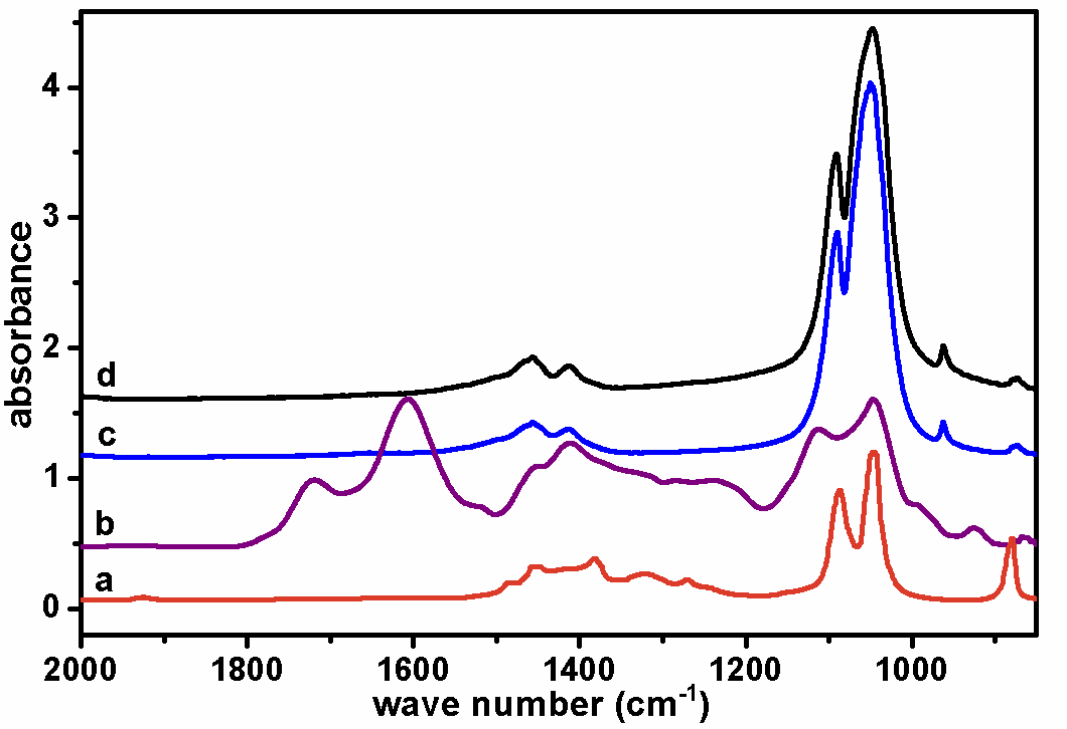

Figure 8.1227: FTIR spectrum (wave number range 2000-850 cm^{-1}) of the red wine (spectrum b), compared with the Ethanol spectrum (a) (NIST Chemistry WebBook) (NIST Chemistry WebBook) and the spectra of the calcined bones (W-W: line c and NE: d line).

FTIR results

In order to obtain information about the possible traces left by the liquids employed to extinguish the pyres in the IR absorption spectra of the burned bones, as a preliminary measurement, the spectrum of the red wine used was analyzed. The collected spectrum (Figure 8.12) was compared with the complex spectrum of the calcined bone extinguished by means of the water/wine mixture (W-W) and with the spectrum of the calcined bone spontaneously extinguished (NE), taken as a control.

In the wine spectrum the main absorption bands can be attributed to the protein content (Amide bands:1800-1500 cm^{-1}) and to the carbohydrate residues (C-O-H, C-O-C groups: 1200-900 cm^{-1}). The two component bands at 1102 and 1055 cm^{-1} are due to the C-O stretching vibrations. Thus, the spectra shown in Figure 8.12, assured us that no feature of the wine absorption bands can contribute to the calcined bone spectra, also given the likely small amount of liquid on the specimens.

In Fig. 8.13, the spectra of the calcined bones are compared with the spectrum of the fresh bone. The main IR-active groups with the associated frequencies (Mantsch and Chapman 1995) are listed in table 8.3 and indicated in the figure by arrows.

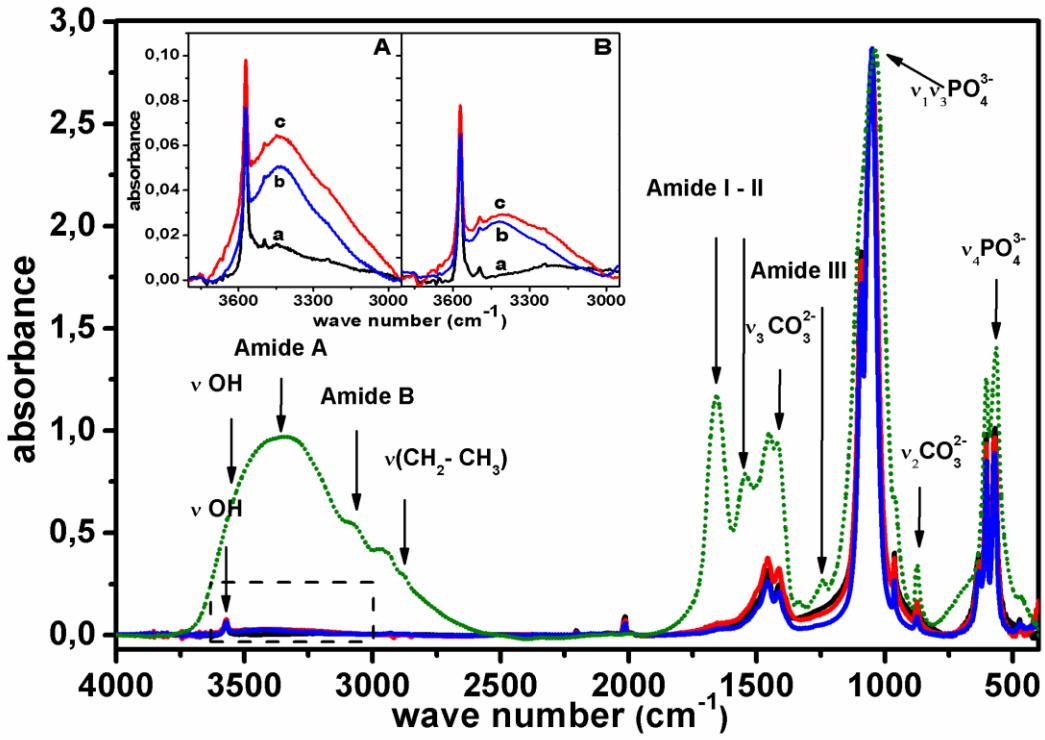

Figure 8.1328: FTIR spectra of the calcined bones compared with the spectrum of the fresh bone. Green dotted line: fresh bone; black line: NE sample; red line: W sample; blue line: W-W sample. The spectra are normalized to the amplitude of the maximum peak ($\nu_3(PO_4^{3-})$). The main absorption peaks are identified and indicated by the arrows. Inset: OH stretching region magnification (4000-2800 cm^{-1}) before (panel A) and after (panel B) dehydration treatment at 80°C for three hours. Curve a: NE sample, curve b: W sample; curve c: W-W sample

In the high wave number region (4000-2000 cm^{-1}, Fig. 8.13, insets A and B) it is easy to observe the differing profile of the ν(OH) bands in the different samples inspected. This result may be considered as a preliminary indirect indication of the changes in the mineral lattice of the samples as a consequence of the extinguishing procedures. The hydration water band of collagen dominates the fresh bone spectrum as a broad absorption band around 3400 cm^{-1}.

Amide A and B bands contribute to the overall band. In the burned bone spectra, the shape of the band is changed.

	Functional Group	Vibrational mode	Wave number (cm^{-1})
Water	R-OH H-O-H R-OH	νOH δ(O-H) ν_L OH	3700–3000 1640 600
Amide A and B	$R\text{-}NH^{3+}$ NH-Amide II	νNH overtone	3300 3075
Lipids and Proteins	$C–CH_3$/ $C–CH_2$	ν_{as} (CH*)*	2950
	$C–CH_3$/ $C–CH_2$	ν_S (CH*)*	2870
Amide I	C=O (75-80%) C-N (20-25%)	ν(C=O) ν(C-N)	1660
Amide II	N-H (40-60%) C-N (20-40%) C-C (10%)	δ(N-H) in-plane ν(C-N)	1545
Carbonates	CO_3^{2-}	$\nu_{3as}(CO_3^{2-})$	1415
Amide III	C-N C-H N-H	ν(C-N) δ(C-H) δ(N-H) in-plane	1240
Phosphates	P-O	$\nu_{3as}(PO_4^{3-})$	1035
	P-O	$\nu_{1s}(PO_4^{3-})$	960
Carbonates	CO_3^{2-}	$\nu_2(CO_3^{2-})$	870
Phosphates	P-O-P	$\nu_{4as}(PO_4^{3-})$	604 - 565

Table 8.3: IR-active groups with the associated absorption frequencies of the fresh bone.

The Amide A and B absorptions are significantly reduced. In the NE sample (black line) two sharp peaks are observed, a strong feature at 3572 cm^{-1} and a weak one around 3496 cm^{-1}, which can be attributed to the hydroxyl groups in hydroxyapatite chemical structure. They are characteristic features in the spectrum of synthetic commercial hydroxyapatite (Rehman and Bonfield 1997). The same bands are present in the spectra of the samples extinguished by means of liquids (red and blue line, corresponding to W and W-W samples respectively), although the sharp OH peaks are superimposed on a broad band peaking around 3440 cm^{-1} and suggesting the presence of molecular water adsorbed in a significant amount in such samples. After submission to a dehydration process by maintaining them in an oven for three hours (see §

Chapter 8, Materials and Methods), the band is shifted to 3410 cm^{-1} and drastically reduced in amplitude (Fig. 8.13, inset B).

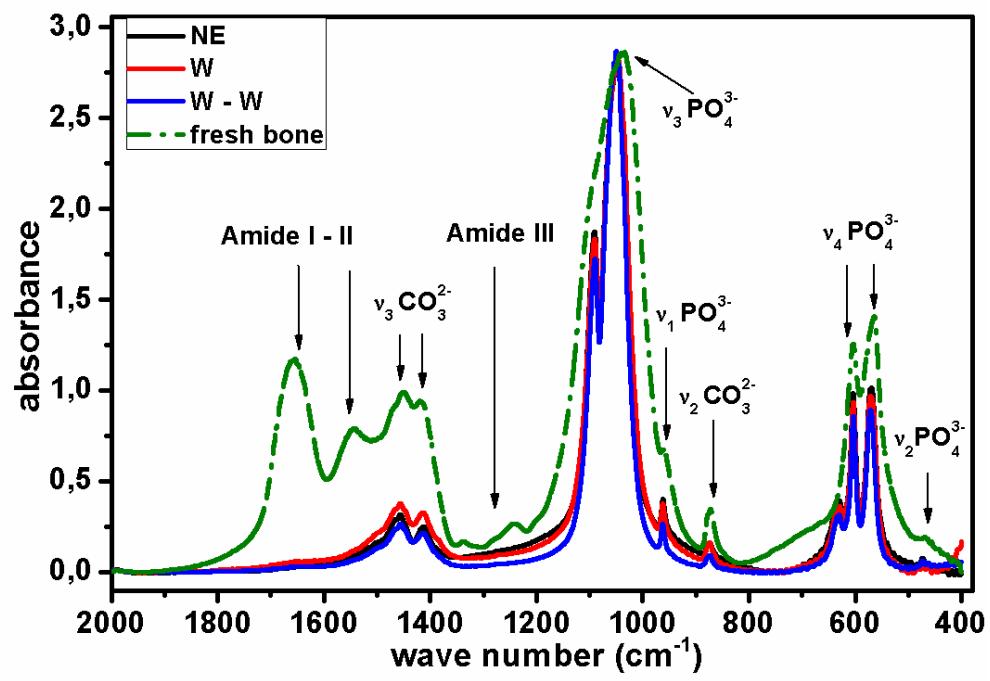

Figure 8.14: FTIR spectra of fresh and calcined bones in the spectral range 2000 - 400 cm^{-1}. Green dotted line: fresh bone; black line: NE sample; red line: W sample; blue line: W-W sample. The spectra are normalized to the amplitude of the maximum peak $\nu_3(PO_4^{3-})$.

Fig. 8.14 displays the low wave number region between 2000-400 cm^{-1}. The fresh bone spectrum appears very different from the spectra of the burned bones, clearly showing that, after burning, the most damaged fraction of the bone is the protein content: in the calcined bone spectra no traces of Amide I, II and III bands can be found and the observation is consistent with the lack of Amide A and B bands, as above reported. The result is in agreement with those of previous studies (Thompson et al. 2009; Rajendran 2011), showing that in bones exposed to temperatures above 700 °C, the organic matrix is completely degraded, the heating inducing the complete damage of the protein content. Therefore the feeble signal around 1650 cm^{-1} may more likely be attributed to the bending vibrations of the OH groups.

The burning treatment also induces deep changes in the inorganic component of the bones. The amplitude of the carbonate peaks is dramatically reduced compared to that of the fresh bone both in the 1470-1400 cm^{-1} ($\nu_3(CO_3^{2-})$) and in the 870-880 cm^{-1} ($\nu_2(CO_3^{2-})$) wave number range, testifying to a loss in structural carbonate as a consequence of the high temperatures (Rehman and Bonfield 1997; Figueiredo et al. 2010). A detailed analysis of these bands was performed and the comparison between the three calcined samples is shown in Fig. 2.12, where the two spectral regions are separately represented. $\nu_3(CO_3^{2-})$ band appears as an asymmetric doublet characteristic of the mixed type AB apatites.

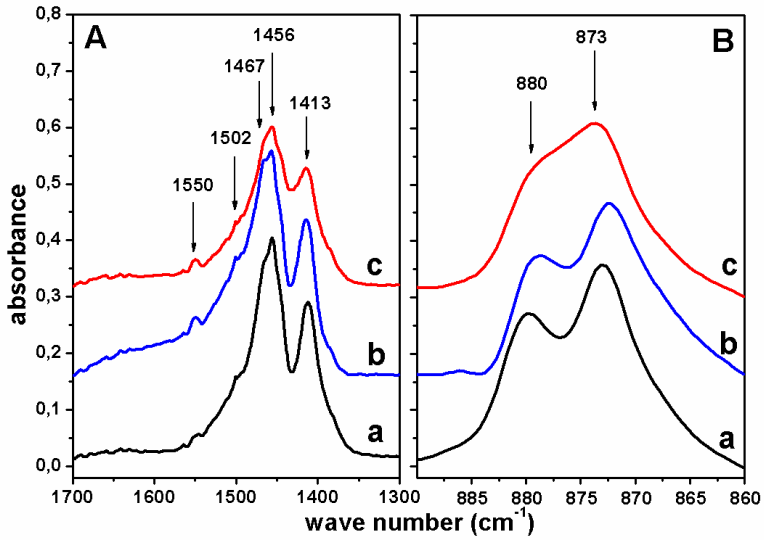

Figure 8.15: Panel A: $\nu_3(CO_3^{2-})$ asymmetric stretching. Panel B: $\nu_2(CO_3^{2-})$ out-of-plane bending. Curve a: W sample; curve b: NE sample; curve c: W-W sample. The characteristic absorption bands of the AB carbonate apatite are indicated by the arrows.

A decrease in the B component is observed (1415 cm^{-1}) compared to that of the A type (1456 cm^{-1}) in the W samples (Fig. 8.15, panel A, c line). The ν_2 band shape confirms the behavior: the two-component band, peaking at 880 and 873 cm^{-1}, in the W sample spectrum (Fig. 8.15 panel B, c line) exhibits a broadened band profile reflecting multiple carbonate local environments whose complexity is different in the different samples (Rajendran, 2011; Figueiredo et al., 2010).

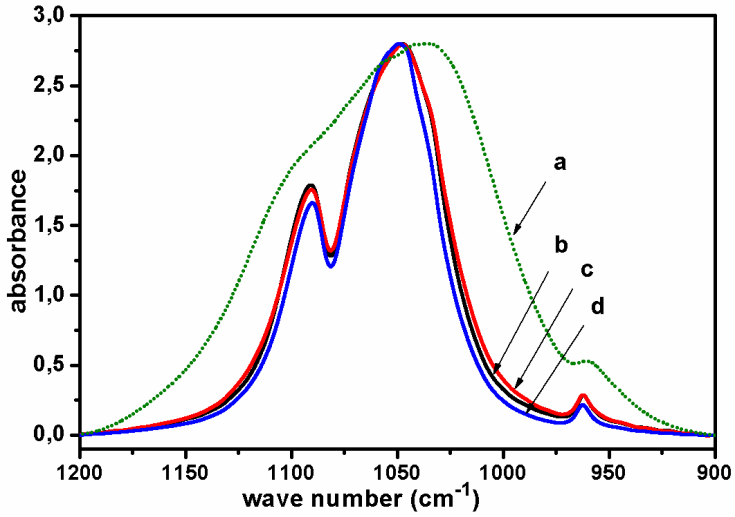

Figure 8.1629: Phosphate stretching absorption band ($\nu_1\nu_3(PO_4^{3-})$). Calcined bone spectra are plotted together with the spectrum of the fresh bone. Curve a: fresh bone; curve b: NE sample; curve c: W sample; curve d: W-W sample

As concerns phosphate bands, they are also modified in profile and position as compared with the fresh bone spectrum, however the changes are quite uniform for the three burned samples. As a general trend, the $\nu_1\nu_3(PO_4^{3-})$ feature (1035 cm^{-1}) narrows down and shifts towards the

higher wave number region, as displayed in Figure 8.16. The fresh bone spectrum (green dotted line) is shaped as a broad featureless band peaking at ~1035 cm^{-1} and displaying a shoulder around 1100 cm^{-1} (ν_3 phosphate asymmetric stretching) and a weaker one on the low wave number side (~960 cm^{-1}) due to the ν_1 phosphate symmetric stretching mode (Figueiredo et al. 2010). The band in the calcined bone spectra (Figure 8.16, b, c and d lines) is considerably narrower and peaks at 1045 cm^{-1}, shifted 10 cm^{-1} upwards.

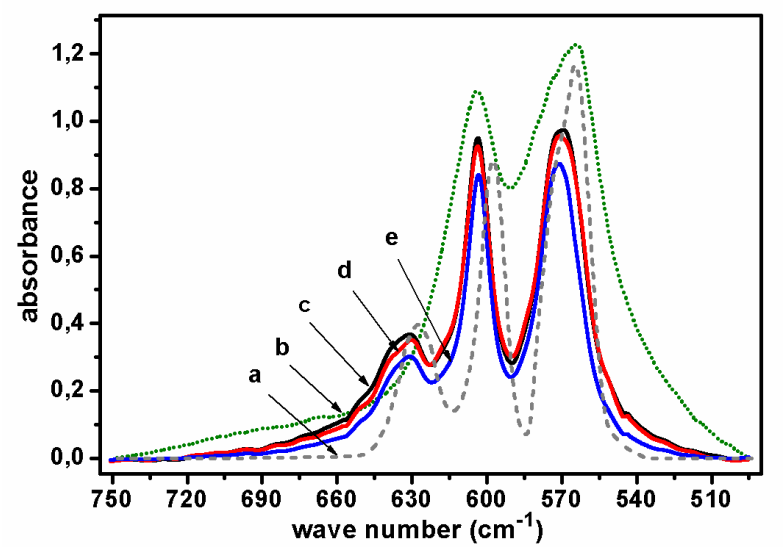

Figure 8.1730 Phosphate asymmetrical bending absorption band (ν_4 (PO_4^{3-})). The intensities of the peaks and of the valley between them are used to calculate the CI splitting factor following Shemesh (Shemesh, 1990). Curve a: synthetic hydroxyapatite (peaks at 632, 603 and 566 cm^{-1}); curve b: fresh bone; curve c: NE sample; curve d: W sample; curve e: W-W sample.

Fig. 8.17 shows the doublet arising from the $\nu_4(PO_4^{3-})$ mode (604-565 cm^{-1}) due to the O-P-O asymmetrical bending mode in tetrahedral (PO_4^{3-}) ions: in burned bones it is reduced in amplitude, thins and displaying a shoulder in the high wave number side, due to the hydroxyl groups librational mode ν_L(OH); (~633 cm^{-1}). The mathematical treatment of the amplitudes and areas of the main absorption bands related to the inorganic fraction may be employed in the development of a series of parameters suitable to describe the mineral phase of the bones and alterations (Olsen et al. 2008). Such indices will be described in detail below and quoted in Table 8.4.

Sample	C/P	CI	Mineral maturity
Fresh bone	0.33	2.9	0.95
NE	0.08	6.9	3.6
W	0.11	6.3	2.9
W-W	0.07	7.1	3.8

Table 8.4: Mineralization indices.

Carbonate/ phosphate ratio (C/P)

C/P index was evaluated as the Abs(1415)/Abs(1035), the amplitude ratio of the absorption peaks at ~1415 cm^{-1} and ~1035 cm^{-1}, by assuming they are proportional to the carbonate and phosphate content. In the calcined bones the phosphate band displays a 10 cm^{-1} shift towards the higher wave number region ($\nu \sim 1045$ cm^{-1}) therefore carbonation in such samples was estimated as the Abs(1415)/Abs(1045) ratio (Thompson et al. 2009). Ratios measured for burned bones are very low as compared with the fresh bone parameter (0.33) as a consequence of the decrease in the carbonate content, and the change may be correlated to an increase in order in the apatite lattice crystals.

Crystallinity index (CI)

The crystalline structure extent of the bones was evaluated by means of the $\nu_4(PO_4^{3-})$ peak splitting. The fresh bone spectrum displays two large bands, peaking at 604 and 565 cm^{-1}, partially overlapping, whereas in the calcined bones (Figure 8.17, c, d and e lines) the two component bands are thinner, well separated and peaking at 604 and 570 cm^{-1}. Their shape is very similar to that recorded for synthetic hydroxyapatite (Figure 8.17, grey dashed line) (Miller et al. 2001). The crystallinity index was calculated following Shemesh (Shemesh 1990). Apatites with larger, more ordered crystals show greater separation of the two peaks, and higher CI. In poorly crystallized apatites, the peaks show overlap and consequently lower CI. Therefore the spectral modifications in charred bones can be attributable to an increase in the degree of crystallinity.

Mineral maturity index

The mineral maturity parameter was developed from the $\nu_1\nu_3(PO_4)$ absorption band (900-1200 cm^{-1}) (Lebon et al. 2010b). It measures the transformation of immature surface-hydrated domains into a mature and more stable apatite lattice, during organism growth. In the samples exposed to a heat source the index can be related to the abrupt changes in the mineral composition produced by the temperature increase and is indicative of the relative amounts of phosphate in stoichiometric or non-stoichiometric apatite, whose ratio provides information about the phosphate ion environments and lattice distortions.

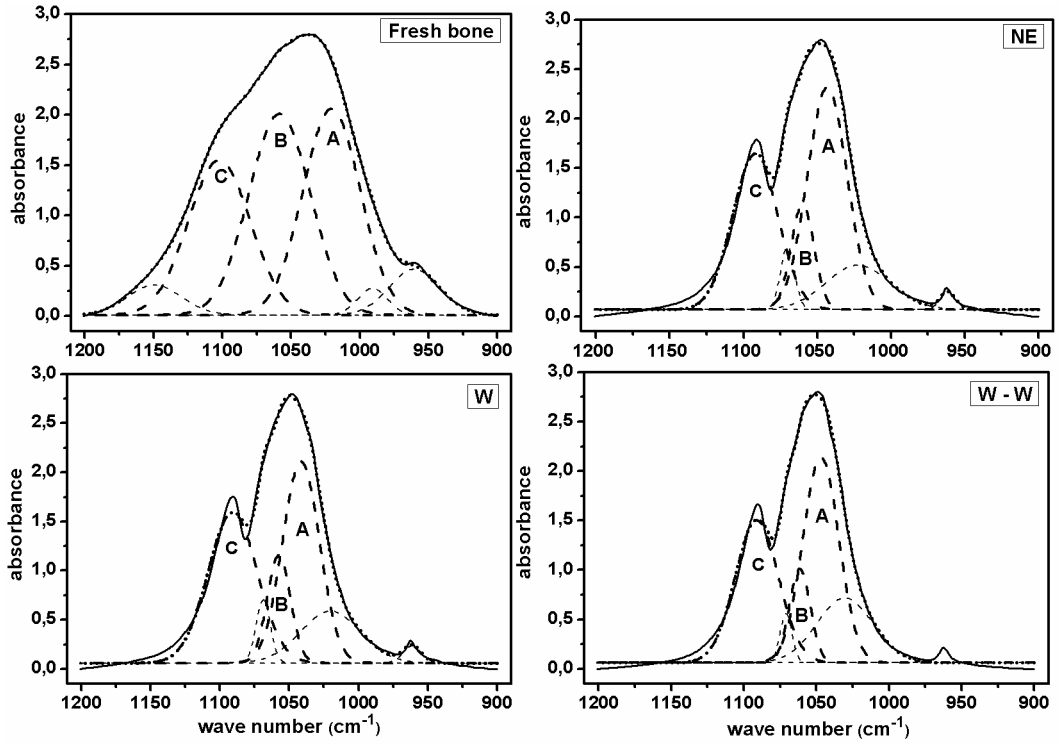

Figure 8.18: Gaussian deconvolution of FTIR spectra in the $\nu_1\nu_3$ phosphate region. The sum of the fitted curves is shown by the thin dotted line, closely overlapping the experimental data trace, which is shown as a full thick line. The individual components are represented by the dashed lines.

To better investigate this point, a Gaussian multipeak analysis was performed on the band of the fresh and calcined bone samples. The results of the deconvolution procedure are shown in Figure 8.18 and in Table 8.5.

	Fresh Bone		NE		W		W-W	
Integral Area	333		212		218		191	
Band	**cm^{-1}**	**Area%**	**cm^{-1}**	**Area%**	**cm^{-1}**	**Area%**	**cm^{-1}**	**Area%**
A	1030	32	1043	36	1041	31	1046	34
B	1058	33	1060	10	1057	11	1061	9
C	1102	26	1092	29	1090	31	1091	28

Table 8.5: Position and percentage areas of the main $\nu_1\nu_3$ (PO_4^{3-}) sub-bands (A, B and C) obtained by the Gaussian multipeak fitting analysis

8.2.3 - Discussion

Concerning FTIR measurements, as a general consideration, burning treatment induces complete decomposition of the collagenous matrix and an enhancement in the crystalline character of the mineral matrix. The IR spectrum of the cremated bones in addition reveal a considerable decrease in the carbonate amount, changes in the shape of the bands corresponding to the four vibrational modes of phosphate groups (ν_1, ν_2, ν_3,and ν_4), and the stretching (ν_s) and librational (ν_L) modes of the hydroxide groups.

The main results related to the spectra of calcined bones can be discussed as follows:

1) The presence of the two OH- stretching (ν_s) vibrations, (3572 cm^{-1} and 3496 cm^{-1}), and of OH- librational (ν_L) modes (~630 cm^{-1}), suggests the activation in the burned samples of the mechanism of orthophosphate decomposition and -OH release observed in synthetic hydroxyapatite during heat treatment followed by cooling in air atmosphere. It highlights the new environment and distribution of OH- ions in the burned bone structure as compared with the fresh one.

   The underlying plateau of elevated background in the spectra of samples collected from the pyres extinguished with liquid (W and W-W sample) may be attributed to molecular water located in submicroscopic pores and to fluid micro-inclusions. By integration of the spectra over the whole water wave number range (3800-3000 cm^{-1}) it is apparent that W and W-W bone samples are ~2 times and ~ 1.5 times respectively more capable of incorporating water than the NE sample, owing to their different microscopic structure (Figure 8.13, inset A).
2) The burning treatment heavily influences the carbonate absorption region (Figure 8.14 and 8.15), which results as being strongly modified in the intensity and shape of the corresponding bands. On the bases of several FTIR studies applied to the characterization of the carbonate bands in bones and teeth (Fleet 2009), charred bones can be considered as belonging to a mixed apatite type, called AB type, whose typical absorption bands appear at 1416, 1452, 1470, 1500 and 1568 cm^{-1}. As illustrated in Figure 8.15, the slight differences among the absorption band shapes of the different samples can be due to the relative prevalence of the amount of one type over that of the other one, depending on bulk composition and local stereo-chemical environments.
3) Phosphate absorption bands provide information about mineral maturity and crystallinity attained by the calcined bone samples. In the wave number region 1200-900 cm^{-1}, $\nu_1\nu_3(PO_4)$ band changes position and shape as a consequence of the exposure of the samples to heat. The peak shift is due to the mineralogical modification induced by heating and can be attributed in particular to the exclusion of carbonate ions from the mineral lattice. Such a

result is in agreement with the severe decrease in the carbonate absorption bands (1470-1400 cm^{-1} and 870-880 cm^{-1}). It is worth noting once more that the band shape closely resembles the feature detected for well-crystallized apatite (Pleshko et al. 1991), the result giving further evidence of the sample recrystallization caused by the transformation of non-stoichiometric apatite components into the stoichiometric one.

The Gaussian deconvolution of the band suggests that in the fresh bone band it is possible to distinguish three main component bands, A, B and C, as discussed by Pleshko et al. (Pleshko et al. 1991). A component (~ 1035 cm^{-1}) may be assigned to the phosphate moieties in stoichiometric apatite, and B component (~1060 cm^{-1}) arises from a disordered phosphate phase not located in a crystalline environment. The percentage area of B band, and the position of A band might be correlated to the apatite crystal size (Pleshko et al. 1991; Lebon et al. 2010b). As shown in Table 8.5, the position of A band shifts from 1030 cm^{-1} for fresh bone towards higher wave numbers (average ν > 1043 cm^{-1}) for calcined samples. The B band area undergoes a sizeable decrease ranging from about 34 % for fresh bone to an average value around 10% for burned specimens. Both the results show a general trend confirming the increase in the crystal size of the calcined bone samples.

A/B band area ratio is a parameter useful to measure mineral maturity. As reported in Table 8.4, the index increases from 0.95 for the fresh bone to higher values for calcined bones. The parameter displays comparable values for the NE and W-W samples, relatively higher than the index detected for the W sample. An increase in the mineral maturity is indicative of an increase in the apatite crystalline order (Pleshko et al. 1991; Sobczak-kupiec et al. 2013); therefore, the result not only indicates the recrystallization of the bone after heating, but also confirms that the sample extinguished with water is seen to contain crystallites of sizes lower than those in the other two bones.

Burning treatments change the shape of the twin band $\nu_4(PO_4^{3-})$ as well (Figure 2.8). The increase in the estimated CI factor from fresh bone to the calcined ones emphasizes once more that high burning temperatures promote the re-crystallization process in the bone (Olsen et al. 2008). According to the literature, CI ≈ 3 is indicative for burning at low temperatures or diagenetic alterations; CI > 4 indicates partial re-crystallization and CI ≈ 7 indicates complete re-crystallization. As shown in Table 8.4, modern fresh bone displays CI = 2.9 typical for a matrix at low crystalline character, but for calcined bones CI values higher than 6 were obtained, confirming that charred bones could experience a complete re-crystallization, promoted by the high burning temperatures (Stiner et al. 1995; Olsen et al. 2008; Rajendran 2011; Sobczak-kupiec et al. 2013). The slight difference ascertained in the CI values obtained,

in particular between the water-extinguished sample and the two others, is considered as being significant, indicating that the NE and W-W samples attain a similarly large CI, whereas the W sample, characterized by a relatively lower CI, contains crystals of smaller sizes.

The coupling of the techniques PSI and FTIR spectroscopy therefore should provide comprehension of damages produced on bone structure by burning and extinguishing, improving the interpretation of the complex diagenetic processes in ancient remains.

Conclusions

This thesis work was carried out with the main purpose of estimating the state of preservation of precious archaeological remains of biological nature, such as mummified skin and fossilised bone. As demonstrated by previous studies, the survival of these remains is guaranteed primarily by the survival of their main protein component: collagen.
Collagen is a very fascinating fibrous protein that owes its strength to its structure. The structure shows an incredible organisation assuring the main functional properties of collagen such as support and tensile strength of the tissues.
The stabilisation and assembly of the protein are favoured by the peculiar organisation of the water molecules wrapping the collagen. Thus, dehydration, followed by the formation of extensive cross-links causing the accumulation of advanced glycation end products, are the main biochemical mechanisms that can influence and modify the protein conformation, leading to the aging of the protein. The powerful combination of several techniques such as FTIR spectroscopy, Circular Dichroism spectroscopy, Scanning Electron Microscopy and histological analyses provided complementary results useful in the comprehension of the great amount of the experimental data.

The first part of this work describes in detail how de-hydration and non-enzymatic glycation influence the collagen structure. The main results can be summarized as follows:

As collagen undergoes dehydration, the desorption of the water molecules wrapping the protein promotes a reorganisation of the hydrogen bond network of the collagen triple helices in the attempt to stabilise the structures and reach a new state of equilibrium. This leads assembly and alignment of the collagen molecules causing a stiffening of the structures. During the re-hydration treatments, the water molecules cannot be completely re-adsorbed in the inner spaces between the triple helices, so that the collagen molecules cannot recover their primitive hydration structure. The collagen secondary structure does not show significant modifications except for an increase in the β-sheet motif amount indicative of an accumulation of the collagen cross-links.

In a living tissue, collagen is embedded in the extracellular matrix, a hydrated gel mainly constituted by glycosaminoglycans. As the tissue dehydrates, as a consequence of aging, collagen lose its cylinder of hydration water and interacts with the extracellular matrix

borrowing the hydroxyl groups from the surrounding sugars, in an attempt to reorganise its structure.

The *in vitro* treatment of the native collagen with different types of sugars was carried out in order to simulate the behaviour of collagen molecules interacting with the extra cellular matrix, and to understand the biochemical mechanisms taking place in a living tissue.
Ribose showed the highest efficiency in the formation of complexes with collagen if compared with glucose. Both the sugars, anyway, cause an increase of the formation of covalent cross-links with the collagen triple helices increasing the stiffening of the collagen structure. The advanced glycation end products (AGEs) obtained represent the main cause of collagen aging. However, they plays a protective action on the collagen fibers stabilising the structure and securing it from the thermal denaturation processes.

In the second part of this work, the results obtained on the pure collagen samples were employed in the interpretation of the results of the archaeological samples and in the comprehension of the biochemical mechanisms triggering the mummification and fossilization processes.

The morphological characterization of the mummified skin samples and their main components, mainly focused on the collagen fibers highlighted their structural modifications and preservation degree in the ancient archaeological remains.
Different conformational changes of collagen occurred in the samples, as a consequence of different types of mummification processes. The main differences among natural and anthropogenic mummification in hot dry environments (Egyptian mummies) and natural mummification in cold dry conditions (Roccapelago mummies) were identified.
The results obtained by means of FTIR spectroscopy showed that the collagen fibers undergo different structural modifications depending on the type of mummification procedures. In natural mummified remains, both Egyptian and from Roccapelago, collagen exhibits an extensive damage of the structure characterised by a partial breakdown of the fibers. A preliminary formation of adipocere has been detected in the natural mummies, both pre-dynastic Egyptian and modern ones from Roccapelago.
In the samples of the Egyptian embalmed mummies, on the contrary, the deconvolution of the Amide I band shows an increase of the cross-linking that causes the stiffening of the collagen fibers.
SEM and histological analyses agree in the representation of collagen bundles modified by the aging, thinned and stretched, if compared with the native macromolecules, as a result of the dehydration, aging and consequently mummification processes.

The extensive modifications of the collagen molecules in the natural mummified remains reveal differences in the structural modifications that these samples underwent as a consequence of the slower exsiccation of the soft tissues than the one occurred to the embalming tissues treated with natron. We can suppose that the slow dehydration probably promoted the initial decomposition processes and the adipocere formation. However, adipocere could probably play an effective role in isolating the body from the external environment and avoiding the re-absorption of humidity from the ambient, favouring the start of the mummification process. The embalming procedures seem to be the best way to obtain a complete and long-lasting mummification, thanks to the very fast dehydration of the bodies produced by natron and, thanks to the sealing action operated by oils, resins and wraps, preventing water reabsorption.
The combined analytical approach enabled us to identify some of the materials used during the Egyptian embalming procedures, traces of Natron used for dehydrating the bodies on the surface of some mummified skin remains, and traces of fungal and insect infestations, causes of dangerous biodegrade of the precious remains studied.

In the study of the osteological remains, the diagenetic processes were investigated: They are the main modification of both the mineral and protein matrix constituting the bone, governed by several factors, such as the burial environment, temperature, pH and composition of the soils and climate conditions. All these parameters can influence the structural properties of both the components of the bone in different ways. A clear comprehension of the diagenetic modification of ancient bones has not been completely achieved yet, but the coupled use of FTIR spectroscopy and Circular Dichroism spectroscopy allows us to obtain several information on the structural modification and, consequently, the state of preservation of both the mineral and organic matrix of some ancient fossilized bones. The main results can be summarised as follows:

- Every bone follows its own diagenetic way depending on the burial environment.
- FTIR analyses permit to evaluate some mineral indices. The results obtained suggest that mineral maturity and crystallinity are not mutually dependent parameters.
- The fossilised collagen did not undergo a proper denaturation but a structural re-arrangement within the bone tissue. The stabilisation of the aged collagen is due to non-enzymatic glycation processes and cross-linking formation leading to the increase of AGEs products such as pyridinolic compounds, which cause a tight aggregation and stiffening of the collagen fibers.

Moreover, the possibility to extract collagen by means of a low temperature procedure, in order to avoid a further modification of the collagen structure permits to analyse it without any interference by the mineral matrix contribution and to calculate specific indices that provide information about the accumulation of the advanced glycation end products.

The experimental archaeology studies had the main purpose to investigate in the field of two of the widely debated archaeological questions of the last years. The first one regards the Egyptian embalming procedures and it is about the employment of natron in dry or liquid formulation. The second one is focused on the funerary practices of cremation used by the Ancient Veneti population.

In the first case of study, the experimental work was applied on pigskin. The results suggest that in the pigskin treated with dry natron, dehydration process is faster and more efficient in the water removal than in the tissues treated with salt solution. Fiber cross-linking and stiffening is induced by this rapid humidity subtraction. No remarkable changes in the collagen structure were observed.

Pigskin samples treated with natron solution revealed interaction of the salt with the tissue that induce strong modifications of the collagen structure, highlighted by a dramatic increase of the Amide II band intensity with respect to the Amide I. This result may be correlated with the strong modification of the collagen structure observed in the *in vitro* analyses, and could be interpreted as due to a severe unwrapping of the collagen triple helices treated with alkaline solutions.

The samples collected from Alan's body, mummified with liquid natron, exhibit the same changes of the Amide II band profile.

Thus, the change in the Amide II band may represent the "signature", allowing us to distinguish the mummified skin treated with dry natron and the one handled with liquid natron.

The second case of study had the main purpose to understand how the structural changes occurring in the burned bones could be experimentally correlated to the different methods of the pyres extinguishing, by means of liquids such as wine.

The coupling of the techniques PSI and FTIR spectroscopy therefore should provide comprehension of damages produced on bone structure by burning and extinguishing, improving the interpretation of the complex diagenetic processes in ancient remains.

The burned bones collected from pyres extinguished in three different ways (spontaneously, by quenching the fire with water and with a mixture of water/wine) showed different colors, measured in terms of the chromatic coordinates L*a*b*, which may be attributed to structural differences in the bone mineral matrix.

Such differences are not concerning the mineral composition of burned bones, which show similar changes in the carbonate and phosphate bands as shown by FTIR spectra.

However, FTIR measurements revealed slight but significant differences among the structural properties of charred bones, suggesting that the differences in the extinguishing procedures give rise to differences in the crystalline texture of the samples.

The results obtained were explained by assuming that during exposure of the bones to heat, atoms of the mineral phase gain high kinetic energy and diffuse much faster than at physiological temperature. The faster diffusion speeds up the phase transition from amorphous to crystalline hydroxyapatite. For this reason, heat treatment increases the crystallinity in all the burned samples. When the fire is extinguished by means of a liquid, the vapor produced by the liquid coming in contact with the very hot surface of the bone can produce an abrupt thermal expansion of the mineral matrix. In fact, the liquid penetrating into the bone tissue will boil before it evaporates. The steam produced exerts expansive pressure and creates a porous structure. It is reasonable to suppose that pore sizes will critically depend on the vaporization heat of the liquid employed, thus modulating the matrix roughness and crystal sizes, water producing the smallest ones.

The differences in the crystal sizes and in porosity were confirmed by the differences in the colors and is reflected by the differences in the wettability of the samples examined. The NE samples, where the hydroxyapatite crystallization process was completely accomplished, accommodate a very small quantity of water compared with the other two samples. It is reasonable therefore to hypothesize that it could be characterized by large smooth crystals, forming large pores, where water can be easily desorbed. When the crystallization process is stopped by quenching the fire with liquid, smaller crystals are formed, the size of which is dependent on the heat of vaporization of the liquids employed for the extinguishing. They lead to smaller pores in the bone structure and to an increase in coating roughness resulting in higher propensity to water adsorption.

References

Abdel-kareem, O., 2010a, FUNGAL DETERIORATION OF HISTORICAL CONTROL IN EGYPT, **7**, 40–7.

Abdel-kareem, O., 2010b, MONITORING , CONTROLLING AND PREVENTION OF THE FUNGAL DETERIORATION OF TEXTILE ARTIFACTS IN THE MUSEUM OF JORDANIAN HERITAGE, *Mediterranean archaeology and archaeometry*, **2**, 85–96.

Abdel-maksoud, G., and El-amin, A., 2013, THE INVESTIGATION AND CONSERVATION OF A GAZELLE MUMMY FROM THE LATE PERIOD, *Mediterranean archaeology and archaeometry*, **1**, 45–66.

Alberts, B., 2001, *Molecular Biology of The cell*, Vol. 40.

Allison, S. D., Chang, B., Randolph, T. W., and Carpenter, J. F., 1999, Hydrogen bonding between sugar and protein is responsible for inhibition of dehydration-induced protein unfolding., *Archives of biochemistry and biophysics*, **365**(2), 289–98.

Antonioli, G., Fermi, F., Oleari, C., and Reverberi, R., 2004, Spectrophotometric Scanner for imaging of paintings and other works of art., In *CGIV 2004: The Second European Conference on Colour Graphics, Imaging and Vision*, 219–24.

Avery, N. C., and Bailey, a J., 2006, The effects of the Maillard reaction on the physical properties and cell interactions of collagen., *Pathologie-biologie*, **54**(7), 387–95.

Azémard, C., Vieillescazes, C., and Ménager, M., 2014, Effect of photodegradation on the identi fi cation of natural varnishes by FT-IR spectroscopy, *Microchemical Journal*, **112**(2014), 137–49.

Bailey, a J., Paul, R. G., and Knott, L., 1998, Mechanisms of maturation and ageing of collagen., *Mechanisms of ageing and development*, **106**(1-2), 1–56.

Bailey, a J., 2001, Molecular mechanisms of ageing in connective tissues., *Mechanisms of ageing and development*, **122**(7), 735–55.

Barth, A., and Zscherp, C., 2002, What vibrations tell about proteins, *Quarterly Reviews of Biophysics*, **35**(4), 369–430.

Belbachir, K., Noreen, R., Gouspillou, G., and Petibois, C., 2009, Collagen types analysis and differentiation by FTIR spectroscopy., *Analytical and bioanalytical chemistry*, **395**(3), 829–37.

Bella, J., Brodsky, B., and Berman, H. M., 1995, Hydration structure of a collagen peptide., *Structure (London, England : 1993)*, **3**(9), 893–906.

Bridelli, M. G., and Crippa, P. R., 2010a, Infrared and water sorption studies of the hydration structure and mechanism in natural and synthetic melanin., *The journal of physical chemistry. B*, **114**(29), 9381–90.

Bridelli, M. G., and Crippa, P. R., 2010b, Infrared and water sorption studies of the hydration structure and mechanism in natural and synthetic melanin., *The journal of physical chemistry. B*, **114**(29), 9381–90.

Bridelli, M. G., Dell'Anna, A., and Stani, C., 2011, FT-IR spectroscopy and microspectroscopy of ancient Egyptian embalmed heads from the Museum of Anthropology and Ethnography of the University of Turin., In *2nd Bolzano Mummy Congress- Mummies from the ice*, Bolzano.

Bridelli, M. G., Dell'Anna, A., and Stani, C., 2012, The preservation state of the skin of some embalmed heads from the Museum of Anthropology and Ethnography of the University of Turin: FTIR investigation of protein secondary structure., *Journal of Biological Research - Bollettino della Società Italiana di Biologia Sperimentale*, **875**, 340–1.

Bryan, M. a, Kar, K., Amin, P., Persikov, A. V, Mohs, A., Wang, Y.-H., and Brodsky, B., 2006, Self-association of collagen triple helic peptides into higher order structures., *The Journal of biological chemistry*, **281**(44), 33283–90.

Buckley, S. a, Stott, a W., and Evershed, R. P., 1999, Studies of organic residues from ancient Egyptian mummies using high temperature-gas chromatography-mass spectrometry and sequential thermal desorption-gas chromatography-mass spectrometry and pyrolysis-gas chromatography-mass spectrometry., *The Analyst*, **124**(4), 443–52.

Buckley, S. a, Clark, K. a, and Evershed, R. P., 2004, Complex organic chemical balms of Pharaonic animal mummies., *Nature*, **431**(7006), 294–9.

Byler, D. M., and Susi, H., 1986, examination of the secondary structure of proteins by deconvolved FTIR spectra, *Biopolymers*, **25**(3), 469–87.

Cai, S., and Singh, B. R., 1999, Identification of $^{N}_{L}$ -turn and random coil amide III infrared bands for secondary structure estimation of proteins.

Canci, A., and Minozzi, S., 2005, *Archeologia dei resti umani. Dallo scavo al laboratorio.*, Carocci, Roma.

Chen, K., Baxter, T., Muir, W. M., Groenen, M. a, and Schook, L. B., 2007, Genetic resources, genome mapping and evolutionary genomics of the pig (Sus scrofa)., *International journal of biological sciences*, **3**(3), 153–65.

Cimmino, F., 1994, *vita quotidiana degli Egizi*, Rusconi Libri.

Collins, M. J., Nielsen-Marsh, C. M., Hiller, J., Smith, C. I., Roberts, J. P., Prigodich, R. V., Wess, T. J., Csapo, J., Millard, a. R., and Turner-Walker, G., 2002, The survival of organic matter in bone: a review, *Archaeometry*, **44**(3), 383–94.

Colombini, P. M., Modugno, F., Silvano, F., and Onor, M., 2011, CHARACTERIZATION OF THE BALM OF AN EGYPTIAN MUMMY FROM THE SEVENTH CENTURY B . C ., **45**(1), 19–29.

Cotte, M., Walter, P., Tsoucaris, G., and Dumas, P., 2005, Studying skin of an Egyptian mummy by infrared microscopy, *Vibrational Spectroscopy*, **38**(1-2), 159–67.

Curry, J. ., 2006, *The Structure of Bone Tissue" Bones: Structure and Mechanics*, Princeton U. Press, Princeton.

DeOliveira, D. B., Trumble, W. R., Sarkar, H. K., and Singh, B. R., 1994, Secondary Structure Estimation of Proteins Using the Amide III Region of Fourier Transform Infrared Spectroscopy: Application to Analyze Calcium-Binding-Induced Structural Changes in Calsequestrin, *Applied Spectroscopy*, **48**(11), 1432–41.

Donadoni Roveri, A. M., 1988, *Civiltà degli Egizi. Le credenze religiose*, Electa.

Do-Seon, L., Lee, I. S., Choi, K.-J., Lee, S. D., Oh, C. S., Kim, Y.-S., Bok, G. D., Kim, M. J., Yi, Y. S., Lee, E.-J., and Shin, D. H., 2008, The potential for non-invasive study of mummies: validation of the use of computerized tomography by post factum dissection and histological examination of a 17th century female Korean mummy., *Journal of anatomy*, **213**(4), 482–95.

Duday, H., 2006, *Lezioni di Archeotanatologia. Archeologia funeraria e antropologia di campo.*, Erma, Roma.

Dunand, F., and Lichtenberg, R., 1997, *Le mummie, viaggio nell'eternità.*, Electa.

Edwards, H., Currie, K., Ali, H., Villard, S., David, A., and Denton, J., 2007, Raman spectroscopy of natron: shedding light on ancient Egyptian mummification, *Analytical and Bioanalytical Chemistry*, **10**, 1007.

Farlay, D., Panczer, G., Rey, C., Delmas, P. D., and Boivin, G., 2010, Mineral maturity and crystallinity index are distinct characteristics of bone mineral., *Journal of bone and mineral metabolism*, **28**(4), 433–45.

Figueiredo, M. M., Gamelas, J. A. F., and Martins, A. G., 2010, Characterization of Bone and Bone-Based Graft Materials Using FTIR Spectroscopy, In *Infrared Spectroscopy - Life and Biomedical Science*.

Fleet, M. E., 2009, Infrared spectra of carbonate apatites: v2-Region bands., *Biomaterials*, **30**(8), 1473–81.

Forbes, S. L., Dent, B. B., and Stuart, B. H., 2005, The effect of soil type on adipocere formation., *Forensic science international*, **154**(1), 35–43.

Friess, W., and Lee, G., 1996, Basic thermoanalytical studies of insoluble collagen matrices., *Biomaterials*, **17**(23), 2289–94.

Habermehl, J., Skopinska, J., Boccafoschi, F., Sionkowska, A., Kaczmarek, H., Laroche, G., and Mantovani, D., 2005, Preparation of ready-to-use, stockable and reconstituted collagen., *Macromolecular bioscience*, **5**(9), 821–8.

Hall, A. C., and Guyton, J. E., 2005, *Textbook of medical physiology*, W.B. Saunders, Philadelphia.

Harvey, R. A., *Lippincott's Illustrated Reviews: Biochemistry, 5e*.

Kawahara, K., Nishi, Y., Nakamura, S., Uchiyama, S., Nishiuchi, Y., Nakazawa, T., Ohkubo, T., and Kobayashi, Y., 2005, Effect of hydration on the stability of the collagen-like triple-helical structure of [4(R)-hydroxyprolyl-4(R)-hydroxyprolylglycine]10., *Biochemistry*, **44**(48), 15812–22.

Koller, J., Baumer, U., Kaup, Y., and Weser, U., 2005, Herodotus' and Pliny'S Embalming Materials Identified on Ancient Egyptian Mummies*, *Archaeometry*, **47**(3), 609–28.

Kothi, S., and Jayanthi, B., 2014, Innovare Academic Sciences EVALUATION OF ANTIOXIDANT AND ANTIMICROBIAL ACTIVITY OF STINGLESS BEE PROPOLIS (TETRAGONULA IRIDIPENNIS) OF TAMILNADU , INDIA, *internal journal of pharmacy and pharmaceutical science*, **6**(8), 81–5.

Lebon, M., Reiche, I., Bahain, J.-J., Chadefaux, C., Moigne, a.-M., Fröhlich, F., Sémah, F., Schwarcz, H. P., and Falguères, C., 2010a, New parameters for the characterization of diagenetic alterations and heat-induced changes of fossil bone mineral using Fourier transform infrared spectrometry, *Journal of Archaeological Science*, **37**(9), 2265–76.

Lebon, M., Reiche, I., Bahain, J.-J., Chadefaux, C., Moigne, A.-M., Fröhlich, F., Sémah, F., Schwarcz, H. P., and Falguères, C., 2010b, New parameters for the characterization of diagenetic alterations and heat-induced changes of fossil bone mineral using Fourier transform infrared spectrometry, *Journal of Archaeological Science*, **37**(9), 2265–76.

Leslie, P., Gartner, J., and Hiatt, L., 2009, *Istologia*, Edises.

Łucejko, J. J., Lluveras-Tenorio, A., Modugno, F., Ribechini, E., and Colombini, M. P., 2012, An analytical approach based on X-ray diffraction, Fourier transform infrared spectroscopy and gas chromatography/mass spectrometry to characterize Egyptian embalming materials, *Microchemical Journal*, **103**, 110–8.

Mallamace, F., Chen, S.-H., Broccio, M., Corsaro, C., Crupi, V., Majolino, D., Venuti, V., Baglioni, P., Fratini, E., Vannucci, C., and Stanley, H. E., 2007, Role of the solvent in the dynamical transitions of proteins: the case of the lysozyme-water system., *The Journal of chemical physics*, **127**(4), 045104.

Mantsch, H. H., and Chapman, D. (eds.), 1995, *Infrared Spectroscopy of Biomolecules*, Wiley-Liss, Inc., New York.

Marchesini, M., and Barresi, A., 2009, I minerali di Wadi Natrun, *Rivista Mineralogica Italiana*, **4**, 228–57.

Marshall, A., 2011, Simulation of prehistoric cremation: experimental pyres, and their use for interpretation of archaeological structures., In *Experimental Archaeology: 1. Early Bronze Age Cremation Pyres – 2. Iron Age Grain Storage.*, 2–79, British Archaeological Reports.

Mary, Y. S., Ushakumari, L., Harikumar, B., Varghese, H. T., and Panicker, C. Y., 2009, FT-IR, FT-Raman and SERS spectra of L-Proline, *Journal of the Iranian Chememical Society*, **6**(1), 138–44.

Mays, S., 2010, *The Archaeology of Human Bones* 2nd ed., Taylor & Francis, London.

Miller, L. M., Vairavamurthy, V., Chance, M. R., Mendelsohn, R., Paschalis, E. P., Betts, F., and Boskey, a L., 2001, In situ analysis of mineral content and crystallinity in bone using infrared micro-spectroscopy of the v4P043- vibration., *Biochimica et biophysica acta*, **1527**(1-2), 11–9.

Montella De Carlo, S., 1998, La ricerca archeobotanica e le terre di rogo, In *"Presso l'Adige ridente": recenti rinvenimenti archeologici da Este a Montagnana, Padova.*, 54–61, Adle, Padova.

Murray, K., Rodwell, V., Bender, D., and Botham, K., 2009, *Harper's Illustrated Biochemistry. 28*.

Nakamoto, K., Margoshes, M., and Rundle, R. E., 1955, Stretching frequencies as a function of distances in hydrogen bonds, **9**, 6480–6.

NIST Chemistry WebBook, NIST Chemistry WebBook, URL: http://webbook.nist.gov/cgi/cbook.cgi?ID=C64175&Type=IR-SPEC&Index=3#IR-SPEC.

Olsen, J., Heinemeier, J., Bennike, P., Krause, C., Margrethe Hornstrup, K., and Thrane, H., 2008, Characterisation and blind testing of radiocarbon dating of cremated bone, *Journal of Archaeological Science*, **35**(3), 791–800.

Onori, G., and Santucci, A., 1993, Ir investigation of water stricture in aerosolOT reverse micellar aggregates, *Journal of Physical Chemistry*, **97**, 5430–4.

Ottaviani, G., 2008, *Manuale di anatomia topografica*, Santa Croce, Parma.

Payne, J., and Veis, A., 1988, Fourier Transform IR Spectroscopy of Collagen and Gelatin Solutions : Deconvolution of the Amide I Band for Conformational Studies, *Biopolymers*, **27**, 1749–60.

Pleshko, N., Boskey, A., and Mendelsohn, R., 1991, Novel infrared spectroscopic method for the determination of crystallinity of hydroxyapatite minerals., *Biophysical journal*, **60**(4), 786–93.

Popescu, M.-C., Vasile, C., and Craciunescu, O., 2010, Structural analysis of some soluble elastins by means of FT-IR and 2D IR correlation spectroscopy., *Biopolymers*, **93**(12), 1072–84.

Rabotyagova, O., Cebe, P., and Kaplan, D., 2011, Collagen Structure Hierarchy and Susceptibility to Degradation by Ultraviolet Radiation, *Materials science & engineering. C, Materials for biological applications*(617), 1420–9.

Rajendran, J., 2011, Xanes and ftir study on dried and calcined bones, , The University of Texas at Arlington.

Rehman, I., and Bonfield, W., 1997, Characterization of hydroxyapatite and carbonated apatite by photo acoustic FTIR spectroscopy., *Journal of materials science. Materials in medicine*, **8**(1), 1–4.

Rest, M. Van der, and Garrone, R., 1991, Collagen family of proteins., *The FASEB Journal*(60).

Roy, R., Boskey, A., and Bonassar, L. J., 2010, Processing of type I collagen gels using nonenzymatic glycation., *Journal of biomedical materials research. Part A*, **93**(3), 843–51.

Samadelli, M., Roselli, G., Fernicola, V. C., Moroder, L., and Zink, A. R., 2013, Theoretical aspects of physical-chemical parameters for the correct conservation of mummies on display in museums and preserved in storage rooms, *Journal of Cultural Heritage*, **14**(6), 480–4.

Sandison, A., 1963, The Use of Natron in Mummification in Ancient Egypt, *journal of near eastern studies*, **22**(4), 259–67.

Schmidt, C. W., and Symes, S. A., 2008, *The Analysis of Burned Human Remains* 1 edition ed., Academic Press, New York.

Schmidt, D. A., 2007, Structural Correlations in Liquid Water : A New Interpretation of IR Spectroscopy(Figure 1), 10119–22.

Schmidt, D. A., and Kazushi, M., 2007, Structural correlations in liquid water: a new interpretation of IR spectroscopy., *The journal of physical chemistry. A*, **111**(40), 10119–22.

Schmitt, A., 2006, *Forensic Anthropology and Medicine*, Humana Press, Totowa, NJ.

Do Seon, L., Lee, I. S., Choi, K. J., Lee, S. D., Oh, C. S., Kim, Y. S., Bok, G. D., Kim, M. J., Yi, Y. S., Lee, E. J., and Shin, D. H., 2008, The potential for non-invasive study of mummies: validation of the use of computerized tomography by post factum dissection and histological examination of a 17th century female Korean mummy, *Journal of anatomy*, **213**, 482–95.

Shemesh, A., 1990, Crystallinity and diagenesis of sedimentary apatites, *Geochimica and Cosmochimica Acta*, **54**(9), 2433–8.

Shortland, A., 2004, Evaporieties of the Wadi Natrun: seasonal and annual variation and its implication for ancient exploitation, *Archeometry*, **46**(4), 497–516.

Shoulders, M. D., and Raines, R. T., 2009, Collagen structure and stability., *Annual review of biochemistry*, **78**, 929–58.

Sobczak-kupiec, A., Wzorek, Z., and Kijkowska, R., 2013, Effect of calcination conditions of pork bone sludge on behaviour of hydroxyapatite in simulated body fluid, *Bulletin of Material Science*, **36**(4), 755–64.

Stani, M., Baraldi, A., Boano, R., Cinquetti, R., and Bridelli, M. G., 2014, Study of skin degradation in ancient Egyptian mummies: complementarity of Fourier transform infrared spectroscopy and histological analysis, *Journal of Biological Research - Bollettino della Società Italiana di Biologia Sperimentale*, **87**(1), 2–4.

Steele, D. G., and Bramblett, C. A., 1988, *The Anatomy and Biology of the Human Skeleton.*, Texas A&M University Press.

Stiner, M. C., Kuhn, S. L., Weiner, S., and Bar-Yosef, O., 1995, Differential Burning, Recrystallization, and Fragmentation of Archaeological Bone, *Journal of Archaeological Science*, **22**(2), 223–37.

Stuart, B. H., Forbes, S., Dent, B. B., and Hodgson, G., 2000, Studies of adipocere using diffuse reflectance infrared spectroscopy, *Vibrational Spectroscopy*, **24**(2), 233–42.

Stuart, B. H., 2007, Studies of adipocere using attenuated total reflectance infrared spectroscopy B.H. Stuart, 1–13.

Thompson, T. J. U., Gauthier, M., and Islam, M., 2009, The application of a new method of Fourier Transform Infrared Spectroscopy to the analysis of burned bone, *Journal of Archaeological Science*, **36**(3), 910–4.

Tiffany, M. L., and Krimm, S., 1972, Effect of temperature on the circular dichroism spectra of polypeptides in the extended state., *Biopolymers*, **11**(11), 2309–16.

Ubelaker, D. H., and Zarenko, K. M., 2011, Adipocere: what is known after over two centuries of research., *Forensic science international*, **208**(1-3), 167–72.

Vidal, B. D. C., and Mello, M. L. S., 2011, Collagen type I amide I band infrared spectroscopy., *Micron (Oxford, England : 1993)*, **42**(3), 283–9.

Whitford, D., 2005, *Proteins: structure and function*.

Wright, L. E., and Schwarcz, H. P., 1996, Infrared and Isotopic Evidence for Diagenesis of Bone Apatite at Dos Pilas, Guatemala: Palaeodietary Implications, *Journal of Archaeological Science*, **23**(6), 933–44.

Young, B., Luwe, J., Stevens, A., and Health, J., 2007, *Istologia e anatomia microscopica*, Elsevier, Amsterdam.

Zhang, Z. K., Li, G. Y., and Shi, B., 2006, Physicochemical properties of collagen, gelatin and collagen hydrolysate derived from bovine limed split wastes, *Journal of the Society of Leather Technologists and Chemists*, **90**(1), 23–8.